DASA 2638
(3SR - 502)
December 1970

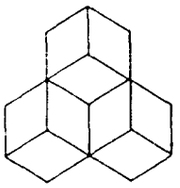

SYSTEMS, SCIENCE AND SOFTWARE

DISLOCATION DYNAMICS AND THE FORMULATION OF CONSTITUTIVE EQUATIONS FOR RATE-DEPENDENT PLASTIC FLOW IN METALS

by
H.E.Read
J.R.Triplett
R.A.Cecil

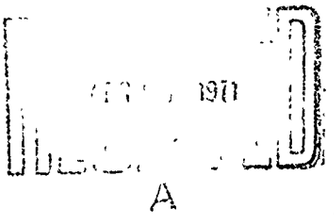

P O. BOX 1620, LA JOLLA, CALIFORNIA 92037, TELEPHONE (714) 453-0060

DASA 2638

(3SR - 502)

December 1970

SYSTEMS, SCIENCE AND SOFTWARE

DISLOCATION DYNAMICS AND THE FORMULATION OF CONSTITUTIVE EQUATIONS FOR RATE-DEPENDENT PLASTIC FLOW IN METALS

by

H.E.Read

J.R.Triplett

R.A.Cecil

This work sponsored by the Defense Atomic Support Agency under NWER/Subtask AA 106

Contract DASA 01 - 70 - C - 0055

P O BOX 1620, LA JOLLA, CALIFORNIA 92037, TELEPHONE (714) 453 0060

ABSTRACT

A rate-dependent constitutive model is developed which describes a broad spectrum of elastic-plastic response in isotropic metals, ranging from quasi-static behavior through the thermally activated intermediate strain rate regime, up to the high strain rate region, where phonon viscosity and relativistic effects appear to control the flow process. Upon reverse straining from a plastically prestrained state, the constitutive model exhibits a rate-dependent Bauschinger effect.

An attempt has been made to utilize, wherever possible, current knowledge in the theory of dislocation dynamics in formulating the constitutive model. It is not the intent, however, to imply that the model developed necessarily has physical significance at the microstructural level. The micromechanical mechanisms which govern the mobility and multiplication of dislocations at high strain rates are not well understood at the present time. In most cases, only simple models of governing deformation mechanisms can be constructed and, even to accomplish this, considerable speculation is required. Where dislocation theory is unable to provide guidance in defining and characterizing a particular mechanism, a phenomenological approach has been followed.

The advanced constitutive model developed here has been incorporated into the one-dimensional, finite-difference RIP code. The application of this model to 6061-T6 aluminum is described.

FOREWORD

This technical report describes the results of a study conducted by Systems, Science and Software (S^3) to develop constitutive models for predicting the dynamic response of metals to impulsive loading. The work reported here was performed for the Defense Atomic Support Agency (DASA), Aerospace Systems Division, as part of the PREDIX Program under Contract DASA 01-70-C-0055. The inclusive dates of research were January 1969 through September 1970.

The overall effort at S^3 on the PREDIX Program, of which the present report describes only a portion, was conducted under the general supervision of Dr. Robert A. Kruger, who served as the Principal Investigator. The material presented in this report appears also as a chapter in the following report:

> R. A. Kruger, R. H. Fisher, H. E. Read, and J. R. Triplett, "A Theoretical Investigation of the Dynamic Response of Metals," Systems, Science and Software report, No. 3SR-308, December 1970,

which documents the entire S^3 PREDIX effort to date pertaining to metals. Other chapters in the report cited above deal with the related problems of (1) radiation transport and deposition, (2) front surface physics, and (3) dynamic fracture.

The authors wish to thank Messrs. W. Isbell, D. Christman, and S. Babcock of the General Motors Materials and Structures Laboratory for their cooperation in supplying the majority of the experimental data used in this study, as well as for a number of informative discussions. Thanks are also extended to Dr. C.J. Maiden, who reviewed the manuscript and made several pertinent suggestions.

CONTENTS

I. INTRODUCTION

During the past ten years, there has been a substantial continuing effort to develop techniques for predicting the dynamic response, and damage thresholds, of reentry vehicles exposed to sudden doses of nuclear radiation. Conceptually, the general response of such a vehicle can be separated into an initial phase and a final phase. In the initial phase, the incident radiation generates thin stress pulses which propagate through the structure in a localized manner. During this time, the stress intensity is high and considerable attenuation of the loading wave occurs; the distribution of stress may be sufficiently localized to produce material damage. In the final phase of response, the incident radiative energy has been transmitted throughout the structure by stress wave propagation, and the stress distribution is much less localized than in the initial phase. The response of the vehicle during the final phase is principally of a structural nature, consisting of elastic vibration, plastic deformation, buckling and (possibly) fracture in varying degrees, depending on the intensity of the incident radiation.

A large part of the effort to understand, and model, the response of reentry vehicles to radiation loading has been devoted to studies, both experimental and theoretical, of the constituent materials, such as the metallic backup materials and the composite ablative materials. In most analyses, the metallic materials have been described by simple elastic-plastic models, and for the purpose of systems studies these appear to provide sufficient accuracy, at least in analyses of the final response phase.

During the initial phase, however, where the propagation and attenuation of thin stress pulses are of great concern, recent studies have cast considerable doubt on the use of the simple elastic-plastic constitutive model, especially for

metals such as α-titanium, beryllium, and tantalum, which exhibit relatively strong strain hardening and strain rate effects. As is generally known, the simple elastic-plastic constitutive model, while computationally attractive, cannot account for increases in the flow stress due to strain hardening and strain rate effects, or changes in the nature of the strain hardening on reverse loading from a prestrained state (Bauschinger effect). It has been apparent for some time, however, that many metals adopted for use in reentry vehicles exhibit to some degree dynamic response features which the simple elastic-plastic model does not account for. Moreover, experimental evidence accumulated during the past few years indicates that some of the more complex effects not exhibited by the simple elastic-plastic model may have significant influence on the calculation of thin pulse propagation and damage thresholds in metals.

Significant discrepancies between theoretical predictions based on simple elastic-plastic models and experimental observation have been reported for a number of metals*. Evidence of elastic precursor decay and strain rate effects during wave propagation in a variety of metals has been reported by Jones, Neilson, and Benedict,[2] Taylor and Rice,[3] Barker, Butcher and Karnes,[4] Karnes[5] and Isbell, Christman, Babcock, Michaels and Green.[6] Barker, Lundergan and Herrmann[7] experimentally measured the loading and unloading dynamic stress-strain relation for 6061-T6 aluminum and observed a disagreement with predictions based on the simple elastic-plastic model which they attributed to strain rate effects and a Bauschinger effect. Additional evidence of a significant Bauschinger effect in 6061-T6 aluminum was reported by Hartman,[8] who measured the residual strain

*For a review of elastic-plastic wave propagation phenomena in metals, the reader is referred to a recent survey paper by Herrmann.[1]

after release from a shock compressed state. Erkman and Christensen,[9] in a study of stress wave propagation in 2024 aluminum, did not observe the two-step shape in the release wave profile, which is characteristic of simple elastic-plastic theory. Thin pulse attenuation in 2024 aluminum was studied by Curran,[10] who found that the simple elastic-plastic theory resulted in a more delayed attenuation than that which was experimentally observed. Barker[11] observed release wave profiles in 6061-T6 aluminum using a laser interferometer and found that the data could be fit reasonably well if the simple elastic-plastic theory was modified to include strain hardening and a strong Bauschinger effect.

In view of the studies mentioned above, it appears that the simple elastic-plastic theory, while sufficiently adequate for many applications, may not provide an accurate enough description of material response when thin pulse attenuation and spallation are of primary concern. When this is the case, it appears that a more sophisticated and realistic material model is needed and a number of attempts in this direction have been made.*

Recent advances in the basic understanding of dislocation behavior have given considerable insight into the physical processes which govern the dynamic plastic response of metals. As pointed out by Dorn, Mitchell and Hauser[13] in a survey paper on dislocation dynamics, significant progress has been made recently in identifying the rate-controlling mechanisms for plastic flow over a wide range of strain rates up to about 10^3 sec^{-1}. It appears that it may now be possible to mathematically model with some degree of realism several of the dislocation mechanisms of importance to plastic wave propagation.

*In this connection, see a recent topical report by Herrmann, Lawrence and Mason[12] in which the effects of strain hardening, strain rate, and Bauschinger phenomena on thin pulse attenuation are discussed.

Using such information, functional forms suggested by dislocation theory may be synthesized to form constitutive equations for describing dynamic material response over a wide range of strain rates. Such an approach has been followed, for example, by Taylor,[14] Gilman,[15] Wilkins,[16] and Johnson and Barker.[17]

A research program, termed PREDIX, was initiated some time ago by the Defense Atomic Support Agency (DASA) for the purpose of developing techniques (both theoretical and numerical) for predicting the response and damage thresholds of solids exposed to sudden doses of nuclear radiation. This program involves a coordinated effort by personnel from several independent research organizations, and has combined the talents of theoreticians, experimentalists, and numerical code specialists. A large part of the effort within the PREDIX program to date has been devoted to the development of constitutive models for high strain rate elastic-plastic deformation of metals. This report describes the research performed at S^3 under the PREDIX program in this connection.

In the work reported here, an attempt has been made to avoid the purely phenomenological approach to constructing constitutive models, which has been followed frequently in the past, by making as much use as possible of the present knowledge of dislocation dynamics. Following this philosophy, a rate-dependent constitutive model has been developed which describes a broad spectrum of mechanical response ranging from quasi-static behavior, through the thermally activated intermediate strain rate regime, up to the high strain rate region, where phonon viscosity and relativistic effects appear to control the plastic flow process. Upon reversed loading from a prestrained state, the model exhibits a Bauschinger effect. This advanced constitutive model has been incorporated into the one-dimensional, finite-difference RIP code and applied successfully thus far to 6061-T6 aluminum.

It should finally be noted that the present constitutive model is designed primarily to describe high strain rate plastic flow, for which the governing micromechanical mechanisms are extremely complicated and not well understood at present. In most instances, only simple models of these mechanisms can be constructed and, even to accomplish this, considerable uncertainty is unavoidable. But because of the approach followed here, it appears that the present constitutive model can be readily modified to accommodate any improvements which may be suggested in the future as further understanding of high strain rate plastic flow in metals is achieved.

II. SALIENT FEATURES OF SHOCK-INDUCED PLASTIC DEFORMATION

There are a number of features that distinguish plastic deformation under shock loading from that which occurs under quasi-static or moderate strain rate conditions. Inasmuch as shock loading is of principal interest in this study, we shall briefly discuss some of the salient effects that shock loading has on the plastic deformation modes and mechanical properties of metals. For a more extensive discussion of this subject, the reader is referred to Ref. 18, where Maiden has given a survey of the literature up to 1965 dealing with the effect of shock waves on the properties of metals.

It has been fairly well established that the mechanical properties of most metals are usually different after they have been shock loaded than when the loading has occurred under quasi-static or moderate strain conditions. In many metals quasi-static loading produces a much greater hardness than shock loading to the same maximum stress level. Conversely, for the same amount of strain, the shock-loaded specimen is much harder than a statically loaded specimen.[19] The significant changes observed in the dislocation substructure and strength characteristics, as well as the hardness between shock and nonshock-loaded specimens seems to indicate that the modes of plastic deformation may be quite different.

It should be noted at this point that there are two basic modes by which plastic deformation may take place in polycrystalline metals, name, slip and twinning. Depending upon the nature of the deformation process, these modes may operate exclusively or jointly. In one respect, twinning differs from slip in that the interatomic movements within the crystal structure are only a small fraction of the atomic spacing, and it appears that the total shear deformation is generally small. While slip is the likely mode of deformation in most metals at room temperature and low-to-moderate rates of strain, twinning can be the dominant mode at high strain rates under

shock loading. According to Tegart,[20] twinning can occur in bcc and fcc metals (such as copper, iron, tantalum, and nickel) at room temperature under shock loading; there is indication that twinning may be expected to be an important, if not dominant, deformation mode in hcp metals (such as α-titanium and beryllium) at room temperature under both moderate and high strain rates.

Recent experimental studies on several metals tend to support the conclusions expressed above. Nolder and Thomas,[19] for example, found that the deformation in nickel changed from slip to slip-twinning for shock loading at stresses near 350 kbar. Similarly, Johari and Thomas[21] investigated the deformation modes of pure copper and copper alloy specimens subjected to shock loading and found that the deformation mode changed from slip to twinning above a critical stress that depended on the percent alloy in the copper. For pure copper, this critical stress was in the range of 16-28 kbar. In addition to these studies, it has been known for some time that iron and iron-base alloys exhibit extensive twinning (Neumann bands) after shock loading. Additional studies, recently reported in Reference 22, provide further confirmation that a change in the deformation mode occurs in certain metals under shock loading.

From the preceding discussion it appears that although slip may be the most favorable mode of plastic deformation at low-to-moderate strain rates near room temperature, twinning may be the dominating mode at high strain rates in some metals under shock loading. As Gilman has pointed out,[23] profuse twinning may occur in some metals under impulsive loading. Therefore, in developing a constitutive equation for high strain rate processes on the basis of the physical processes occurring at the substructure level, twinning as well as slip may have to be given appropriate consideration.

If an attempt is made to formulate this approach, one immediately encounters a difficulty which arises from the fact that while the equation relating the plastic strain rate to the various dislocation characteristics has been well established for slip deformation, the same is not true for twinning deformation. If plastic deformation is solely by slip, it can be shown that the plastic strain rate, $\dot{\gamma}$, is given by[23]

$$\dot{\gamma} = bN_m v \tag{2.1}$$

where

b = Burgers vector (cm)
N_m = density of the mobile dislocations (cm^{-2})
v = mean velocity of the mobile dislocations (cm/sec).

On the other hand, the state of knowledge of twinning deformation is not as advanced as that of slip. However, several equations have been proposed for describing the plastic strain rate during twinning. The most recent of these has been suggested by Gilman,[23] and it prescribes the plastic strain rate due to twinning, $\dot{\gamma}_{twin}$, according to the following relation:

$$\dot{\gamma}_{twin} = sN_t\dot{A} \tag{2.2}$$

where

s = twinning shear strain (dimensionless)
N_t = density of twins intersecting an arbitrary plane (cm^{-2})
$\dot{A}$ = mean rate of change of cross-sectional area per twin (cm^2/sec).

However, inasmuch as twinning will not be the primary topic of discussion here, we shall not go into further detail on this topic. Instead, the reader is referred to References 24 and 25, where comprehensive accounts of twinning deformation may be found.

III. FORMULATION OF THE RATE-DEPENDENT CONSTITUTIVE EQUATION

The basic formulation of the rate-dependent constitutive equation is given in this section. Particular attention is given to an examination of the various functional forms (some of which are taken from dislocation theory and others simply postulated) that have been adopted in synthesizing the material model. Wherever possible, attempts are made to compare the viewpoints adopted in formulating the constitutive equation with those put forth by others.

A. Plastic Deformation by the Slip Process

Polycrystalline metals, when viewed on the microscale, are inhomogeneous and possess a large number of crystal defects, termed dislocations. Inhomogeneities also arise from entrained impurities, precipitates, and the general nonuniformity of the grain structure. When an external load is applied either statically or dynamically, plastic flow results from the motion of dislocations (edge and screw) along various glide planes. Under the action of applied forces, the mobile dislocations move rapidly along glide planes until their motion is arrested by short-range obstacles (energy barriers) lying in their paths. These obstacles may result from entrained impurities, precipitates, fixed dislocations, or grain boundaries. Through the process of thermal activation, large (random) thermal vibrations assist the dislocation in overcoming the obstacles. After this has occurred, the dislocation accelerates rapidly to a high velocity, the magnitude of which is usually governed by some viscous-like mechanism. The dislocation continues to travel at this high velocity until it encounters another obstacle and the same process is repeated.

In the sequel, it will be assumed that the major portion of the plastic flow at a point occurs along slip planes on which the resolved shear stress has its maximum value.* We

*For a more general treatment of slip deformation, see Ref.26.

shall denote by τ the maximum resolved shear stress on these planes and by γ the component of plastic strain in the direction of τ. The one-dimensional uniaxial stress and uniaxial strain configurations play an important role in the developments which follow and, because of this we shall list here some special features of these configurations for future reference.

Under uniaxial stress conditions, the maximum shear stress τ occurs on planes inclined at 45^{o} to the axis of the only nonvanishing principal stress component σ; the magnitude of the maximum shear stress on these planes is given by

$$\tau = \frac{\sigma}{2} \tag{3.1}$$

We shall employ the symbol ε_1 to denote the strain component in the direction of the stress σ.

In the case of uniaxial strain, the maximum shear stress acts on planes inclined at 45^{o} to the only nonvanishing principal strain ε, and its magnitude on these planes is defined by the equation

$$\tau = \tfrac{1}{2}(\sigma_1 - \sigma_2) \tag{3.2}$$

where σ_1 denotes the principal stress in the direction of ε and σ_2 is a principal stress component orthogonal to σ_1.

Unless otherwise noted, the natural (or logarithmic) definition of strain is employed throughout this work. On this basis, the strain ε is defined in the following manner for the case of uniaxial strain

$$\varepsilon = \ell n\ (\rho/\rho_o) \tag{3.3}$$

where ρ_o and ρ denote, respectively, the initial and current mass density of material. From the above definition, it is seen that the strain ε is positive when the material is compressed.

In the one-dimensional configurations considered herein, we shall find it convenient to refer to the plastic strain component in either the direction of uniaxial stress or in the direction of uniaxial strain; in either case, this component of plastic strain will be denoted by ε_p. By invoking the condition of incompressibility of the plastic state, it can be shown that, for these one-dimensional configurations, one may write

$$\varepsilon_p = \frac{4}{3}\gamma \tag{3.4}$$

Therefore, when reference is made in the sequel to τ, γ, ε_p, σ, σ_1, ε, and ε_1, the definitions given above will be implied.

When plastic flow takes place by the slip process, the plastic strain rate $\dot{\gamma}$ is given by Eq. (2.1). In the developments that follow, no attempt will be made to distinguish between dislocation types, such as edge and screw dislocations, and their corresponding mean velocities. Instead, we shall treat the terms appearing on the right-hand side of Eq. (2.1) as suitable weighted averages over the various dislocation types.

Figure 1 illustrates some of the typical features of plastic flow in metals for a wide range of strain rates. In this figure a plot of $\dot{\gamma}$ versus τ for a fixed value of the plastic strain γ is depicted for an arbitrary material. For purposes of comparison, the curve corresponding to the simple elastic-plastic model has been included. The figure shows the various regions of mechanical response and cites the dislocation mechanism which is rate-controlling in each region. For

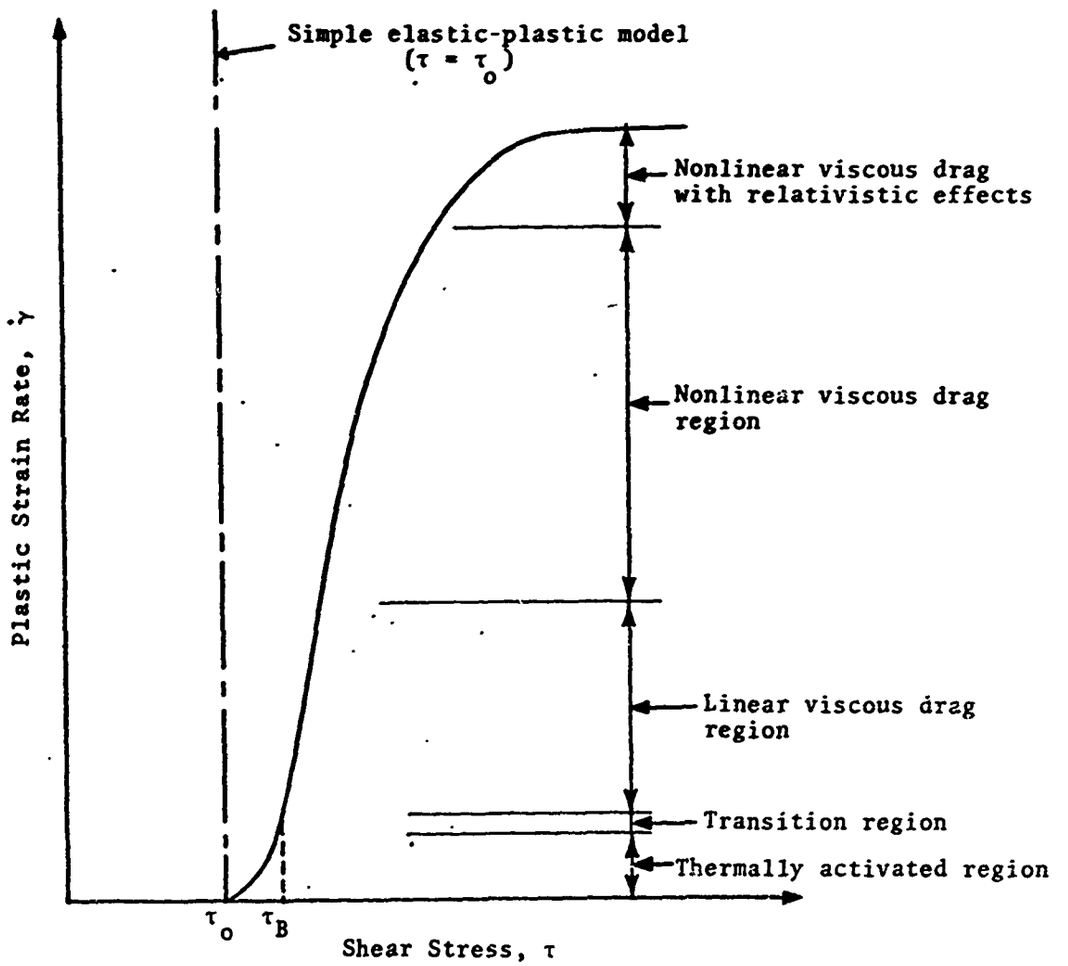

Figure 1. Dependence of the plastic strain rate on the applied shear stress for constant plastic strain.

shear stresses less than the quasi-static yield stress τ_o, there is no plastic flow and the response is purely elastic. At very small strain rates, where rate effects are insignificant, the stress-strain relationship depends primarily on the strain-hardening characteristics of the metal. For intermediate strain rates, the rate-controlling mechanism is thermal activation; it is in this region where one typically finds that $\tau \sim \log(\dot{\gamma})$. As the strain rate is increased, the so-called back stress τ_B is reached, above which it appears that viscous drag controls the plastic flow process. As the shear stress τ is further increased, the plastic strain rate eventually begins to approach a limiting value due to the influence of relativistic effects, which place an upper bound on the maximum velocity at which a dislocation can travel.*

B. Mean Velocity of Mobile Dislocations

For a deformation process such as we are considering here, an expression for the mean velocity v, appearing in Eq. (2.1), can be derived in the following manner: suppose that the average dislocation travels a path of length L in time t, and that there are m types of obstacles, such as immobilized dislocations, impurities, etc., distributed in some manner along this path. The number of obstacles of type i in the interval L is

$$n_i = \frac{L}{\ell_i} \tag{3.5}$$

*It should, however, be noted that considerable uncertainty still remains regarding the dislocation mechanisms and the shape of the curve in Figure 1 for strain rates above the linear viscous drag region. Because of the limitations on present experimental techniques, measurements of dislocation velocities have not been made for velocities greater than about one-half the shear wave velocity (see Ref. 13), and it is not at all clear what the maximum dislocation velocity is.

where ℓ_i is the mean interval between obstacles of type i. The time t required for the mobile dislocation to cover the distance L is the sum of the activation time t_a and the glide time t_g:

1. The activation time is the time that elapses while the dislocation waits to be thermally activated over each of the obstacles. This is given by the expression

$$t_a = \sum_{i=1}^{m} \frac{n_i}{\omega_i} \exp\left(\frac{H_i}{kT}\right) \tag{3.6}$$

where ω_i denotes a vibration frequency which depends on the nature of the obstacle, H_i is the activation energy corresponding to the ith type of obstacle, k is the Boltzmann constant, and T is the temperature.

2. The glide time is the time required for the dislocation to travel between the obstacles over the distance L. After the dislocation has been thermally activated over an obstacle, it very rapidly accelerates to some high steady-state glide velocity u_g. If the acceleration time is neglected,* the glide time can be expressed in the form**

$$t_g = \frac{L}{|u_g|} \tag{3.7}$$

*As Dorn pointed out,[13] dislocations can accelerate to extremely high velocities for moderate shear stresses in less than 10^{-11} sec. The neglect of acceleration time appears, therefore, to be justified.

**The absolute value sign is introduced to ensure that t_g will be a positive quantity regardless of the sign of u_g.

The mean velocity of the dislocation over the distance L is, by definition, given by the following expression,

$$v = \frac{L}{t_a + t_g} \tag{3.8}$$

Upon combining this equation with Eqs. (3.5), (3.6), and (3.7), we reach the result

$$v = \frac{u_g}{1 + |u_g| \sum_{i=1}^{m} \frac{1}{\ell_i \omega_i} \exp\left(\frac{H_i}{kT}\right)} \tag{3.9}$$

At a fixed temperature, there is evidence that one type of short-range obstacle is usually rate-controlling when thermal activation is the dominant mode of plastic flow. Then, with m=1 and $L=\ell_1$, Eq. (3.9) reduces to the following form:

$$v = \frac{u_g}{1 + \frac{|u_g|}{L\omega} \exp\left(\frac{H}{kT}\right)} \tag{3.10}$$

which forms a very important part of the analysis that follows in the sequel. If the short-range obstacles to dislocation motion are not significantly affected by straining, the distance L can be taken as constant in the above expression.

C. The Mobile Dislocation Density

An inspection of Eq. (2.1) will reveal that it is the density of the mobile dislocations that is required in formulating the constitutive equation. Unfortunately, present

experimental methods cannot provide any direct insight into the dependence of the mobile dislocation density on the deformation state. Current techniques for examining dislocation substructures with electron microscopes reveal, at best, only the total dislocation density. If one attempts to develop a constitutive equation for plastic response by starting from Eq. (2.1), it thus becomes necessary to make speculations regarding the mobile dislocation density. The basic lack of understanding of this all important component of the governing equation for plastic flow is so severe that it ranges from the one extreme of considering all dislocations mobile to the other extreme of assigning no importance at all to this parameter.[27] Several other investigators[15,16] have assumed that the mobile dislocation density, N_m, is some fixed fraction, f, of the instantaneous total dislocation density, N, while others have assumed that N_m remains fixed in magnitude throughout the entire deformation.[14] Regardless of the approach adopted, considerable guesswork is unavoidable. As Dorn and his co-workers have noted,[13] the magnitude of the mobile dislocation density, especially under dynamic conditions, is still open to considerable question.

From the standpoint of dislocation theory, it seems likely that, under rapid dynamic loading conditions, the mobile dislocation density depends on the excess of the dynamic flow stress over the quasi-static flow stress, as well as on the plastic strain. However, for simplicity, we shall restrict N_m here to depend only on the plastic strain ε_p.

In view of the existing uncertainty in the mobile dislocation density, the present approach will be to postulate a seemingly reasonable functional form for the mobile dislocation density, N_m, instead of attempting to derive an expression for it, as some have done by starting from some highly simplified models of the complex multiplication and annihila-

tion process.[28,29] Nonetheless, it should be kept in mind that these models indicate that, during initial plastic straining, the mobile dislocation density initially increases with plastic strain, reaches a maximum, and then decreases with further increases in the plastic strain, asymptotically approaching a saturated value. A functional form for N_m which exhibits these general features and has been adopted in the present work is

$$N_m = N_{m\infty} + (N_{mo} - N_{m\infty} + M_1\varepsilon_p^2) \exp(-A_1\varepsilon_p) \qquad (3.11)$$

In this expression, N_{mo} denotes the initial mobile dislocation density; $N_{m\infty}$ is the saturation value of the mobile dislocation density; M_1 is a multiplication coefficient, and A_1 is an annihilation coefficient.

Unfortunately, it is not possible to experimentally validate the plausibility of the functional form for N_m adopted above inasmuch as there are no experimental techniques at the present time for determining mobile dislocation densities. Because of this, the coefficients which appear in Eq. (3.11) cannot be evaluated directly from dislocation density measurements; it becomes necessary to resort to some other (indirect) technique for evaluating these coefficients and, for this purpose, plastic wave profiles have been utilized. This approach will be described in detail in Sec. IV C.

D. Decomposition of the Applied Shear Stress

The notion of decomposing the applied shear stress τ into a thermal component τ^*, which depends on the temperature T and the plastic strain rate, $\dot{\gamma}$, and an athermal component τ_μ, which depends on the temperature only through the shear modulus μ, was apparently first suggested by Seeger.[30] Accord-

ing to this view, τ, which represents the shear stress in the slip plane and along the slip direction, may be written in the following form:[31]

$$\tau = \tau_\mu + \tau^* \tag{3.12}$$

Physically, τ^* can be thought of as that part of the shear stress τ which is assisted by thermal vibrations in activating dislocations past short-range obstacles. On the other hand, the athermal component τ_μ is associated with long-range obstacles which require such large energies to overcome that thermal vibrations are unimportant.

The form of stress decomposition suggested by Seeger, and given in Eq. (3.12) above, is valid only for low-to-moderate strain rates, since no provision for viscous drag effects was made. At high strain rates, which are of special interest to the present inquiry, provision must be made in the stress decomposition for a viscous drag contribution to the total stress. It has been shown by Kumar, Hauser and Dorn[32] that the stress decomposition appropriate for high strain-rate conditions is given by

$$\tau = \tau_\mu + \tau^* + \tau_D \tag{3.13}$$

where τ_D is the part of the total stress that arises from dislocation drag, and the other symbols have the same meaning as before. When the applied stress is so large that viscous drag is the rate-controlling mechanism, the time spent by the dislocation while waiting to be thermally activated over the obstacle is very small. In this case, the component of the stress due to short-range barriers, τ^*, is not significantly reduced by thermal activation. Then, as shown in Ref. 32, the decomposition given in Eq. (3.13) can be placed in the form

$$\tau = \tau_B + \tau_D \tag{3.14}$$

where the back stress τ_B is defined as the sum of the athermal stress component τ_μ and the thermal component τ^* evaluated at $0^\circ K$.

E. Athermal Stress Component

The athermal stress τ_μ represents the component of the applied stress τ necessary to overcome the resistance of long-range obstacles to dislocation motion. Long-range obstacles are sufficiently distant from the dislocation that thermal activation plays no role in aiding the dislocation to overcome them. The nature of these long-range obstacles forms the basis of the various theories of strain hardening. Without exception, all of the present theories of strain hardening lead to the same expression for the athermal stress τ_μ, namely,*

$$\tau_\mu = \alpha b \mu \sqrt{N} \tag{3.15}$$

where α is a dimensionless constant whose magnitude is between 0.2-0.6, b is the Burgers vector, μ represents the shear modulus, and N is the total dislocation density. Although τ_μ is termed the athermal stress, it exhibits a small dependence on temperature through the shear modulus μ.

The relationship given in Eq. (3.15) has been experimentally verified for initial loading of a large class of metals under quasi-static and low strain rate conditions; it

*A survey of the various theories of work hardening can be found in Ref. 33. The dependence of τ_μ on N is also discussed at length in Ref. 34.

is not known, however, if such a relation is valid for initial loading at high strain rates during plastic wave propagation.*

When unloading phenomena are a critical aspect of plastic wave propagation analyses - as they are when thin pulse attenuation and spall are of importance - there is a critical need for a theory of strain hardening relating τ_μ and γ which can realistically describe reverse plastic deformation from a prestrained state as well as initial plastic deformation from an unstrained state. The need for such a theory arises because the majority of metals exhibit a reduction in the flow stress and a temporary increase in the rate of strain hardening when the material undergoes reverse plastic strain from an initially prestrained state. A metal exhibiting such a property is said to have a Bauschinger effect. To account for such an effect in the present constitutive model, the athermal stress τ_μ is taken to have a different dependence on plastic strain during initial loading than on reverse loading. In this section, we shall confine our attention to initial plastic loading and reserve the discussion of reverse loading phenomena for Sec. III.I.

As noted above, considerable speculation is required regarding the dependence of the athermal stress τ_μ on the plastic strain γ at the high strain rates of interest to the present study. Until evidence to the contrary becomes available,

---

* In a recent survey article, Dorn et al. have stated[13] "Before much progress can be made in using dislocation theory for the determination of plastic wave propagation effects, it will be necessary to ascertain how the values of τ_μ, ... depend on strain.... At present, the only recourse is the experimental evaluation of the needed relationships and these are somewhat questionable because it is usually assumed that they are independent of the stress."

it will be assumed that the dependence given in Eq. (3.15), which has been confirmed for low strain rate plastic deformation, is also valid at high strain rates for initial loading. A relationship between the athermal stress τ_μ and the plastic strain γ may then be obtained if the dependence of the total dislocation density N on the plastic strain γ can be determined.

Considerable insight into the dependence of the dislocation density on plastic strain has been gained through experimental examination of metal substructures with electron microscopes. Results have been reported for several metals, mostly high-purity, for straining under quasi-static conditions.

More important to the present study, however, is the dependence of the dislocation structure on straining under shock loading conditions. In this connection, only two experimental studies pertaining to dislocation structure could be traced. In the first of these, Gilbert, Wilcox and Hahn have studied the effect of strain rate on the dislocation density-plastic strain relationship in molybdenum.[35] In this work, dislocation densities were measured at various strains for strain rates of 2×10^{-5} sec^{-1} and $2\times10^{3}sec^{-1}$. The results obtained indicated that the increase in strain rate by a factor of 10^8 produced only a slight increase in the dislocation density. Similar results were recently reported by Kaybyshev, et al. for copper.[22]

From the results for copper and molybdenum described above, it appears that the effect of strain rate on the dislocation multiplication process is quite small. The increase in strain rate apparently causes the mean dislocation velocity to increase rather than the dislocation density.

Bearing the preceding comments in mind, we shall assume that the total dislocation density depends on the plastic strain in the following manner:

$$N = N_o + C_1(\gamma)^m \tag{3.16}$$

where N_o denotes the initial dislocation density and C_1, m are coefficients. This expression may be rewritten in the form*

$$N = N_o + C_2(\varepsilon_p)^m \tag{3.17}$$

when use is made of Eq. (3.4), and the coefficient C_2 is defined as $C_2 = (3/4)^m C_1$.

Upon combining Eqs. (3.15) and (3/17), we reach the result

$$\tau_\mu = \tau_o\sqrt{1+a(\varepsilon_p)^m} \tag{3.18}$$

where we have set

$$\tau_o = \alpha b\mu\sqrt{N_o} \tag{3.19}$$

$$a = C_2/N_o$$

Equation (3.18) gives the expression for the athermal stress τ_μ during initial loading which will be adopted in the present work. An inspection of this equation reveals that there are three constants which must be evaluated for a given material, namely, τ_o, a, and m. The procedure for evaluating these constants for a specific material will be described later in Sec. IV.A.1 of this report.

F. Thermally Activated Stress Component

Under certain conditions, the applied stress alone may not be sufficient to drive the dislocations past the short-

*Expressions having the form of Eq. (3.17) have been used by others (e.g., see Refs. 35 and 36) to correlate dislocation density-plastic strain data.

range obstacles, such as impurities, immobilized dislocations, etc., that tend to arrest their motion. If the obstacles are localized, large random vibrations stemming from thermal excitation of the crystal lattice may assist the dislocations in overcoming these obstacles. When this occurs, the rate at which the dislocations are able to surmount the obstacles governs the character of the plastic flow, and the deformation process is said to be thermally activated.

It should be noted at this point, however, that it is not at all clear that it is even necessary to make provision for thermally activated processes in a constitutive equation designed primarily to treat plastic wave propagation, where the principal features of interest occur at strain rates considerably above that at which thermal activation ceases to be important. It is possibly important, nonetheless, for some metals and affects the interpretation of yield and strain-hardening experimental data.

The activation energy H_i, which appears in Eq. (3.6) given earlier, represents the energy due to thermally induced vibrations which is required to move the dislocation past the ith type of obstacle. Theoretical and experimental studies performed on a large class of metals indicate that the activation energy depends primarily on the thermal stress component τ^*.[37] On the basis of these observations, it appears that one may write with some degree of confidence that

$$H_i = H_i(\tau^*) \tag{3.20}$$

where the (unknown) function H_i is, of course, different for each type of short-range obstacle. As Conrad has noted,[31] the rate-controlling obstacle not only changes in a given material with temperature but it varies from one crystal class to another. At low temperatures ($T < 0.25\ T_m$), for example,

it appears that the most likely rate-controlling mechanisms are (1) the intersection of dislocations in fcc metals, (2) the inherent resistance of the crystal lattice (Peierls-Nabarro stress) in bcc metals, and (3) either cross-slip, the Peierls-Nabarro stress, or impurity atoms in hcp metals.[34] One cannot expect, therefore, that a specific form of H_i which is applicable to one crystal class will be generally applicable over a wide temperature range to a variety of metals from different crystal classes. Thus, any attempt to use a single expression that is not completely general to describe the activation energy for a group of metals having different crystal structures clearly involves some approximation.

The need for including more than one activation energy in the equation governing thermally activated flow is uncertain at this time and it has received little or no attention in the literature. For the majority of metals, it is usually found that at a fixed temperature the experimental data in the thermally activated region can be correlated quite well by assuming that only one type of obstacle governs the process,* and such a point of view will be adopted here. We shall, therefore, restrict the discussion which follows to showing how a simple, and in many ways typical, model for thermal activation can be incorporated into the proposed general framework. It is not to be inferred,however, that we are advocating the general use of the thermal activation model discussed below in constitutive model development; it is well known that many metals exhibit a more complex dependence of the activation energy H on the shear stress τ^* than that which is given below. Nevertheless, in most cases considerations similar to those given below would apply to models for other thermal activation mechanisms.

---

*In this connection Dorn has stated,[38] "... the strain rate for dislocation motion past a series of different kinds of obstacles depends essentially on the rate of nucleation past the most difficult surmountable obstacle."

In fcc metals such as aluminum and copper at low temperatures ($T < 0.25\ T_m$), Conrad has concluded that it is the intersection of forest dislocations which controls the thermally activated process.[34] For such an intersection mechanism, Seeger has developed a model for describing the thermally activated process.[30] In this model the vibration frequency ω appearing in Eq. (3.10) is given by

$$\omega = \frac{\nu_D b}{L} \tag{3.21}$$

where ν_D denotes the Debye frequency, b is the Burgers vector, and L is the mean spacing of the forest dislocations being intersected. The energy H which must be supplied by a vibrational fluctuation in order to complete the intersection is given in the Seeger model by

$$H = H_o - v^*\tau^* \tag{3.22}$$

where H_o is the total energy necessary to form a jog on the intersecting dislocation, v^* is an activation volume, and the thermally activated stress

$$\tau^* = \tau - \tau_\mu \tag{3.23}$$

is interpreted as the net stress available for assisting the intersection after the long-range barriers have been overcome. The stress decomposition appearing in Eq. (3.23) is not as general, however, as that adopted in the present formulation, namely,

$$\tau = \tau_\mu + \tau^* + \tau_D \tag{3.24}$$

but this is of no consequence to the theory of thermal activa-

tion which is based generally on experiments at strain rates where τ_D is negligible compared with τ_μ. In the constitutive model, however, the activation energy is related to the mean dislocation velocity - and hence to the strain rate - through Eq. (3.10), where u_g, the glide velocity, is a function of τ_D and vanishes when $\tau_D = 0$. Therefore, in this general context, it may be necessary to retain the general stress decomposition given in Eq. (3.24) in order to provide for a nonzero (but perhaps small) viscous drag component τ_D in the thermal activation process. The need for using the general stress decomposition becomes even more acute in the transition region where the rate-controlling mechanism is shifting from thermal activation to viscous drag (see Fig. 1). In this region τ_D and τ^* are of the same order of magnitude and the neglect of τ_D, implied by Eq. (3.23), is clearly not justified.

G. Viscous Drag Stress Component

It is now generally accepted that when the applied stress τ becomes greater than the back stress τ_B, dislocations can move along glide planes past short-range obstacles without assistance from thermal activation. A considerable amount of experimental evidence has been accumulated during the past several years which indicates that the mechanisms governing the dislocation motion under such conditions are viscous in nature. Although the viscous-like mechanisms are rate-controlling at high strain rates, they are also operative - and dissipate energy - at the lower strain rates where thermal activation is rate-controlling; their influence at these low strain rates, however, is generally small compared with thermal activation.

It is convenient at this point to introduce the term "switch-over strain rate," which is defined as the (nominal) strain rate at which the rate-controlling mechanism changes from thermal activation to viscous drag as the applied stress

is increased. For a relatively limited range of strain rates above the switch-over strain rate, a linear dependence of the applied stress on the plastic strain rate has been experimentally observed in a number of metals.[13,32,39] The results of these studies can be correlated by an equation of the form

$$\tau - \tau_B = \eta \dot{\varepsilon}_p \tag{3.25}$$

where η is a coefficient which exhibits a slight dependence on temperature. The form of Eq. (3.25) indicates that a viscous-like mechanism is operative. Consequently, the dislocation motion must be damped by some energy absorbing (dissipative) mechanism. Similar damping of dislocation motion has been observed by a number of investigators. Some of these have used ultrasonic methods and others have made direct dislocation mobility measurements. The results of such investigations are typically discussed in terms of a drag coefficient B, defined by the equation

$$F = Bu_g \tag{3.26}$$

where F denotes the net force on the dislocation, and u_g is the dislocation glide velocity. During viscous motion it can be shown that the net force F on the dislocation is given by

$$F = b\tau_D \tag{3.27}$$

where τ_D is the viscous drag component of the applied shear stress. Combining Eqs. (3.26) and (3.27) leads to the following result,

$$\tau_D b = Bu_g \tag{3.28}$$

which is compatible with Eq. (3.25) - inferred from macroscopic measurements - if we make the identification

$$\eta = \frac{3}{4}\frac{B}{b^2 N_m} \tag{3.29}$$

It has therefore been confirmed by a number of different experimental approaches that the viscous drag on dislocations is linear for strain rates above, but of the same order of magnitude as, the switch-over strain rate.

On the contrary, very little is presently known regarding the rate-controlling dislocation mechanisms at considerably higher strain rates, say 10^4-10^7 sec^{-1}. This lack of understanding is due, in part, to the paucity of direct experimental data for metals deforming at strain rates considerably greater than the switch-over strain rate. It seems reasonable, however, to expect that as the strain rate (or dislocation velocity) is increased, the viscous drag stress τ_D will begin to exhibit a nonlinear dependence on the dislocation velocity. Therefore, in the present work we shall generalize the result given in Eq. (3.28) to include nonlinear viscous effects in the following manner,

$$B\Phi(\tau_D) = B^* u_g \tag{3.30}$$

where Φ is a nonlinear function of τ_D, and B^* is the generalized drag coefficient.

As the stress is increased, it seems likely that the dislocation will eventually reach a limiting velocity. As a number of investigators have shown,[41-43] a screw dislocation, for instance, cannot travel faster than the elastic shear wave velocity due to limitations imposed by relativistic considerations. Therefore, to make provision for relativistic effects at high dislocation velocities, the generalized drag coefficient B^* appearing in Eq. (3.30) will be taken in the form†

†This approach to including relativistic effects was first suggested by Taylor[23]. For different approaches, see Refs. 40 and 44.

$$B^* = \frac{B}{\sqrt{1 - u_g^2/u_\infty^2}} \tag{3.31}$$

where B denotes, as before, the usual (linear) drag coefficient, and u_∞ is the limiting dislocation velocity. In the present work, we shall assume that u_∞ is equal to the elastic shear wave velocity, C_s.

Upon combining Eqs. (3.30) and (3.31), we obtain the expression

$$u_g = \frac{\Phi(\tau_D)}{\sqrt{1 + \frac{\Phi^2(\tau_D)}{C_s^2}}} \tag{3.32}$$

which relates the dislocation glide velocity u_g to the drag stress τ_D for a specified function Φ. In the work carried out to date, we have found that a functional dependence of the form

$$\Phi = \alpha_1 \tau_D + \alpha_2 \tau_D^2 \tag{3.33}$$

appears to be adequate. In this expression, α_1 and α_2 denote constants to be evaluated from experimental data. Note that if we set

$$\alpha_1 = \frac{b}{B} \quad , \tag{3.34}$$

Equation (3.32) includes the usual (linear) drag expression given in Eq. (3.28) as a limiting case when τ_D becomes small.

H. Synthesis of the Constitutive Equation

In the foregoing sections, an attempt has been made to review and discuss the various aspects of dislocation theory

which have particular significance to plastic wave propagation. Against this background, models of the necessary component mechanisms, developed and adopted in the present study , were presented. In this section, these notions will be synthesized to form a constitutive equation. In later sections, procedures for evaluating the coefficients in this equation will be illustrated, and theoretical results based on the use of this constitutive equation will be compared with experimental observations.

As pointed out earlier, the present constitutive model is designed to treat the slip mode of plastic deformation and, when plastic flow occurs by this mode, the plastic strain rate is defined by the equation

$$\dot{\varepsilon}_p = \frac{4}{3} bN_m v \tag{3.35}$$

Expressions for N_m and v, based on models of the various dislocation mechanism developed in the preceding sections, will now be combined according to Eq. (3.35) to form the constitutive equation. In order to avoid having the following discussion become overly complicated, we shall restrict attention to initial loading at a fixed temperature.

The basic formulation is based on the concept that the applied stress τ may be decomposed in the following manner:

$$\tau = \tau_\mu + \tau^* + \tau_D \tag{3.36}$$

where τ^* is the thermal component, τ_D is the viscous drag component and τ_μ is the athermal component. The athermal component is given by the equation

$$\tau_\mu = \tau_o \sqrt{1 + a(\varepsilon_p)^m} \tag{3.37}$$

The specific form adopted for the mobile dislocation density N_m is

$$N_m = N_{m\infty} + (N_{mo} - N_{m\infty} + M_1\varepsilon_p^2)\exp(-A_1\varepsilon_p) \qquad (3.38)$$

For the mean dislocation velocity, we have derived the following result[†]

$$v = \frac{u_g}{1 + \frac{|u_g|}{L\omega}\exp(H/kT)} \qquad (3.39)$$

Upon combining the preceding equation with the expression for the activation energy in the Seeger model for dislocation intersection, namely,

$$H = H_o - v^*\tau^* \qquad (3.40)$$

we reach the result

$$v = \frac{u_g}{1 + \beta|u_g|\exp\left(-\frac{v^*\tau^*}{kT}\right)} \qquad (3.41)$$

where we have set:

$$\beta = (L\omega)^{-1}\exp(H_o/kT) \qquad (3.42)$$

Finally, the glide velocity u_g is taken to have the form

$$u_g = \frac{\Phi}{\sqrt{1 + \Phi^2/C_s^2}} \qquad (3.43)$$

where the function Φ is given by

[†]It has been assumed here that at a fixed temperature, only one type of short-range obstacle dominates the deformation when thermal activation is the rate-controlling mechanism.

$$\Phi = \alpha_1 \tau_D + \alpha_2 \tau_D^2 \tag{3.44}$$

The preceding results may now be combined according to Eq. (3.35) to yield the following expression for the plastic strain rate:

$$\dot{\varepsilon}_p = \frac{4}{3} \frac{b u_g [N_{m\infty} + (N_{mo} - N_{m\infty} + M_1 \varepsilon_p^2) \exp(-A_1 \varepsilon_p)]}{1 + \beta |u_g| \exp(-\frac{v^* \tau^*}{kT})} \tag{3.45}$$

where the general stress decomposition, Eq. (3.36), is implicit, and u_g is defined according to Eq. (3.43) and (3.44). Equation (3.45) gives the form of the constitutive equation developed in the present work for initial loading. An inspection of this equation reveals that it is of the general form

$$\dot{\varepsilon}_p = \xi(\varepsilon_p, \tau) \tag{3.46}$$

where the function ξ depends in a nonlinear manner on both ε_p and τ.

For those metals in which thermal activation does not play an important role at a given temperature, the thermal component τ^* may be neglected. When this is the case, the general constitutive equation, Eq. (3.45), reduces to the following simplified form†

$$\dot{\varepsilon}_p = \frac{4}{3} \frac{b \Phi [N_{m\infty} + (N_{mo} - N_{m\infty} + M_1 \varepsilon_p^2) \exp(-A_1 \varepsilon_p)]}{\sqrt{1 + \Phi^2 / C_s^2}} \tag{3.47}$$

†To effect this simplification, the exponential function in the denominator of Eq.(3.45) must be replaced by twice the hyperbolic sine. This will account for the effect of thermal fluctuations which oppose the applied stress at small values of τ^* (see Ref. 45).

where now, since τ^* is being neglected, we have $\tau_D = \tau - \tau_\mu$; therefore,

$$\Phi = \alpha_1(\tau - \tau_\mu) + \alpha_2(\tau - \tau_\mu)^2 \qquad (3.48)$$

with τ_μ defined according to Eq. (3.37). The constitutive equation given in Eq. (3.47) has ten coefficients, namely, $a, m, \tau_o, A_1, M_1, N_{mo}, N_{m\infty}, \alpha_1, \alpha_2$ and C_s, which require evaluation for a given material. We shall describe in Section IV of this report the procedures which have been used to evaluate these coefficients for 6061-T6 aluminum.

I. Reversed Straining from a Prestrained Plastic State for Metals which Exhibit a Bauschinger Effect

It has been found experimentally that, under quasi-static loading conditions, many metals exhibit mechanical properties during reverse straining from plastically prestrained states which differ significantly from those observed during initial loading. For such materials, the shear stress required to initiate plastic flow during reverse straining is smaller than the flow stress at the end of the initial loading process; in addition, the strain hardening rate during reverse straining typically has a temporary increase over that present during initial loading. Metals which exhibit such characteristics follow anisotropic strain hardening laws and are said to have a Bauschinger effect.

A number of recent investigations[7,8,11] indicate that metals which show a Bauschinger effect under quasi-static conditions also exhibit such an effect under rapid dynamic loading conditions, such as occur during elastic-plastic wave propagation. Other studies have shown that the Bauschinger effect can exert significant influence on the shape of the release wave and, consequently, on stress wave attenuation.[12] When reverse plastic straining occurs under rapid dynamic conditions--such as in the release wave during plastic wave

propagation--the presence of strain rate effects and a large hydrostatic component of stress can add further complication to the reversed straining process.

Unfortunately, there is no experimental technique at the present time whereby the separate effects of strain rate and strain hardening (Bauschinger effect) can be isolated in the release portion of a plastic wave. Despite the fact that some insight into the separate influences of these effects can be obtained in the loading portion of a plastic wave through elastic precursor decay and steady wave analysis, such information is not available for the release portion of the wave. This results from the fact that the release wave is dispersive (and therefore never attains a steady state) and the amplitude of the elastic portion of the release wave, which exhibits decay in a manner similar to the precursor, is extremely difficult to measure with any accuracy experimentally. Thus, at the present time, there is no satisfactory experimental method by which the separate influences of strain hardening and strain rate effects on the release wave can be determined. Only one investigation (Ref. 46) could be traced which even remotely touched on this subject but, as the authors cautioned, the results and conclusion given are not applicable to plastic wave propagation phenomena where short recovery times are involved.

Although a few attempts have been made to develop simple dislocation models to explain the Bauschinger effect during quasi-static unloading, it still remains as one of the least understood areas of metal plasticity.* The task becomes even more complicated for rapid dynamic unloading conditions where strain rate effects may be present. In view of this, no attempt

*For a discussion of the Bauschinger effect from the micromechanical viewpoint see, for example, the paper by Mott.(47) A recent attempt to develop a dislocation model for describing the Bauschinger effect can be found in Reference 48.

will be made here to construct a micromechanical model for the reverse loading process during plastic wave propagation; instead, a simple phenomenological model will be developed which reflects a number of salient features observed experimentally in many metals which exhibit anisotropic strain hardening.* Other phenomenological models for describing the Bauschinger effect have been proposed by Duwez,[49] Mróz,[50] Como and D'Agostino,[51] and Barker.[11]

In the following portions of this section, the approaches adopted in the present work for treating the rate-independent shear stress τ_μ, the mobile dislocation density N_m, and the viscous drag coefficients α_1 and α_2 during a reversed straining process from a prestrained state will be described.

The treatment of the rate-independent shear stress component τ_μ, although phenomenological, is designed to reflect the following salient features characteristic of the quasi-static deformation of many metals having a Bauschinger effect:

1. Upon reverse straining from a plastically prestrained state plastic flow begins at a shear stress whose magnitude is smaller than that of the flow shear stress at the end of the initial loading process.
2. After reversed plastic flow has been initiated, the rate of strain hardening is much more rapid than during the initial loading process.
3. In some metals, such as aluminum and copper, the reverse strain hardening path rapidly approaches the hardening path that would have been followed if the material obeyed an isotropic hardening law.

*The treatment of isotropic strain hardening is straightforward and will not be discussed here.

4. For metals which do not have a sharp yield point - which is the case with most metals of practical interest - the following continuity condition between the elastic and plastic states

$$\frac{d\tau_\mu}{d\varepsilon_p} = \infty \tag{3.49}$$

holds at the onset of initial plastic flow, as well as at the initiation of reversed plastic flow from a prestrained state.[52]

In order to elucidate the present treatment of the shear stress component τ_μ in greater detail, let us turn to Fig. 2, where the dependence of τ_μ on ε_p according to the present model is schematically depicted. Initial plastic straining occurs along the path a-b after the applied shear stress exceeds the initial yield stress τ_o. The strain hardening path a-b is described by some appropriate functional dependence of the form

$$\tau_\mu = f(\varepsilon_p) \tag{3.50}$$

where the function f is taken in the present work to have the specific form

$$f(\varepsilon_p) = \tau_o \sqrt{1 + a(\varepsilon_p)^m} \tag{3.51}$$

in accordance with Eq. (3.18). Point b represents the final state reached during the initial loading process and, for future reference, we will designate the plastic strain and corresponding shear stress at this point, respectively by ε_p^* and τ_μ^*. Between points b and c, elastic unloading takes place which consists of a decrease in shear stress but no change in the plastic strain. At point c, the shear stress τ_μ has been completely unloaded. If the applied shear stress is now reversed, elastic loading takes place between c and d. At d,

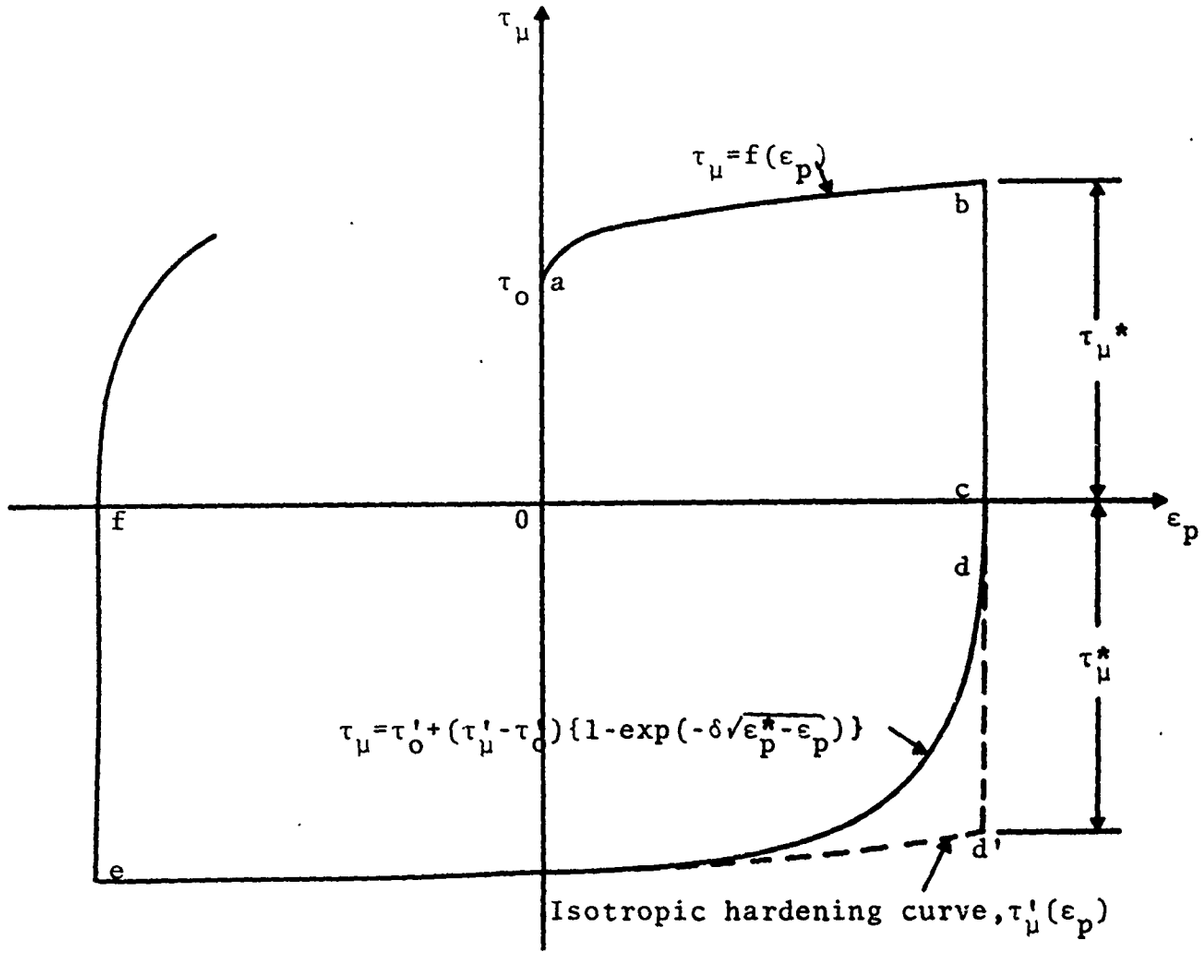

Figure 2. The dependence of τ_μ on ε_p according to the present model for a material which exhibits a Bauschinger effect.

the material yields and then subsequently exhibits a rapid rate of strain hardening, as shown. The following functional form for τ_μ, which exhibits the four general features of the reverse straining process enumerated above, has been adopted in this study to describe the strain hardening path from d to e:

$$\tau_\mu = \tau'_o + (\tau'_\mu - \tau'_o)\left\{1-\exp\left(-\delta\sqrt{\varepsilon^*_p-\varepsilon_p}\right)\right\},\ \tau_\mu \leq \tau'_o \qquad (3.52)$$

Here, τ'_o denotes shear stress at which yield first occurs on reverse straining, δ is a coefficient which governs the rate of strain hardening,[†] and τ'_μ, defined by the expression

$$\tau'_\mu = -\tau_o\sqrt{1+a(2\varepsilon^*_p-\varepsilon_p)^m} \qquad (3.53)$$

describes the strain hardening path that would be followed during the reverse straining process if the material obeyed an isotropic hardening law. Therefore, once the parameters a, m, and τ_o have been determined for the initial loading path, τ'_μ is completely specified; the additional parameters that must be evaluated to complete the specification of this model are τ'_o and δ. The evaluation of these parameters from quasi-static experimental data is described in Section IV.A.2 for 6061-T6 aluminum.[††] An alternative model for incorporating a Bauschinger effect into the general constitutive framework has also been developed, and is discussed in the Appendix.

[†]Although δ and τ'_o are treated as constants in the present model, they can be expected to depend in general on the plastic prestrain.

[††]In using quasi-static data to evaluate a strain hardening model for use under dynamic conditions, it must be assumed that the strain-rate effect influences only the dynamic flow stress but not the actual quasi-static flow stress; clearly such an approach involves some degree of approximation. Moreover, the identification of τ_μ with the quasi-static flow stress is permissible only when the thermal component of the shear stress, τ^*, is negligible compared with τ_μ.

The mobile dislocation density during the reversed straining process is described in the present model by the following expression

$$N_m = N'_{m\infty} + (N_{m*} - N'_{m\infty}) \exp(-A_2 \bar{\varepsilon}_p^2) \qquad (3.54)$$

In the above equation, $\bar{\varepsilon}_p$ denotes the reversed plastic strain, defined as

$$\bar{\varepsilon}_p = \varepsilon_p^* - \varepsilon_p \quad ; \qquad (3.55)$$

N_{m*} is the magnitude of the mobile dislocation density at the end of the initial loading process; A_2 and $N'_{m\infty}$ are coefficients which must be evaluated from experimental data. The functional form for N_m given above maintains continuity in the mobile dislocation density during reversal of the shear stress†, and allows for saturation of the mobile dislocation density at a finite, non-zero value.

Turning finally to the viscous drag shear stress component, τ_D, it is assumed that, during a reversed straining process from a prestrained plastic state, the glide velocity u is related to τ_D in the same manner as that adopted for the initial straining process (see Eqs. (3.32) and (3.33). Moreover, the viscous drag coefficients α_1 and α_2 are taken to have the same values on reversed straining as on initial straining. While this approach assumes that the u_g-τ_D relationship is unaffected by plastic prestrain, it does not, however, imply that the τ-$\dot{\varepsilon}_p$ relationship is likewise unaffected; even when the u_g-τ_D relationship is the

†The continuity assumption, made primarily for convenience, is perhaps questionable from the standpoint of dislocation theory. If one considers that the dislocations which have been immobilized by piling up against obstacles in the microstructure may be remobilized when the direction of the applied shear stress is reversed, it seems likely that a discontinuity will exist in the mobile dislocation density during shear stress reversal.

same, changes in the mobile dislocation density between initial and reversed straining lead to differences in the τ-$\dot{\varepsilon}_p$ relationship.

IV. EVALUATION OF THE COEFFICIENTS FOR 6061-T6 ALUMINUM

In this section, the constitutive equation developed in the preceding sections will be applied to 6061-T6 aluminum at room temperature. The constants in the constitutive equation will be evaluated from the extensive experimental data available for this metal, in particular quasi-static stress-strain curves, elastic precursor decay data and plastic wave profiles.

We consider first a simplification which can be made in the general constitutive equation. Turning to Fig. 3, a plot of some experimental data for 6061-T6 aluminum at room temperature, obtained by Isbell, et al.,[6] shows the effect on the compressive axial stress of changing the strain rate from 5×10^{-3} to 10^{3} sec^{-1}†. An inspection of this figure reveals that there is essentially no change in the stress for an increase in the strain rate of about a factor of 10^{6}; this clearly demonstrates that within this range of strain rates the material is strain-rate insensitive. It is in the range of strain rates from 10^{-3} to 10^{3} sec^{-1}, however, where one would normally expect thermal activation to be the rate-controlling mechanism; but, inasmuch as no rate sensitivity is observed, it appears that τ^* may be very small compared with τ_μ. This is further confirmed by noting in Fig. 3, that a change in the strain from plastic yield to 6% resulted in a substantial increase in the stress. The flow stress, therefore, appears to be dominated in this range of strain rates by the athermal component τ_μ. In view of this it appears that the thermally activated stress τ^* is very small compared with τ_μ and can be neglected, and we shall therefore adopt the simplified constitutive equation** given earlier in Eq. (3.47).

---

†The data shown in this figure were obtained under uniaxial stress conditions and are consistent with the data in Ref.53.

**Such a simplification is not likely to be possible at higher temperatures where the thermally activated component τ^* exerts more influence on the plastic flow process.

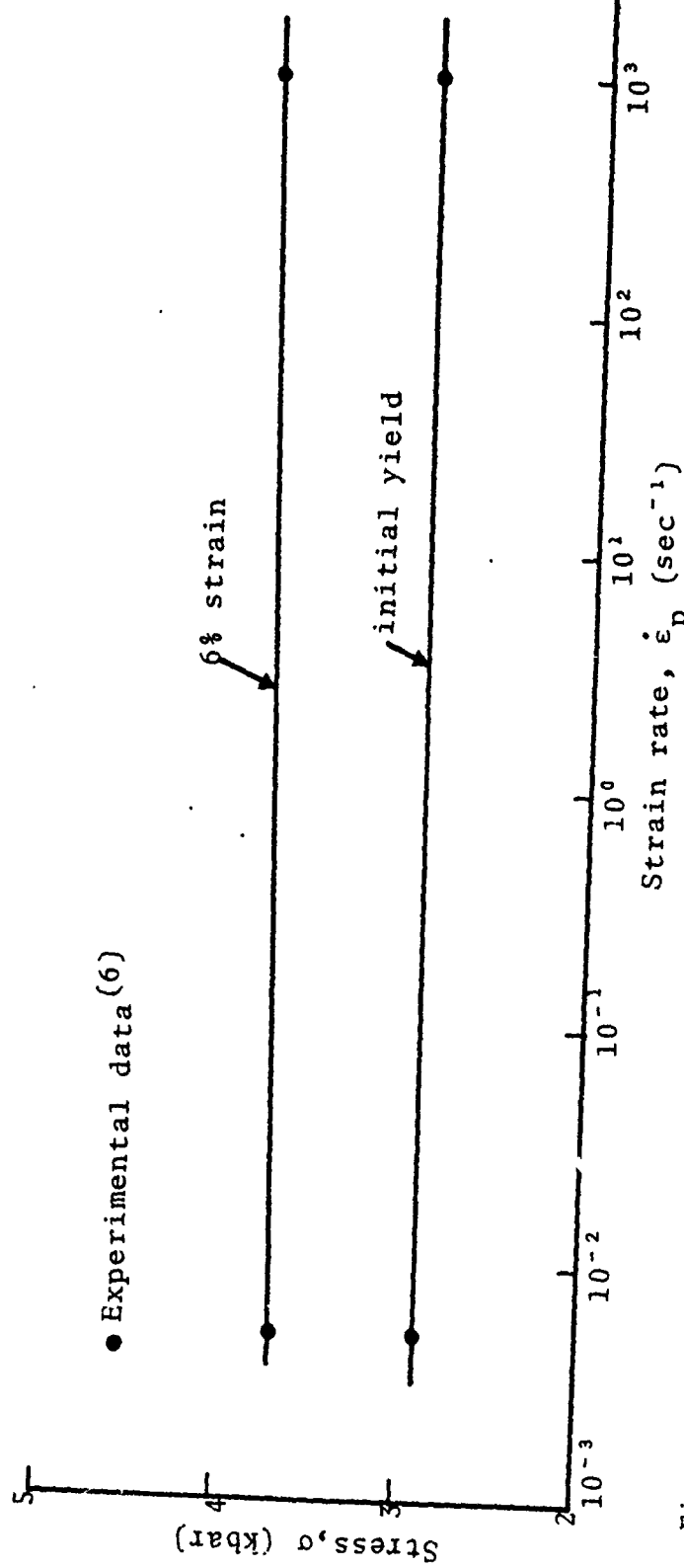

Figure 3. Dependence of the stress on the strain rate in 6061-T6 aluminum at room temperature.

A. Strain Hardening

When the shock loading of a metal is carried out under uniaxial strain conditions, attempts to make direct experimental measurement of the strain hardening characteristics are complicated by the presence of strain rate effects and rarefactions. Because of these apparently unavoidable features, there is, to date, no satisfactory technique for measuring in a direct manner the strain hardening properties of a metal in uniaxial strain during shock loading. Such data, if it could be obtained, would obviously be of interest to those concerned with developing constitutive models for plastic wave propagation in metals. In the absence of such data, it has been customary in the past to either neglect strain hardening effects altogether, or to construct hardening models for use in one-dimensional (uniaxial strain) codes from hardening data obtained from uniaxial stress tests carried out under quasi-static conditions. It has been recognized for some time, however, that shock loading produces a different amount of strain hardening in metals than quasi-static loading, when the two are compared on the basis of equal plastic strain.

When hardening data obtained from uniaxial stress tests are used to construct hardening models for uniaxial strain, it becomes necessary to invoke some assumptions regarding the general hardening law, so that the hardening characteristics measured in uniaxial stress can be transformed to those in the uniaxial strain configuration. For this purpose, some isotropic form of strain hardening, in which the radius of the yield surface increases with either the plastic work or the generalized plastic strain, has been adopted in most cases in the past. The required transformation of the strain hardening properties is then effected through a procedure originally due to Fowles.[54] The assumption of isotropic hardening, which is implicit in Fowles' procedure, provides considerable analytical and computational convenience. However, many (if not most)

metals exhibit to some degree a Bauschinger effect on reverse loading from a plastically prestrained state and when this is the case, the strain hardening is not of an isotropic nature. For such materials the procedure suggested by Fowles is not appropriate, and some other method for transforming the hardening data is required. The procedure adopted in the present work for this purpose is described in that which follows.

As noted earlier, it has been assumed that the major portion of the plastic flow occurs on those slip planes for which the resolved shear stress has its maximum value, regardless of whether the deformation occurs under conditions of uniaxial stress or uniaxial strain. Moreover, it will be assumed that an expression of the form

$$\tau = F(\gamma) \tag{4.1}$$

relates the maximum shear stress τ to the corresponding plastic strain γ in both the uniaxial stress and uniaxial strain configurations under quasi-static conditions. By making use of the result

$$\gamma = \frac{3}{4} \varepsilon_p \tag{4.2}$$

given earlier, Eq. (4.1) may be rewritten in the form

$$\tau = F(\varepsilon_p) \tag{4.3}$$

where ε_p may denote either the plastic strain component in the direction of the axial stress in a uniaxial stress configuration, or the plastic strain component in the direction of the only nonvanishing strain component in a uniaxial strain configuration. Thus, on the preceding assumption, the function F is identical in both the uniaxial stress and uniaxial strain configurations, and it may be determined for a particular material from quasi-static uniaxial stress data. In the case of 6061-T6 aluminum,

the athermal stress, τ_μ, may be equated to the applied flow stress τ for quasi-static loading at room temperature since rate effects can be neglected and τ^* is small compared with τ_μ. Therefore, under these conditions, Eq. (4.3) reduces to the expression

$$\tau_\mu = F(\varepsilon_p) \tag{4.4}$$

which will be used here to describe the strain hardening characteristics of 6061-T6 aluminum.

1. Initial Strain Hardening and the Coefficients a, m, and τ_o

The particular form of Eq. (4.4) adopted in the present work for initial plastic straining is, from Eq. (3.18),

$$\tau_\mu = \tau_o \sqrt{1+a(\varepsilon_p)^m} \tag{4.5}$$

where τ_o is the initial yield stress, and a, m are coefficients. In the evaluation of τ_o, a and m, the experimental results of Maiden and Green[55] have been used. These data, reported in terms of engineering definitions of stress and strain, were transformed to true stress and natural (logarithmic) strain for use in the present work; the results so obtained are presented in Table I, where both stress and strain are taken as positive in compression.

Let us now consider Eq. (4.5), which may be solved for the coefficient m to give

$$m = \frac{d\left\{\ell n\left[\left(\frac{\tau}{\tau_o}\right)^2 - 1\right]\right\}}{d\left\{\ell n \varepsilon_p\right\}} \tag{4.6}$$

where the subscript μ has been omitted from τ, since the athermal component τ_μ is equal to the applied flow stress τ, according to our discussion above. Inasmuch as the initial

conditions, and the material was first compressed quasi-statically to a prescribed strain, unloaded and then immediately subjected to quasi-static reverse loading under tensile stress. The results from these tests on 6061-T6 aluminum indicated the existance of a pronounced Bauschinger effect, in accordance with the observations of others.[8,12]

To evaluate the coefficients τ_o' and δ in the present model, the experimental data, originally reported in terms of axial engineering stress versus engineering strain, were transformed to true shear stress τ versus natural strain ε_1 in the usual manner. The results so obtained are depicted in Fig. 7. An inspection of the experimental curves in this figure will reveal that the material does not have a well defined yield point for reverse loading. In this case, of course, a yield point can be prescribed by some criterion--such as 0.2% offset from the elastic path--but, inasmuch as this is arbitrary, it was decided simply to assume that plastic flow begins on reverse loading when the shear stress is zero. In Eq. (3.52) we thus set

$$\tau_o' = 0 \tag{4.11}$$

In order to make a direct comparison with the quasi-static experimental reverse loading curves, the present model was specialized to uniaxial stress conditions by setting

$$\varepsilon_p = \varepsilon_1 - \frac{2\tau_\mu}{Y} \tag{4.12}$$

in Eqs. (3.52) and (3.53), and by identifying τ_μ as the quasi-static flow stress, τ.[†] Under these conditions, Eq. (3.57) takes the form

$$\tau = \tau_\mu' \left[1-\exp\left(-\delta\sqrt{\varepsilon_p^*-\varepsilon_1 + \frac{2\tau}{Y}}\right)\right] \tag{4.13}$$

[†]Such an assumption is justified in the case of 6061-T6 aluminum at room temperature since the thermally activated stress component, τ^*, is small compared with τ_μ.

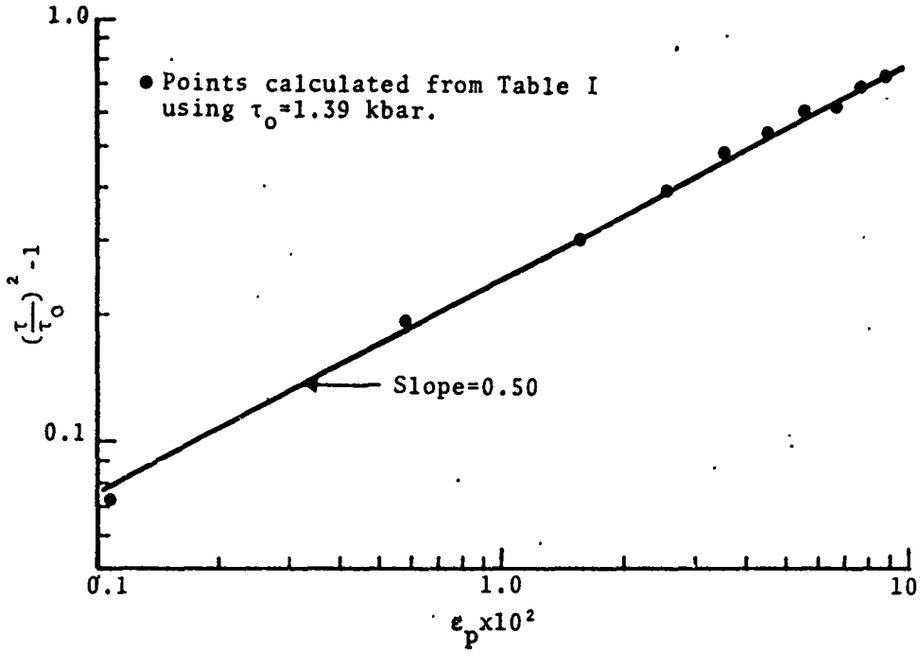

Figure 4. Dependence of $[(\tau/\tau_o)^2-1]$ on the plastic strain ε_p for 6061-T6 aluminum.

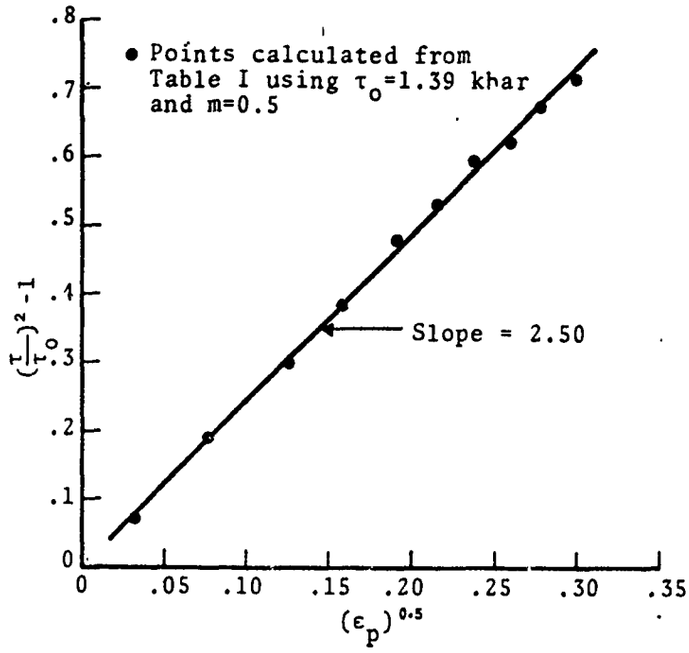

Figure 5. Dependence of $(\tau/\tau_o)^2-1$ on the square root of the plastic strain ε_p for 6061-T6 aluminum.

The experimental data have also been plotted in terms of $[(\tau/\tau_o)^2-1]$ versus $(\varepsilon_p)^{0.5}$, as shown in Fig. 5. As an inspection of this figure will reveal, the data fall along a straight line, the slope of which is 2.50. Therefore, in view of Eq. (4.8), we have

$$a = 2.50 \ .$$

For initial plastic straining in 6061-T6 aluminum at room temperature, the athermal component τ_μ can thus be described by Eq. (4.5) with the following values of the coefficients:

$$\begin{aligned} \tau_o &= 1.39 \text{ kbar} \\ a &= 2.50 \\ m &= 0.5 \end{aligned} \tag{4.9}$$

The extent to which this model correlates the experimental data for 6061-T6 aluminum presented in Ref. 55 is shown in Fig. 6. To accomplish this, the expression for τ_μ, given by Eq. (4.5) with the coefficients listed above, was recast in terms of engineering definitions of stress and strain, and then combined with the following equations for uniaxial stress conditions, where Y denotes Young's modulus,

$$\begin{aligned} \sigma &= 2\tau_\mu \\ \varepsilon_1 &= \frac{\sigma}{Y} + \varepsilon_p \end{aligned} \tag{4.10}$$

to produce the results shown. An inspection of Fig. 6 will confirm that the present model for initial strain hardening correlates the experimental results very well.

2. The Bauschinger Effect and the Coefficients δ and τ_o'

The reverse loading paths for 6061-T6 aluminum were experimentally determined for a range of plastic prestrains by Babcock.[6] The experiments were performed under uniaxial stress

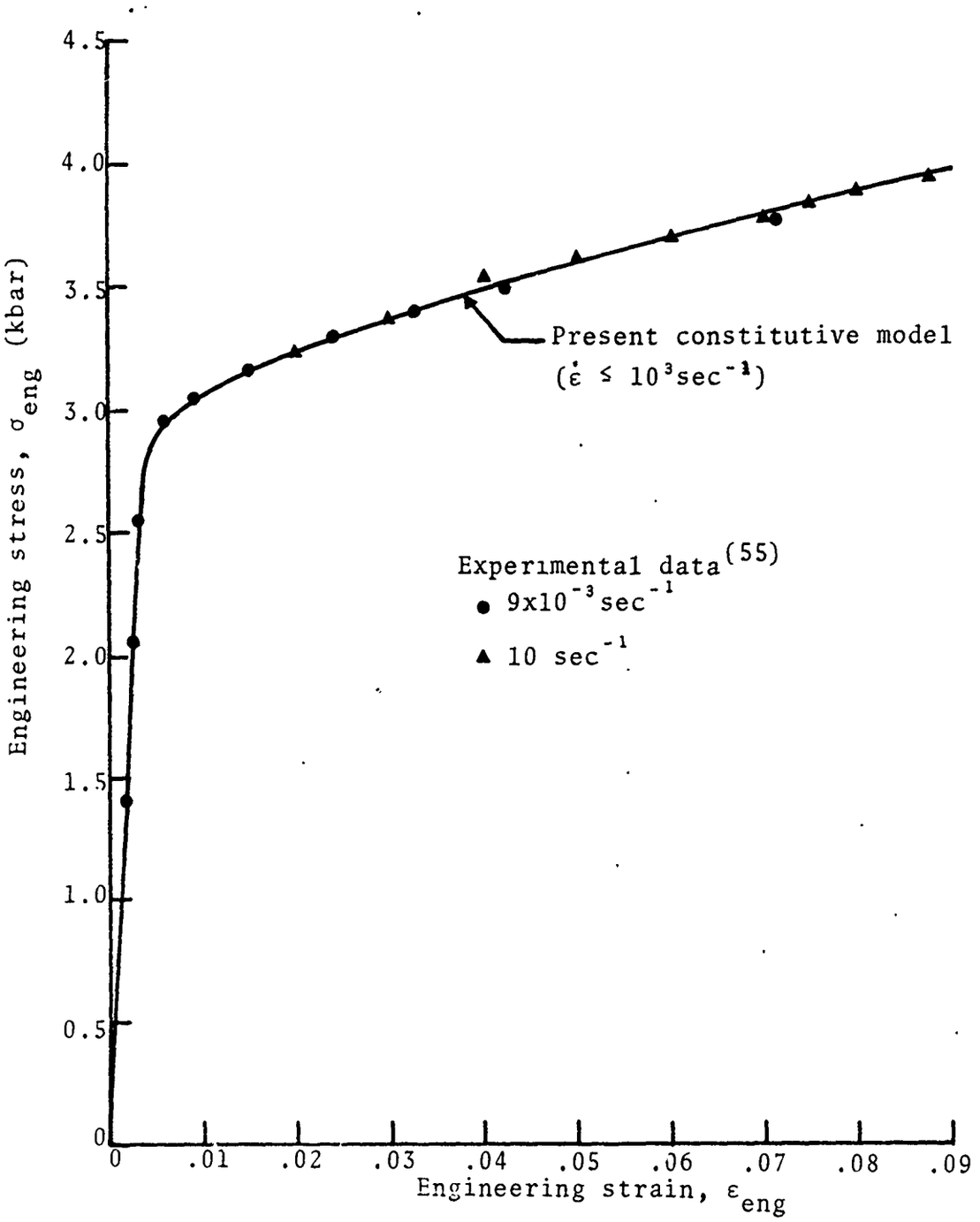

Figure 6. Compressive stress-strain relationship in 6061-T6 aluminum at 72°F, for strain rates not greater than $10^3 sec^{-1}$.

conditions, and the material was first compressed quasi-statically to a prescribed strain, unloaded and then immediately subjected to quasi-static reverse loading under tensile stress. The results from these tests on 6061-T6 aluminum indicated the existance of a pronounced Bauschinger effect, in accordance with the observations of others.[8,12]

To evaluate the coefficients τ_o' and δ in the present model, the experimental data, originally reported in terms of axial engineering stress versus engineering strain, were transformed to true shear stress τ versus natural strain ε_1 in the usual manner. The results so obtained are depicted in Fig. 7. An inspection of the experimental curves in this figure will reveal that the material does not have a well defined yield point for reverse loading. In this case, of course, a yield point can be prescribed by some criterion--such as 0.2% offset from the elastic path--but, inasmuch as this is arbitrary, it was decided simply to assume that plastic flow begins on reverse loading when the shear stress is zero. In Eq. (3.52) we thus set

$$\tau_o' = 0 \tag{4.11}$$

In order to make a direct comparison with the quasi-static experimental reverse loading curves, the present model was specialized to uniaxial stress conditions by setting

$$\varepsilon_p = \varepsilon_1 - \frac{2\tau_\mu}{Y} \tag{4.12}$$

in Eqs. (3.52) and (3.53), and by identifying τ_μ as the quasi-static flow stress, τ.[†] Under these conditions, Eq. (3.57) takes the form

$$\tau = \tau_\mu' \left[1-\exp\left(-\delta\sqrt{\varepsilon_p^*-\varepsilon_1 + \frac{2\tau}{Y}}\right)\right] \tag{4.13}$$

[†]Such an assumption is justified in the case of 6061-T6 aluminum at room temperature since the thermally activated stress component, τ^*, is small compared with τ_μ.

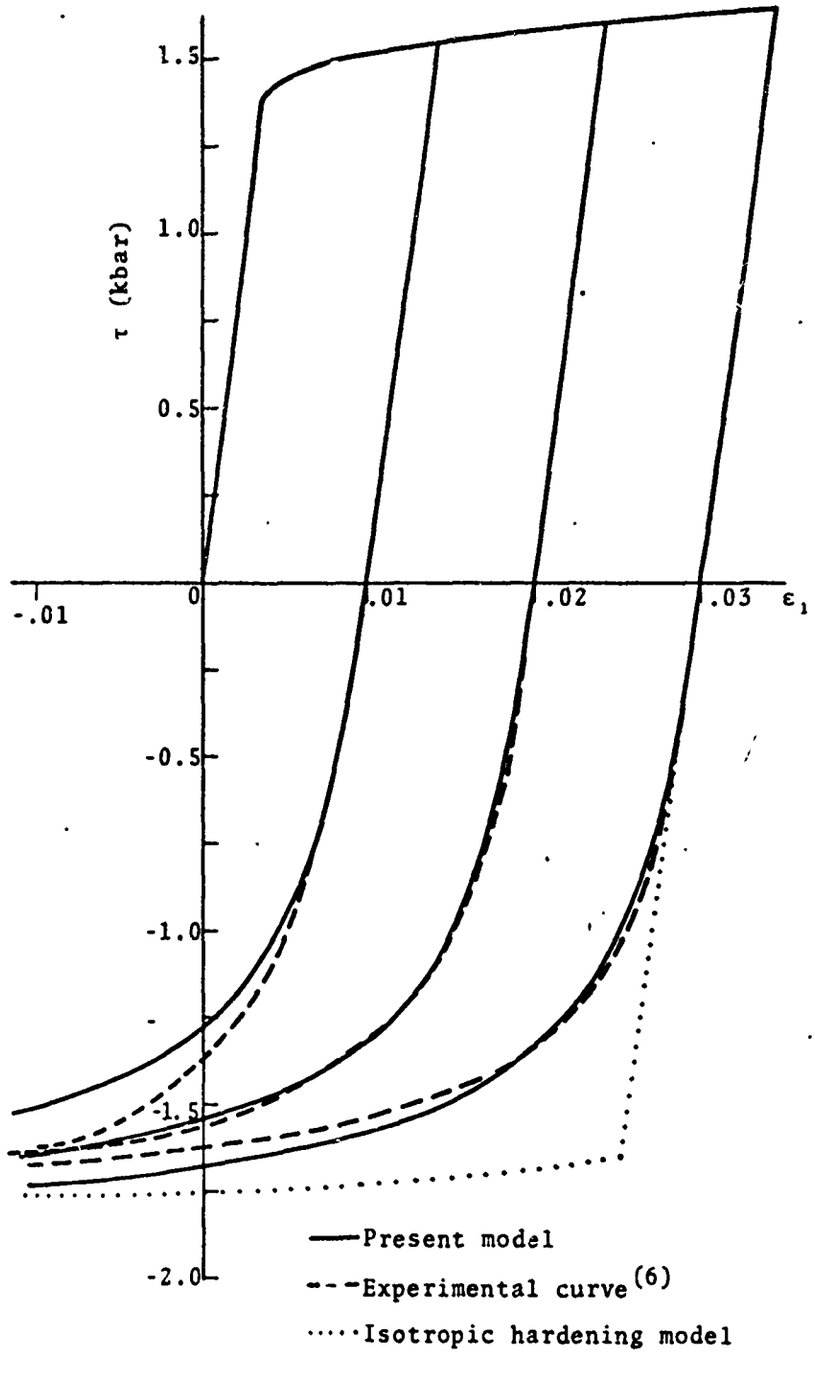

Figure 7. Reverse loading paths determined by the present model and those determined experimentally for several values of plastic prestrain in 6061-T6 aluminum.

where we have set $\tau_o' = 0$. Equation (4.13) is a transcendental equation which may be solved to give τ as a function of ε_1 for a prescribed value of δ. Using this approach, it was found that the best agreement with the experimental data was obtained for

$$\delta = 20 \ , \tag{4.14}$$

which actually represents a compromise of the best fit values for the three experimental paths shown.

A comparison between the reverse loading paths determined by the present model, using $\tau_o' = 0$ and $\delta = 20$, and those determined experimentally for several values of plastic prestrain is given in Fig. 7. Here, it is seen that the reverse loading paths predicted by the present model are in excellent agreement with the experimental results, except perhaps for the smallest plastic prestrain, where there would be more uncertainty in the data. For the purpose of depicting the differences between the present (anisotropic hardening) model and an isotropic hardening model, the reverse loading path for an isotropic model has also been included in Fig. 7 for 0.03 prestrain.

B. Elastic Precursor Decay and the Coefficients α_1, α_2, and N_{mo}

In order to obtain insight into the dependence of the strain rate on the viscous drag stress τ_D, it is advisable to perform experiments in which the strain rates are high but complications introduced by the processes of dislocation multiplication, strain hardening, and thermal activation are minimized. As was recognized by Duvall,[56] the decay of the elastic precursor wave provides information of just this sort.

In materials for which the elastic Hugoniot stress-engineering strain relationship has positive curvature, the precursor wave is an initially unsteady shock, moving at a slightly supersonic velocity U relative to the stationary material

ahead*. Denoting by u the particle velocity, the velocity of the wave relative to the material behind it, namely, U-u, is correspondingly slightly subsonic; as a result, signals emanating from behind the elastic wave front are able to overtake it. It was shown by Ahrens and Duvall,[58] and later by Herrmann,[1] that the stress decay at the elastic wave front under these conditions is given by $D\sigma_1/Dt$, where†

$$\frac{D\sigma_1}{Dt} = \frac{1}{B}\left[A\,\frac{\partial\sigma_1}{\partial x} - 2\mu\dot{\varepsilon}_p\right] \tag{4.15}$$

In this expression, the quantities A and B are defined as

$$A = \frac{(U-u)^2 - C_L^2}{U-u} \tag{4.16}$$

$$B = \frac{3}{2} + \frac{1}{2}\,\frac{C_L^2}{(U-u)^2}$$

where C_L denotes the longitudinal elastic wave speed immediately behind the elastic shock, and $(\partial\sigma_1/\partial x)$ represents the stress gradient at this point. The first term on the right side of Eq. (4.15) represents a correction due to signals originating from the region of the plastic wave behind the elastic front, and it is the result of having a nonlinear elastic Hugoniot. The second term on the right side of this equation arises from visco-plastic relaxation of the material at the elastic front.

The special case of a linear elastic Hugoniot simplifies Eq. (4.15) considerably, since the elastic shock is then exactly

*In materials having a negative elastic Hugoniot curvature, e.g., fused quartz, the precursor wave is a compression fan and Eq. (4.15), which is based on the jump conditions across a flow discontinuity, does not apply.

†The symbol D/Dt denotes the time derivative following the elastic precursor.

sonic. From the jump conditions and the characteristic flow equations,[56] or from Eq. (4.15) with $C_L = U-u$, one has in this case

$$\frac{D\sigma_1}{Dt} = -\mu\dot{\varepsilon}_p$$

or

$$\frac{D\sigma_1}{Dx} = -\frac{\mu}{C_L}\dot{\varepsilon}_p \qquad (4.17)$$

The plastic strain rate $\dot{\varepsilon}_p$ can, in general, be described in the manner $\dot{\varepsilon}_p = \dot{\varepsilon}_p(\tau,\varepsilon_p)$; but, at the elastic precursor, we have $\varepsilon_p = 0$ so that $\dot{\varepsilon}_p$ depends only on the shear stress τ. With this in mind, and making use of the elastic relation for uniaxial strain, namely,

$$\tau = \frac{\mu}{K + \frac{4}{3}\mu}\sigma_1 \qquad (4.18)$$

Equation (4.17) can be integrated at once for x as a function of σ_1. Since the departure of the elastic Hugoniot from linearity is quite small for most metals at low stress levels, the linearized precursor decay equation, Eq. (4.17), may give a reasonable approximation to the more general equation, Eq. (4.15), except possibly during the early stages of the decay when $(\partial\sigma_1/\partial x)$ behind the precursor wave can be large. Indications that this is in fact the case were obtained in the present study, as described below.

An inspection of Eq. (4.15) reveals that it is unsuited for computational purposes, since the first term on the right side can only be determined by calculating the entire flow field. Consequently, if one is to include the effects of a nonlinear elastic Hugoniot, it becomes necessary to resort to numerical methods. Johnson and Band[58] have discussed the use of finite-difference methods for solving the flow equations for stress-relaxing solids, with particular reference to the precursor wave.

They have shown that finite-difference methods can in fact be utilized to study precursor decay, but that certain features of the method must be taken into consideration. First, the finite-difference solution tends to oscillate behind the elastic shock front; it is customary to stabilize these oscillations, which are of numerical origin, by incorporating a small linear artifical viscosity term into the numerical scheme. The addition of such a viscosity term inevitably obscures to some extent the visco-plastic response of the material being analyzed, particularly in the vicinity of the elastic precursor. In the second place, the precursor cannot be treated as discontinuous in the finite-difference approach; it has a finite rise time and, at the top of the wave, significant amounts of dislocation multiplication and plastic strain may therefore have occurred. The dislocation multiplication tends to increase the precursor decay rate, while the stress relief accompanying the plastic strain tends to reduce it. These effects are apparently unavoidable in finite-difference solutions, and clearly have some influence on the calculated decay rate.* Both of the limitations on the finite-difference method noted above can, however, be minimized to some extent by using a small mesh size ($\Delta x, \Delta t$) and by judiciously selecting the artificial viscosity to minimize oscillations behind the precursor.

The linearized precursor decay solution, which has a different type of limitation than a numerical solution, is trivially easy to determine by integration of Eq. (4.17), and can also be

*After the completion of the present work, Herrmann, Hicks and Young[59] reported the results of an investigation in which the use of finite-difference methods for calculating elastic precursor decay was studied. Particular emphasis was given in this investigation to the effects of dislocation multiplication and finite shock thickness on precursor decay. The results obtained indicate that, under certain conditions, the artificial viscosity method may lead to unrealistic precursor decay which is significantly influenced by the numerical scheme employed.

of considerable aid in evaluating coefficients. At the elastic precursor where $\varepsilon_p = 0$, the constitutive equation developed in the present work reduces to the following form:

$$\dot{\varepsilon}_p = \frac{4}{3} \frac{b\Phi N_{mo}}{\sqrt{1 + \frac{\Phi^2}{C_s^2}}} \tag{4.19}$$

Here, we have

$$\Phi = \alpha_1(\tau - \tau_o) + \alpha_2(\tau - \tau_o)^2 \tag{4.20}$$

since both τ and τ_μ are evaluated at zero plastic strain. Upon combining Eqs. (4.18) through (4.20) with Eq. (4.17), one obtains a differential equation of the form

$$\frac{D\sigma_1}{Dx} = F(\sigma_1) \tag{4.21}$$

which can be solved to give the decay of the Hugoniot elastic stress with distance of propagation x. Such a procedure has been followed in the present work to obtain initial estimates of α_1 and α_2, and for this purpose the experimentally determined precursor decay for 6061-T6 aluminum reported in Ref. 6 was used.

At this point, it should be noted that, in the absence of dislocation mobility data for 6061-T6 aluminum, it becomes necessary to make some assumption concerning the initial mobile dislocation density N_{mo}. To this end we have assumed

$$N_{mo} = 10^8 cm^{-2} \tag{4.22}$$

which is of the same order of magnitude as that adopted in Ref.17.

After initial estimates of α_1 and α_2 had been obtained by the procedure described above, further refinements were made in these coefficients through numerical studies carried out on

the finite difference RIP code, using the complete constitutive equation. In these studies, very fine zoning was used ($\Delta x \approx 5\times10^{-4}$ cm), and only sufficient linear artificial viscosity was employed to dampen out small spurious oscillations of numerical origin, which occur immediately behind the precursor when no artificial viscosity is used. The values of the coefficients α_1 and α_2 which gave the best fit to the experimental precursor decay data were found to be

$$\alpha_1 = 5.6\times10^3 \text{ cm/sec/kbar}$$
$$\alpha_2 = 9.0\times10^5 \text{ cm/sec/kbar}^2 \qquad (4.23)$$

Some numerical experimentation was done to determine to what extent the computed precursor decay curve depended on the numerical features, such as the zone size and the computational time step. From the results obtained, it was found that changes in the zone size by a factor of three, and in the time step by a factor of two, had a detectable, but not significant, effect on the calculations.

A comparison of the precursor decay calculated by the finite-difference RIP code (using the values of α_1 and α_2 given above) with that determined experimentally by Isbell, et al.[6] is shown in Fig. 8. In both the calculations and the experiments, the initial elastic impact stress was 20 kbar. It may be noted that the computed precursor decay curve passes through all six of the experimental data points. Although very fine zoning was used, the precursor amplitude could not be accurately determined in the RIP code calculations for propagation distances less than 0.025 cm;* because of this, a dotted line has been used to indicate

*By restricting attention to the region $0 < x < 0.05$ cm, and using finer zoning, the initial stage of precursor decay could be more accurately determined; this was not attempted here, however, due to the absence of experimental data within this region.

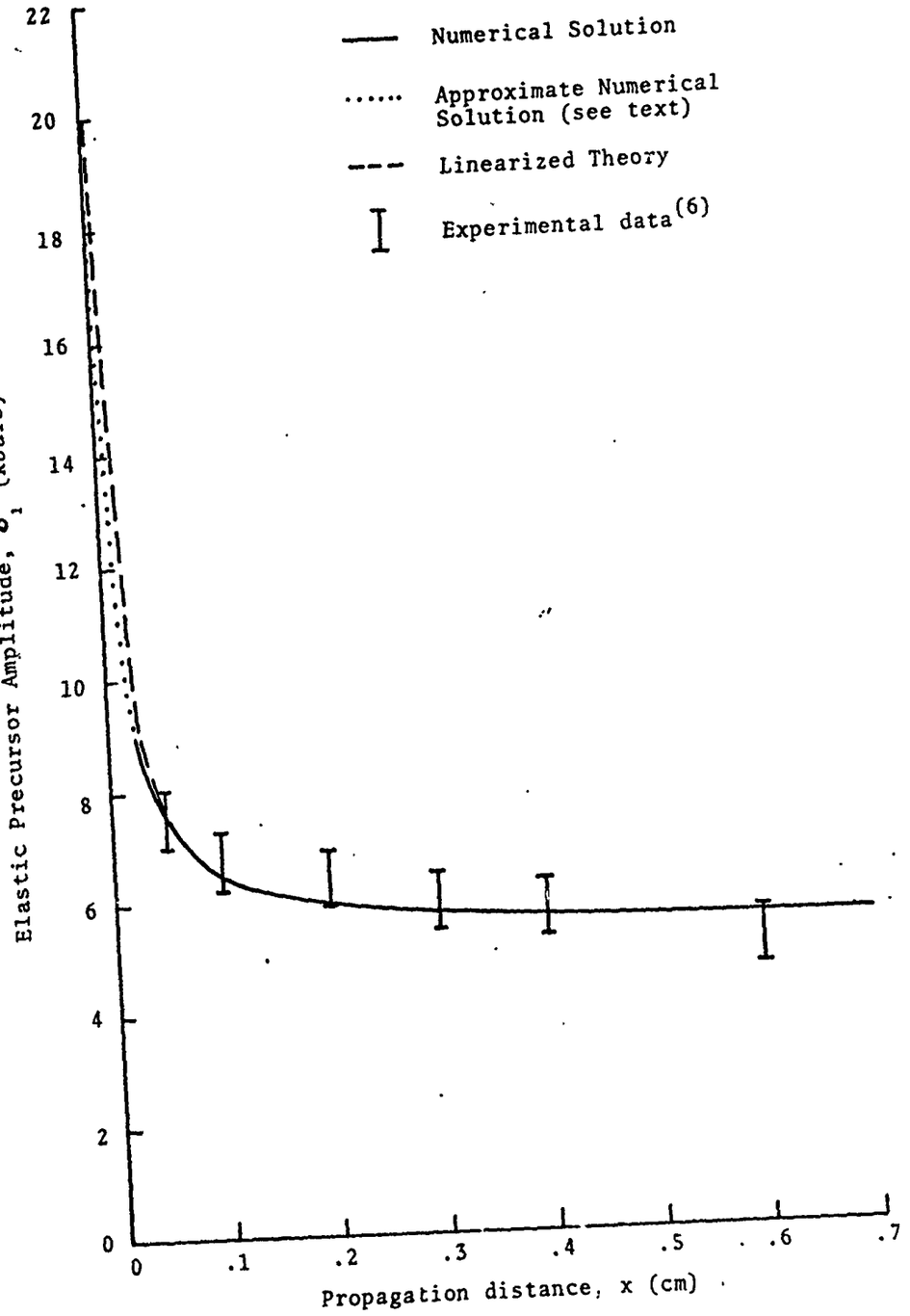

Figure 8. Comparison of calculated and observed elastic precursor decay in 6061-T6 aluminum for an initial impact stress of 20 κbar.

(approximately) the shape of the decay curve in this region. Also shown in Fig. 8 is the precursor decay curve calculated from the linearized theory, Eq. (4.17), using the values of α_1 and α_2 given in Eq. (4.23). From this figure, it is seen that for propagation distances greater than about 0.05 cm, the decay curve predicted by the linearized theory essentially coincides with that determined with the RIP code.

Parenthetically, it is of interest to note that the experimental data shown in Fig. 8 were obtained from specimens of 6061-T6 aluminum which had original stock thicknesses of either 0.32 or 0.64 cm. As shown by Isbell, et al.,[6] the precursor decay for other stock thicknesses varies to some extent from that depicted in Fig. 8 due, most likely, to the different amounts of cold work accumulated during the rolling process.

C. Steady Wave Analysis and the Coefficients A_1, M_1 and $N_{m\infty}$

One of the methods available for study of the dynamical characteristics of a material is the analysis of steady waves, for which the flow equations can be easily integrated. The observed characteristics of the flow can therefore be related to the properties of the material more easily than in the case of a general unsteady flow situation.

Analyses of steady shock waves were presented by Band,[60] and further discussed by Band and Duvall.[61] They showed how the analysis could be used to relate observed wave velocities for shocks of differing strengths to the viscous dissipation rate of the material, so that a mean viscosity parameter could be determined.

More recently, with the development of laser interferometry, a more refined application of steady wave analysis has become possible. The interferometer essentially gives the velocity of a material interface or free boundary, due to an incident wave, as a function of time. From this information, together with some knowledge of the dynamical properties of the materials

involved, the profiles of particle velocity, stress and strain within the incident wave itself can be inferred. If the observed interface velocity profile is essentially steady, as determined by repeated observations at different interface positions, Band's analysis can be applied to the determination of the detailed form of the viscous dissipation function. The analysis requires, in addition to the interferometer data, a knowledge of the elastic constants, quasistatic strain hardening behavior, and shock hydrostat of the material. It also requires, as a practical matter, a constitutive model for the viscous behavior which contains several adjustable parameters. Some of these parameters can be determined by other techniques, such as the analysis of precursor wave decay, but the dislocation multiplication parameters, such as A_1, M_1 and $N_{m\infty}$ in the present model, can best be found from the analysis of the steady wave profile.

Steady wave measurements in 6061-T6 aluminum suitable for this approach were described by Barker[11] and analyzed by Johnson and Barker[17] in terms of a specific constitutive model. In the present study a different constitutive model is proposed, and more data relating to the shock hydrostat, precursor decay and strain hardening have become available. The data presented in Ref. 11 were therefore reanalyzed as described below. The method employed is basically similar to that presented in Ref. 17 but incorporates some refinements which are believed to be justified by the currently available information on the material.

1. Theory Underlying Steady Wave Analysis

In this section the dynamical characteristics of steady waves are reviewed. The following equations describe one-dimensional plane flow:*

*In Sections IV.C.1 and IV.C.2 the symbol σ refers to the stress component σ_1 in the direction of the only nonvanishing strain component. For simplicity, the subscript 1 has been omitted in these sections.

$$\text{Continuity:} \quad \frac{d\rho}{dt} + \rho\frac{\partial u}{\partial x} = 0 \tag{4.24}$$

$$\text{Motion:} \quad \rho\frac{du}{dt} + \frac{\partial \sigma}{\partial x} = 0 \tag{4.25}$$

$$\text{Energy:} \quad \rho\frac{dE}{dt} + \rho\sigma\frac{dV}{dt} + \frac{\partial q}{\partial x} = 0 \tag{4.26}$$

where

$$\frac{d}{dt} = \frac{\partial}{\partial t} + u\,\frac{\partial}{\partial x}$$

represents the substantive derivative along a particle path, σ the total longitudinal stress (positive in compression), u the particle velocity, q the longitudinal heat flux, ρ the density and $V = \frac{1}{\rho}$ the specific volume. These equations may also be written in conservation form as follows:

$$\frac{\partial \rho}{\partial t} + \frac{\partial}{\partial x}(\rho u) = 0 \tag{4.27}$$

$$\frac{\partial}{\partial t}(\rho u) + \frac{\partial}{\partial x}(\rho u^2 + \sigma) = 0 \tag{4.28}$$

$$\frac{\partial}{\partial t}(\rho E + \tfrac{1}{2}\rho u^2) + \frac{\partial}{\partial x}(\tfrac{1}{2}\rho u^3 + \rho u E + u\sigma + q) = 0 \tag{4.29}$$

This set of equations is covariant under the Galilean transformation

$$t' = t \qquad u' = u - U \qquad \rho' = \rho \qquad q' = q \tag{4.30}$$

$$x' = x - Ut \qquad \sigma' = \sigma \qquad E' = E$$

where U is a constant.

A "steady wave" may be said to exist within a space-time region when a unique wave velocity U can be found such that in the moving reference frame defined by Eq. (4.30), the time derivatives of the densities of mass, momentum and total energy vanish:

$$\frac{\partial \rho'}{\partial t'} = 0 \; ; \; \frac{\partial \rho' u'}{\partial t'} = 0 \; ; \; \frac{\partial}{\partial t'} (\rho' E' + \tfrac{1}{2}\rho' u'^2) = 0 \qquad (4.31)$$

It follows from Eqs. (4.27) through (4.31) that between any pair of states A, B within the steady-wave region, the following relations hold:

$$\rho_A(u_A - U) = \rho_B(u_B - U) = M \qquad (4.32)$$

$$\rho_A(u_A - U)^2 + \sigma_A = \rho_B(u_B - U)^2 + \sigma_B \qquad (4.33)$$

$$\tfrac{1}{2}\rho_A(u_A - U)^3 + (\sigma_A + \rho_A E_A)(u_A - U) + q_A = \tfrac{1}{2}\rho_B(u_B - U)^3 \qquad (4.34)$$

$$+ (\sigma_B + \rho_B E_B)(u_B - U) + q_B$$

where M denotes the constant mass flux through the steady wave. These relations define invariants within a region of unsteady flow, in contrast to the Rankine-Hugoniot jump conditions to which they are analogous. For the special cases in which either (i) states A and B are themselves states of steady flow, or (ii) states A and B delimit a flow discontinuity, with $x_A = x_B$, the steady wave relations Eqs. (4.32) through (4.34) can in fact be identified with the Rankine-Hugoniot equations.

From Eqs. (4.32) and (4.33) it follows that

$$\sigma_B - \sigma_A = -M^2(V_B - V_A) \qquad (4.35)$$

so that any pair of states within the wave must lie on a unique straight line in the stress-volume plane. This is termed the "Earnshaw relation" by Band and Duvall.[61] It is the analog of the "Rayleigh line" in fluid mechanics, and is also (perhaps improperly) called by that name. From Eqs. (4.32) and (4.34) one can write the analog of the "Fanno line":

$$E_B + \sigma_B V_B - E_A - \sigma_A V_A = -\tfrac{1}{2}M^2 \left(V_B^2 - V_A^2\right) - \frac{1}{M}\,(q_B - q_A) \qquad (4.36)$$

Additional relations may also be written, such as

$$E_B - E_A + \tfrac{1}{2}(\sigma_B + \sigma_A)\,(V_B - V_A) + \frac{1}{M}\,(q_B - q_A) = 0 \qquad (4.37)$$

$$E_B - E_A = -\,\sigma_A(V_B - V_A) + \tfrac{1}{2}M^2\,(V_B - V_A)^2 - \frac{1}{M}\,(q_B - q_A) \qquad (4.38)$$

$$E_B - E_A = -\frac{1}{2M^2}\left(\sigma_B^2 - \sigma_A^2\right) - \frac{1}{M}\,(q_B - q_A) \qquad (4.39)$$

The first of these is the analog of the Hugoniot equation. All of the above Eqs. (4.32) through (4.39) are valid between any two states A, B on a steady wave profile.

The remaining equations which govern the flow are the equations of state, the equation of heat conduction, and the general quasilinear constitutive relation

$$\frac{1}{\phi(\sigma,E,V)}\,\frac{d\sigma}{dt} + \psi(\sigma,E,V) = -\,\frac{1}{V}\,\frac{dV}{dt} \qquad (4.40)$$

where the first term on the left side represents the "instantaneous response" strain rate (elastic or elastic-plastic behavior), the second term the dissipative strain rate (viscoplastic behavior), and the right side the total strain rate. This relation includes as special cases the viscous fluid, the elastic-plastic solid, and others in addition to the elastic-viscoplastic solid which is the case of present interest.

The elastic modulus ϕ is determined by the elastic equation of state:

$$\phi(\sigma,E,V) = -V(\partial\sigma/\partial V) \tag{4.41}$$

For a steady wave moving with velocity U, Eq. (4.40) may be written

$$\frac{1}{\phi(\sigma,E,V)}\frac{\partial\sigma}{\partial x} + \frac{\psi(\sigma,E,V)}{u-U} = -\frac{1}{V}\frac{\partial V}{\partial x} \tag{4.42}$$

The variables u and σ may be eliminated with the aid of Eqs. (4.32) and (4.35), giving as the result Band's differential equation:

$$-M\left(1 - \frac{M^2V}{\phi(\sigma,E,V)}\right)\frac{\partial V}{\partial x} = \psi(\sigma,E,V) \tag{4.43}$$

where σ is to be evaluated in terms of V and the initial conditions at some prescribed state within, or on the boundary of, the steady wave region. If ϕ and ψ are independent of E, this equation may be integrated at once for the wave profile V(x). This can also be done if the heat flux q can be neglected, by using Eq. (4.38) to evaluate E in terms of V. It will be assumed that the heat flux q is in fact negligible for wave profiles wide enough to be resolved.[53] The alternative assumption, that ϕ and ψ are independent of energy, is not as well justified, although if shock Hugoniot data are employed as reference states in the representation of the state equation, the errors are in general small.

For a wave which loads the material in compression, our sign convention would lead one to expect $\psi(\sigma,E,V)$ to be non-negative throughout the wave profile. This also follows from the Second Law, if ψ is for example proportional to $\sigma - \sigma_{equil}$. Since M and $\partial V/\partial x$ have opposite signs, it follows from Eq. (4.43) that throughout the wave profile

$$M^2V \leq \phi(\sigma,E,V) \tag{4.44}$$

Since $\phi = \rho C_L^2$, where C_L is the effective longitudinal sound speed, this implies that the steady wave velocity must be subsonic with respect to states within the wave. All parts of the wave can then intercommunicate, adjusting their stress and density with the aid of the dissipative mechanism so that each state falls on the same Rayleigh line.

The steady wave region itself, within which Eq. (4.43) applies, must be bounded by states of constant flow, in which $\partial V/\partial x = 0$ and $\psi = 0$, or by a flow discontinuity. The former case occurs for weak waves, which are the cases of present interest. It is apparent from Eq. (4.43) that the x coordinates of the boundaries of the flow are infinitely removed from any point in the interior of the region. As a practical matter, the solution of Eq. (4.43) need not of course be extended beyond points where ψ is negligible. It should also be remarked that such weak waves are not properly termed shocks since they are, throughout their extent, subsonic. Stronger waves may, of course, be true shocks, in which case the wave profile would be expected, by the arguments of the preceding paragraph, to have a discontinuous head at the point where the equality sign holds in Eq. (4.44). The tail portion of the wave would still have a width described by Eq. (4.43).

The Band differential Eq. (4.43) itself is of the simple type in which the independent variable does not explicitly appear, and can be integrated by any numerical quadrature method for x as a function of V.

2. Conditions for Existence of Steady Waves in Metals

The equilibrium stress-strain relation for a typical elastic-viscoplastic metal is schematically illustrated in Fig. 9. (Some of the features of the actual relation are considerably exaggerated for clarity.)

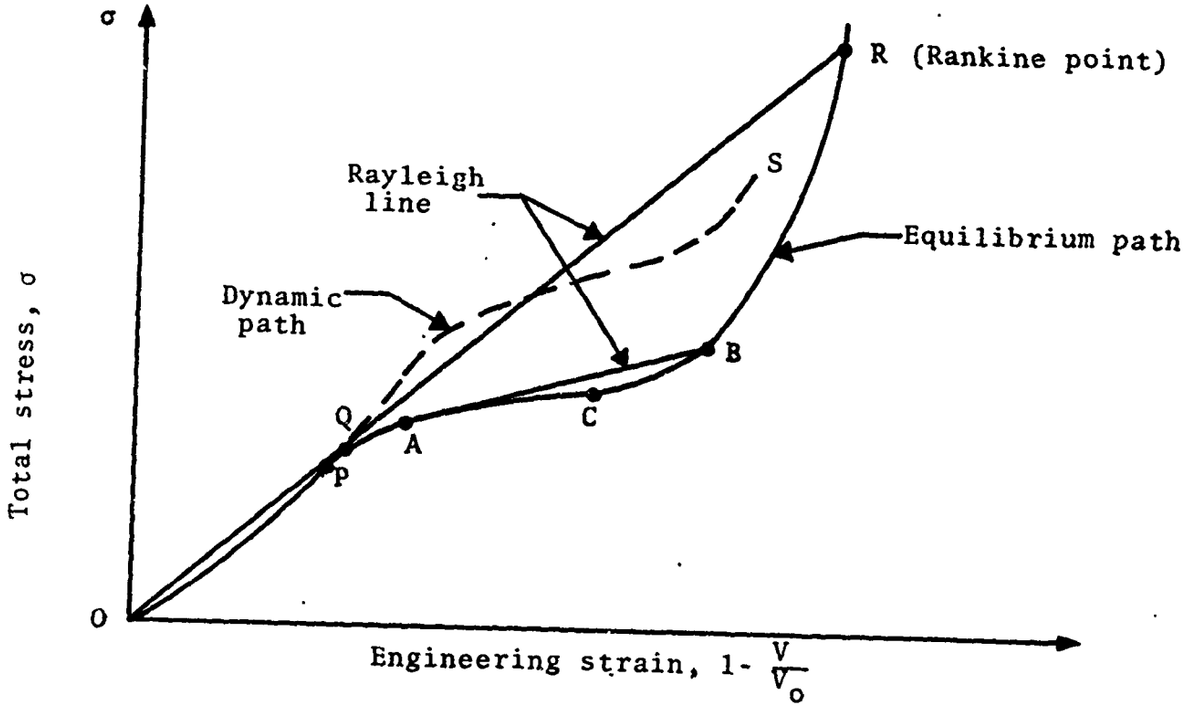

Figure 9. **Stress-strain relation** for elastic precursor and plastic wave.

The section OQ in Fig. 9 follows the Hugoniot, which below the static yield point P is purely elastic in character. Above P the Hugoniot has negative curvature for some distance due to the yield process. The Rayleigh line from the origin is tangent to this yield path at Q, generally very near to P. Above Q the equilibrium path follows an isentrope QAC. At C, the curvature of this isentrope becomes positive, and the equilibrium path follows a modified Hugoniot CBR which can be constructed as follows. At any point B on the segment CBR, a Rayleigh line BA can be drawn tangent to the isentrope at A. The point B must then also lie on the Hugoniot centered at A. These two conditions suffice to determine V_B, V_A and σ_B. Above R (the Rankine point) the equilibrium path follows the Hugoniot centered at O. The path constructed in this way coincides with the static path only below point C; above C it is just the locus of equilibrium states accessible to a system containing steady waves, i.e., one in which transient waves have essentially disappeared.

The wave structure corresponding to this construction is easily described. For wave systems with maximum stress above point R (about 140 kbar for aluminum) a single shock develops. For weaker waves, a two-wave structure appears, eventually consisting of a steady elastic precursor wave in which the internal states lie along a Rayleigh line OQ, and a steady "plastic wave" in which the states lie along a Rayleigh line such as AB. Between these is a compression fan, in which the states lie on the isentrope QA. This dispersive section of the wave system is relatively unimportant in the interpretation of the observed wave profiles (it extends over a stress increment of 0.25 kbar or less for aluminum).

Before the steady wave structure is stabilized, the wave structure is determined by a dynamic yield path such as PS in Fig. 9. The upper portions of this path appear to relax more rapidly than the lower portions which are already closer to

the equilibrium path, as evidenced by the early stabilization of the shape of the upper portions of the plastic wave. A true steady wave does not exist in any part of the profile until the entire yield path has relaxed to its equilibrium position, however.

The range of wave strengths for which this steady-wave profile analysis is at present feasible is rather restricted, being limited above by the resolution of the interferometer and below by the conditions under which a steady uniaxial wave can be established in the laboratory. For waves generated by impacting the end of a bar, the dynamic yield surface must essentially complete its relaxation before the arrival of lateral unloading waves which distort the uniaxial strain states.

Three wave profiles suitable for analysis are presented in Refs. 11 and 17. Of these three profiles, Shot 926 (90 kbar) is at the limit of resolution of the interferometer, and Shot 939 (21 kbar) is apparently not yet quite steady in the lower third of the profile, as noted in Ref. 17.

3. Application to the Present Constitutive Model of 6061-T6 Aluminum

It follows from Hooke's Law, the assumption that the plastic flow is incompressible, and the assumption that total strain is uniaxial, that the constitutive equation must have the form

$$\dot{\sigma}_1 + 2\mu\dot{\varepsilon}_p = \left(\frac{dP}{d\varepsilon} + \frac{4}{3}\mu\right)\dot{\varepsilon} \qquad (4.45)$$

where $\frac{dP}{d\varepsilon}$ (the bulk modulus) is obtained from an equation of state, which for 6061-T6 aluminum was taken in the form given later on in Sec. IV.E. Equation (4.45) conforms to Eq. (4.40) if one identifies $\dot{\varepsilon}$ with the right side of Eq. (4.40), the longitudinal elastic modulus with ϕ:

$$\phi = \frac{dP}{d\varepsilon} + \frac{4}{3}\mu$$

and the dissipative part of the total strain rate as

$$\psi = \frac{2\mu}{\phi}\,\dot{\varepsilon}_p$$

By Eqs. (2.1), (3.4) and (3.11), this quantity ψ depends on the dislocation multiplication parameters A_1, M_1 and $N_{m\infty}$ as follows:

$$\psi = \frac{8}{3}\,\frac{\mu b v}{\phi}\left[N_{m\infty} + (N_{mo} - N_{m\infty} + M_1\varepsilon_p^2)\,\exp(-A_1\varepsilon_p)\right] \qquad (4.46)$$

A series of steady wave profile calculations were carried out in order to establish best values for the constants A_1, M_1 and $N_{m\infty}$ in this expression to fit the data for shots 926, 927 and 939. The quartz-aluminum interface velocities obtained from analysis of the oscillograph fringes were transformed to incident-wave aluminum particle velocities using an elastic-plastic model for aluminum and elastic data for quartz by Johnson and Barker.[17] The transformed data and the steady-wave calculations with

$$\begin{aligned} A_1 &= 180 \\ M_1 &= 2 \times 10^{13}\ \text{cm}^{-2} \\ N_{m\infty} &= 10^{9}\ \text{cm}^{-2} \end{aligned} \qquad (4.47)$$

are shown in Fig. 10. The quoted values of A_1, M_1 and $N_{m\infty}$ represent a compromise of the best-fit values for the three shots. The dependence of the wave shape on these parameters is rather strong, so that a 5% change in either parameter would yield significantly poorer overall agreement with the data. The difference between these results and those of Johnson and Barker[17] can be attributed mostly to the use of different models for viscous drag and strain hardening, and to the use

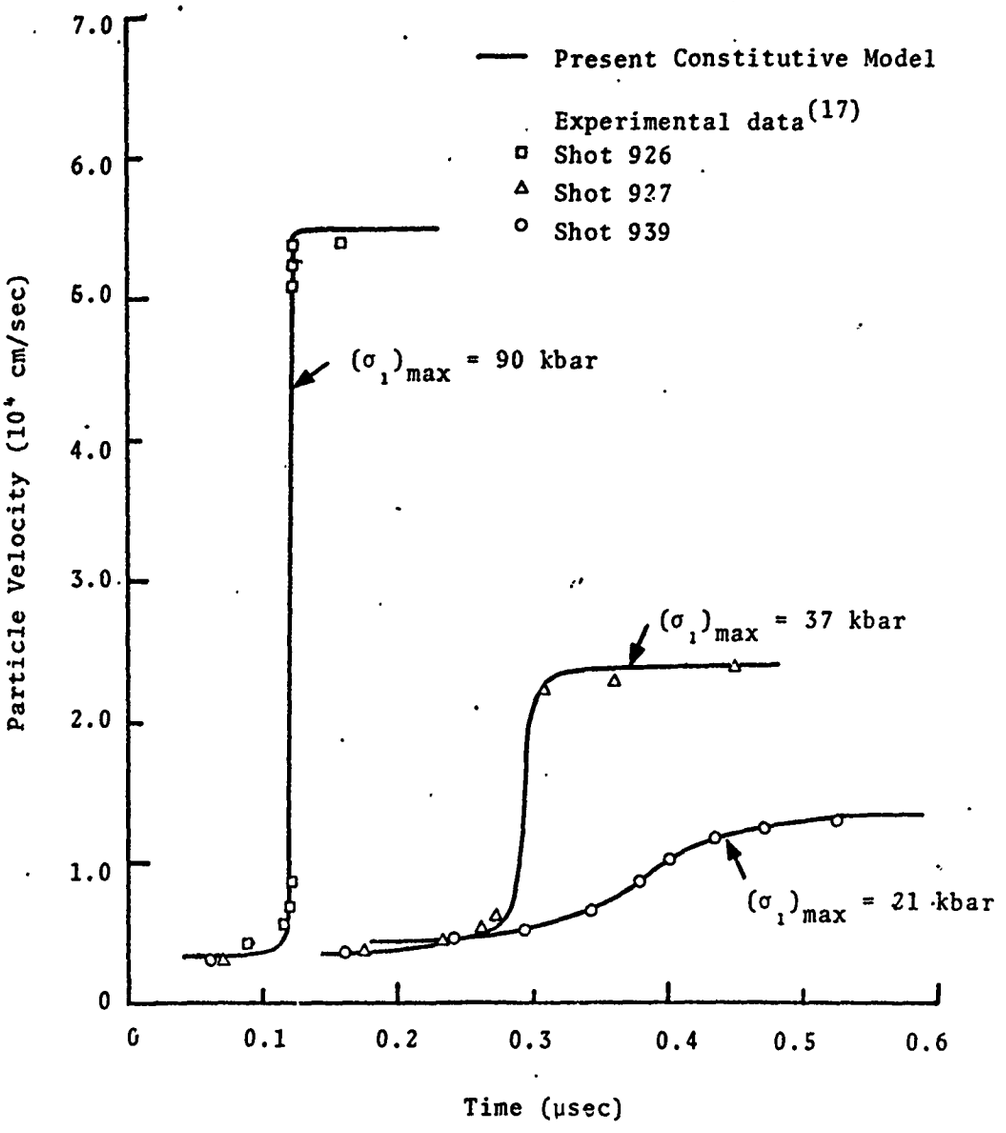

Figure 10. Comparison of calculated and observed particle velocity histories in 6061-T6 aluminum.

of different data for the equation of state. The inclusion of energy dependence in the calculation had only a small effect on the shape of the profile. Finally, in these calculations the Rayleigh line was taken tangent to the strain-hardened yield locus at the lower end, while Johnson and Barker took it through the initial yield point. This modification had a definite effect on some of the calculations, particularly on wave velocities and the shape of the low portion of the plastic wave.

D. Release Waves and the Coefficients A_2 and $N'_{m\infty}$

Earlier in Sec. III.I the expression adopted in the present work for describing the mobile dislocation density during reverse loading from a plastically prestrained state was given as

$$N_m = N'_{m\infty} + (N_{m*} - N'_{m\infty}) \exp(-A_2 \bar{\varepsilon}_p^2) \qquad (4.48)$$

where each of the symbols has been previously defined. This expression has two coefficients, A_2 and $N'_{m\infty}$, which must be evaluated from experimental data and, to accomplish this, the following approach was followed here.

An impact problem, previously investigated experimentally by Barker,[11] was selected for the purpose of evaluating the coefficients A_2 and $N'_{m\infty}$. In this problem, reported as shot 927 in Ref. 11, a 0.650 cm 6061-T6 aluminum flyer plate impacted a target of 1.223 cm 6061-T6 aluminum backed by fused quartz at a velocity of 4.81×10^4cm/sec. Because of the geometry, the release wave in this problem traveled a relatively long distance (about 1.9 cm) without attenuating and, thus, had an opportunity to develop considerable structure.

A series of numerical calculations was performed on the RIP code for the above problem by varying the values of A_2 and $N'_{m\infty}$ in the present constitutive model for 6061-T6 aluminum. In

these calculations the constitutive equation for fused quartz (silica) recently reported in Ref. 62 was used. Successive changes were made in the values of A_2 and $N'_{m\infty}$ until a satisfactory level of agreement had been achieved between the computed and the experimental release wave profiles; after several iterations, it was found that the following values for these coefficients

$$\begin{aligned} A_2 &= 1.2\times 10 \\ N'_{m\infty} &= 5\times 10^7 \text{ cm}^{-2} \end{aligned} \tag{4.49}$$

resulted in a calculated release wave profile which agreed reasonably well with the experimental data.

A comparison of the results computed using the present constitutive model and the above values for A_2 and $N'_{m\infty}$ with experimental data from Ref. 11 is depicted in Fig. 11.* Here, the particle velocity-time history at the aluminum-fused quartz interface is shown. For the purpose of comparison, the corresponding computed results for the simple elastic-plastic model and for the present constitutive model with rate effects removed on unloading have also been included in this figure. By comparing the release wave profiles for the various models, some indication of the influence that the Bauschinger and strain rate effects have can be obtained.

The numerical results shown in Fig. 11 for the various constitutive models were all obtained for the same zone size, as well as for the same form and magnitude of artificial viscosity. The differences which are apparent between the results for the various models are thus of physical origin, and reflect

*To make this comparison, the experimental data was shifted very slightly (about .05 μsec) to the right along the horizontal time axis in Fig. 11 in order to obtain agreement between the computed and the observed arrival time of the elastic precursor.

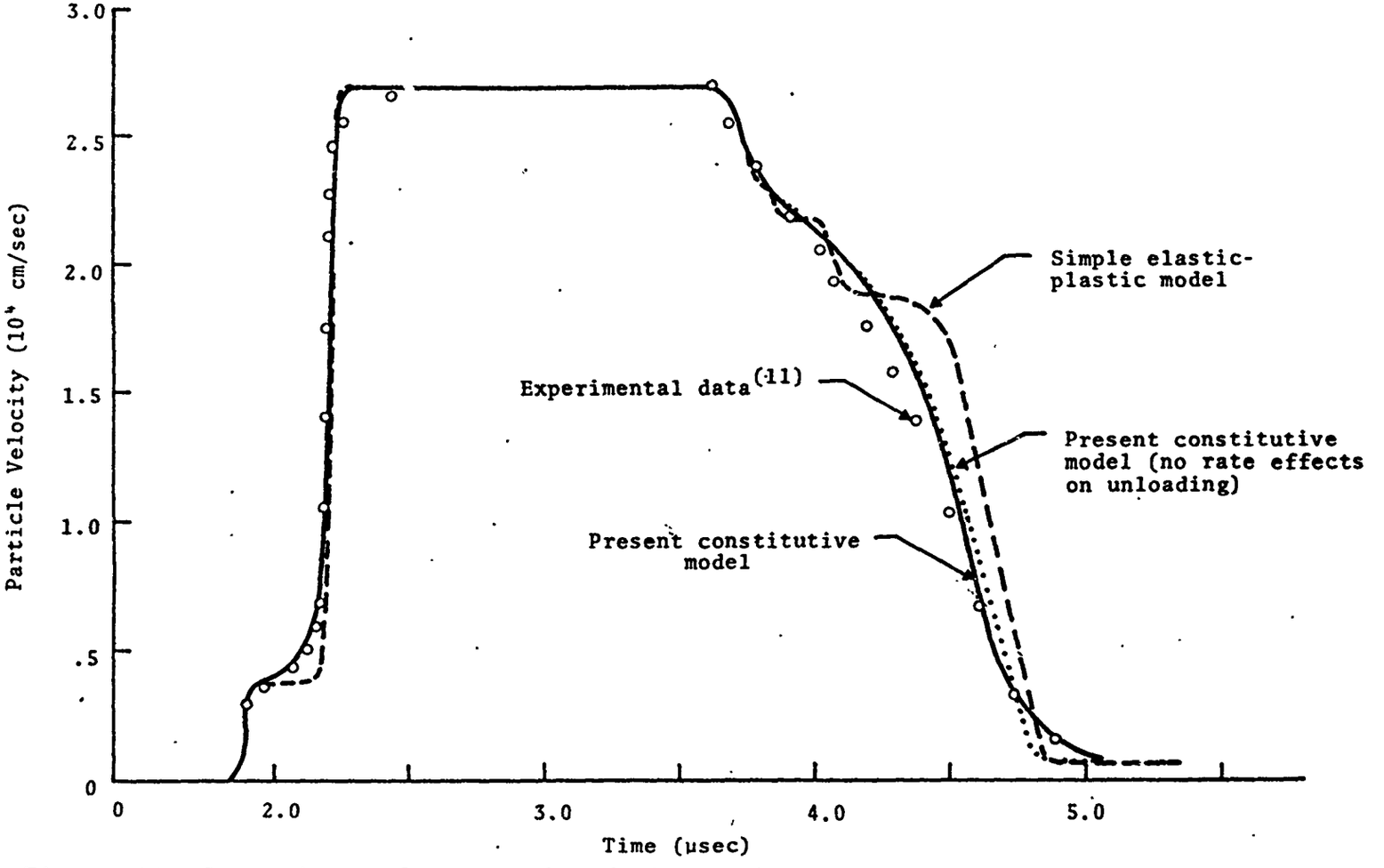

Figure 11. Comparison of computed and observed particle velocity history at aluminum-fused quartz interface for Shot 927.

the basic differences in the dynamic response characteristics of these models.

Finally, an inspection of Fig. 11 reveals that the present constitutive model with a Bauschinger effect, but no rate effects, on unloading gives satisfactory results; only a small improvement in the release wave profile was obtained when strain rate effects were introduced. It is believed that further improvement in the agreement between the computed and observed results could be obtained, however, with additional effort.

E. Summary of Constitutive Model of 6061-T6 Aluminum

In summary, it appears that thermal activation does not play an important role in the room temperature deformation of 6061-T6 aluminum and may be neglected. In this case, the system of equations that describes the present constitutive model of this material is as follows for uniaxial strain conditions:

$$\dot{\varepsilon}_p = \frac{4}{3} \frac{bN_m \Phi}{\sqrt{1+\Phi^2/C_s^2}}$$

$$\tau = \mu(\varepsilon - \frac{3}{2} \varepsilon_p)$$

$$\sigma_1 = P + \frac{4}{3} \tau \qquad (4.50)$$

$$P = f(\rho, E)$$

$$\varepsilon = \ell n \ (\rho/\rho_o)$$

where the symbols Φ, N_m are defined as

$$\Phi = \alpha_1(\tau - \tau_\mu) + \alpha_2(\tau - \tau_\mu)^2$$

$$N_m = \begin{cases} N_{m\infty} + (N_{mo} - N_{m\infty} + M_1\varepsilon_p^2)\exp(-A_1\varepsilon_p), & \text{for initial loading} \\ N'_{m\infty} + (N_{m*} - N'_{m\infty})\exp(-A_2\bar{\varepsilon}_p^2), & \text{for reverse loading} \end{cases}$$

and

$$\tau_\mu = \begin{cases} \tau_o\sqrt{1+a(\varepsilon_p)^m}, & \text{for initial loading} \\ -\tau_o\sqrt{1+a(\varepsilon_p)^m}\left[1-\exp(-\delta\sqrt{\varepsilon_p})\right], & \text{for reverse loading} \end{cases}$$

In the preceding equations, P denotes the thermodynamic pressure, ρ is the mass density, E represents the specific internal energy, and μ is the shear modulus.

Procedures for evaluating the coefficients which appear in the above equations have been described in previous sections, and the final results for 6061-T6 aluminum may be summarized as follows:

$$\begin{aligned} a &= 2.50 \\ m &= 0.5 \\ A_1 &= 180^* \\ M_1 &= 2\times10^{13}\ \text{cm}^{-2} \\ N_{mo} &= 1\times10^{8}\ \text{cm}^{-2} \\ N_{m\infty} &= 10\times10^{8}\ \text{cm}^{-2\,*} \\ \alpha_1 &= 5.6\times10^{3}\ \text{cm/sec/kbar} \\ \alpha_2 &= 9\times10^{5}\ \text{cm/sec/kbar}^2 \end{aligned} \qquad (4.51)$$

*See Section V.5 where revised values for A_1 and $N_{m\infty}$ are suggested for use in conjunction with finite-difference codes.

$$\tau_o = 1.39 \text{ kbar}$$
$$\delta = 20$$
$$A_2 = 1.2\times10^4 \qquad (4.51)$$
$$N'_{m\infty} = 5\times10^7 \text{ cm}^{-2}$$

In addition, the Burgers vector b was assigned the usual value for aluminum of $2.86\ 10^{-8}$ cm, the shear modulus was given the value μ = 277 kbar, and the shear wave velocity C_s was taken as 3.26×10^5 cm/sec.

In the present study the equation of state adopted was:

$$P = \begin{cases} (A\theta+B\theta^2+C\theta^3)\ (1 - \frac{G\theta}{2}) + G\rho E \text{ , for } \theta \geq 0 \\ \rho\left[H+(G-H)\eta^{\frac{1}{2}}\right]\ (E-E_s\{1-\exp[\frac{N}{\eta}(1 - \frac{1}{\eta})]\}), \text{ for } \theta < 0 \end{cases} \qquad (4.52)$$

where

$$\theta = \frac{\rho}{\rho_o} - 1 \qquad (4.53)$$
$$\eta = \frac{\rho}{\rho_o}$$

The constants appearing in the equation of state were assigned the following values:

ρ_o = 2.70 g/cm	C = 2008 kbar	
G = 2.13	H = 0.66	(4.54)
A = 728 kbar	N = 1.056	
B = 1313 kbar	$E_s = 1.2\text{x}10^{11}$ erg/g	

for 6061-T6 aluminum. The values of μ, C_s, A, B, and C given above were determined from experimental data furnished by Isbell, et al.[6]

V. NUMERICAL AND EXPERIMENTAL STUDIES OF THE PROPAGATION AND ATTENUATION OF STRESS WAVES, AND OF INCIPIENT SPALL PHENOMENA

In this section, the results of some numerical studies carried out with the RIP code, using the constitutive equation described in the preceding sections, are given. Qualitative features of computed loading and unloading wave profiles are examined, together with computed stress pulse attenuation, and comparisons of the computed results with experimental data are given. Finally, the influence of strain hardening, strain rate and Bauschinger effects on the calculation of incipient spall thresholds is discussed.

During plastic wave propagation, a material element may be subjected to a very wide range of strain rates. In order to give some graphic indication of how the present constitutive equation behaves over such a range, a plot of the constitutive relation for fixed values of the plastic strain is given in Fig. 12. Experimental data from Ref. 6 have been included to give some indication of how well the present constitutive model agrees with the data. Unfortunately, as noted earlier in the text, there is no direct experimental data on 6061-T6 aluminum for strain rates greater than 10^3 sec^{-1}. Aside from indirect experimental data - such as plastic wave profiles, precursor decay, etc. - the region of the graph above a strain rate of 10^3 sec^{-1} is experimentally unexplored. As this figure reveals, the proposed model is essentially rate-insensitive in the range of strain rates between 10^{-3} and $10^3 sec^{-1}$ in accord with the experimental data. Above a strain rate of about 10^4 sec^{-1}, the viscous terms in the constitutive equation begin to have some noticeable effect, and at the higher strain rates, the influence of the relativistic effect is clearly evident.

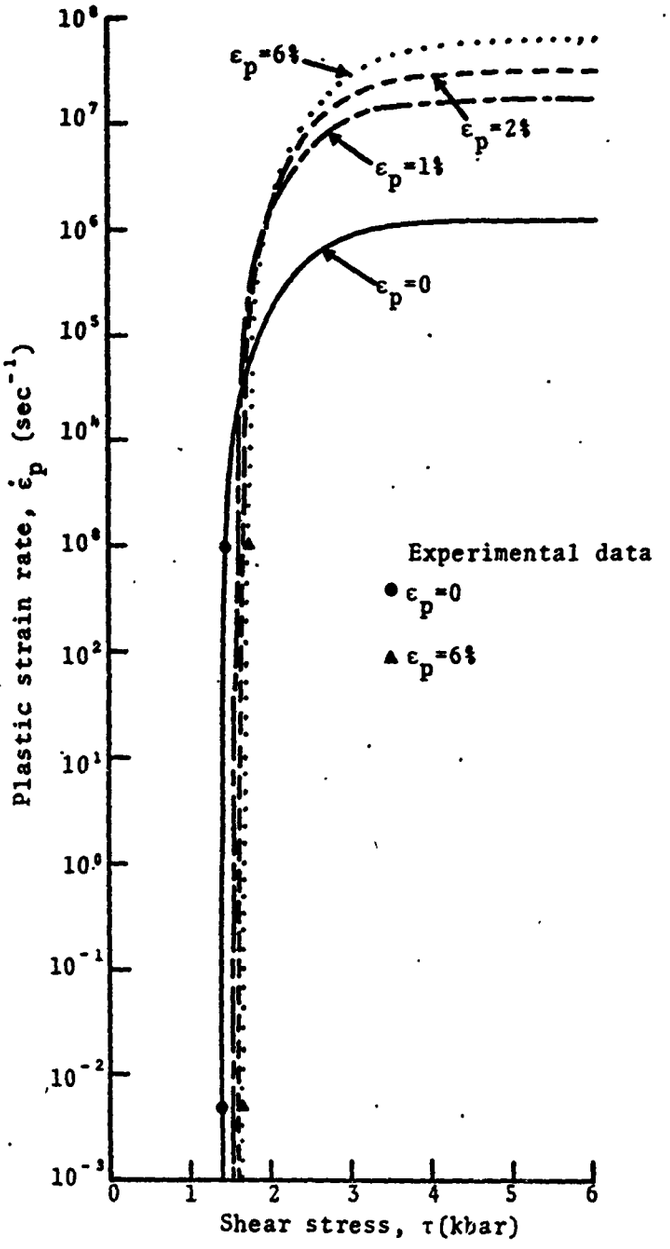

Figure 12. Compressive plastic strain rate-shear stress relationship for present constitutive model of 6061-T6 aluminum.

A. Transient Loading Waves

The results of numerical studies carried out on the impact problems corresponding to shots No. 16, 20 and 51 reported in Ref. 6 are discussed in this section. For convenience, the descriptive aspects of these three problems have been summarized below in Table II. In each case, the flyer plate and the target material was 6061-T6 aluminum, and the rear surface of the target was free.

Table II

Summary of Shots 16, 20 and 51[6]

Shot No.	Flyer Thickness (mm)	Target Thickness (mm)	Impact Velocity (mm/μsec)	Peak Stress (kbar)
16	1.875	3.124	0.257	20
20	1.488	3.132	0.523	40
51	1.483	3.073	0.155	12.5

In Fig. 13, a comparison of the computed and experimentally observed motion of the rear free-surface of the target caused by the reflection of the transient stress wave is shown for the three problems described above. The experimental data was obtained through the use of a laser interferometer. An inspection of Fig. 13 reveals that the present constitutive model predicts the dispersion of the plastic waves very well and, consequently, gives accurate rise times. It appears that the discrepancies between the computed and observed peak free surface velocities for shots No. 16 and 20 are due to uncertainties in the experimental data.* It is important to note that in

*In a private communication from W. Isbell, it was learned that there is some uncertainty in the experimental data shown in Fig. 13 near the top of the profiles for shots No. 16 and 20. It appears, however, that the experimental rise times in the plastic waves for these shots are accurate.

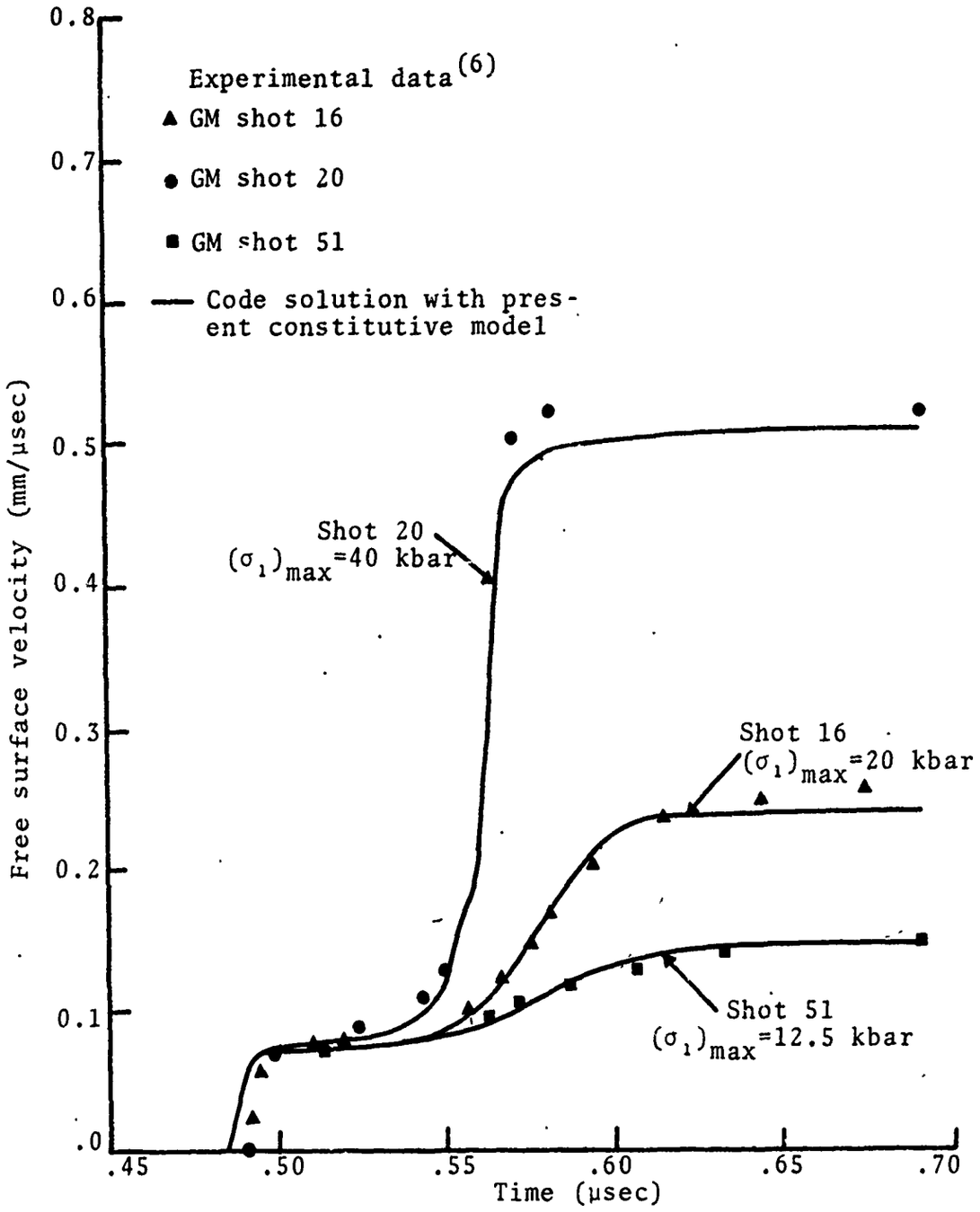

Figure 13. Comparison of computed and observed transient wave profiles in 6061-T6 aluminum.

order to achieve the agreement shown in Fig. 13, it was necessary to make changes in the values of A_1 and $N_{m\infty}$ determined from the steady wave analysis. Specifically, the values

$$A_1 = 60$$
$$N_{m\infty} = 4\times10^8 \text{ cm}^{-2} \tag{5.1}$$

were found to provide the best results, and they have been used in all the numerical studies reported in the sequel. The need for changes in these coefficients apparently arises from the fact that, in the finite-difference solutions, dispersion in the plastic wave occurs not only from the material viscosity and the imposed artificial viscosity, but also from the unavoidable inherent viscosity associated with error terms in the differencing scheme. The steady wave analysis, on the other hand, is not encumbered by such numerical artifacts; only the material viscosity is present. Consequently, in order to compensate in the finite-difference methods for the dispersion effects of numerical origin, less material viscosity than that indicated by the steady wave analysis must be used. Discrepancies between finite-difference methods and steady wave analysis have also been observed by others.*

B. Attenuated Wave Profiles

In order to examine the ability of the present constitutive model to predict the shape of thin attenuated stress pulses in 6061-T6 aluminum, several problems involving attenuated waves were studied numerically, and these results are reported in this section. These problems, for which Isbell, et al. have obtained experimental data, are reported as shots 110-112 in Ref.6. A summary of these shots is given below in Table III; in each

*Private communication with W. Herrmann, Sandia Laboratories.

case, the flyer plate and the target material was 6061-T6 aluminum and the target rear surfaces were free.

Table III

Summary of Shots 110, 111, and 112[6]

Shot No.	Flyer Thickness (mm)	Target Thickness (mm)	Impact Velocity (mm/μsec)	Peak Stress (kbar)
110	0.419	3.970	0.418	32.1
111	0.426	3.992	0.374	28.7
112	0.426	3.993	0.246	19.0

In Figs. 14-16, the numerical results for these problems are depicted, together with the corresponding experimental data and numerical results obtained using a simple elastic-plastic model. Although the combined flyer and target thickness was about the same in each case, the range of impact velocities covered by these three problems leads to considerable differences in the observed wave profiles. Incidentally, the impacts in shots 110 and 111 were intense enough to spall the target material, and the signal which emanated from the spalled region in these shots produced a reversal in the observed free surface velocity, as shown. In the numerical calculations, however, no spallation was permitted. Consequently, it is not meaningful to compare the computed results with the experimental data for shots 110 and 111 beyond the point (located approximately on the figures) where the spall signal first reached the free surface.

An examination of Figs. 14-16 shows that the numerical results based on the present constitutive model are in excellent agreement with the experimental data, and they provide significant improvement over the corresponding results for the simple elastic-plastic model. Perhaps the most apparent

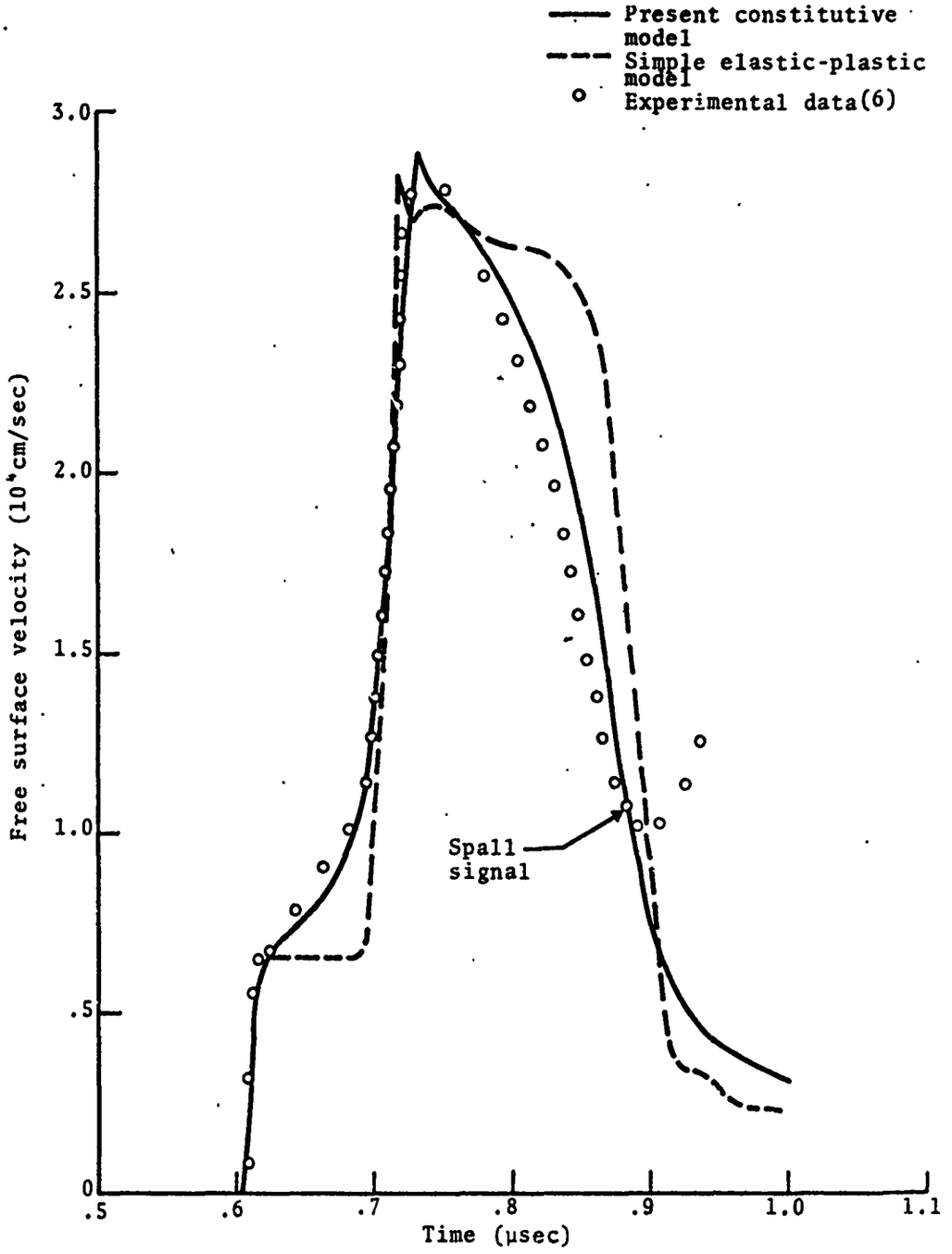

Figure 14. Comparison of computed and observed free surface velocity history for shot 110.

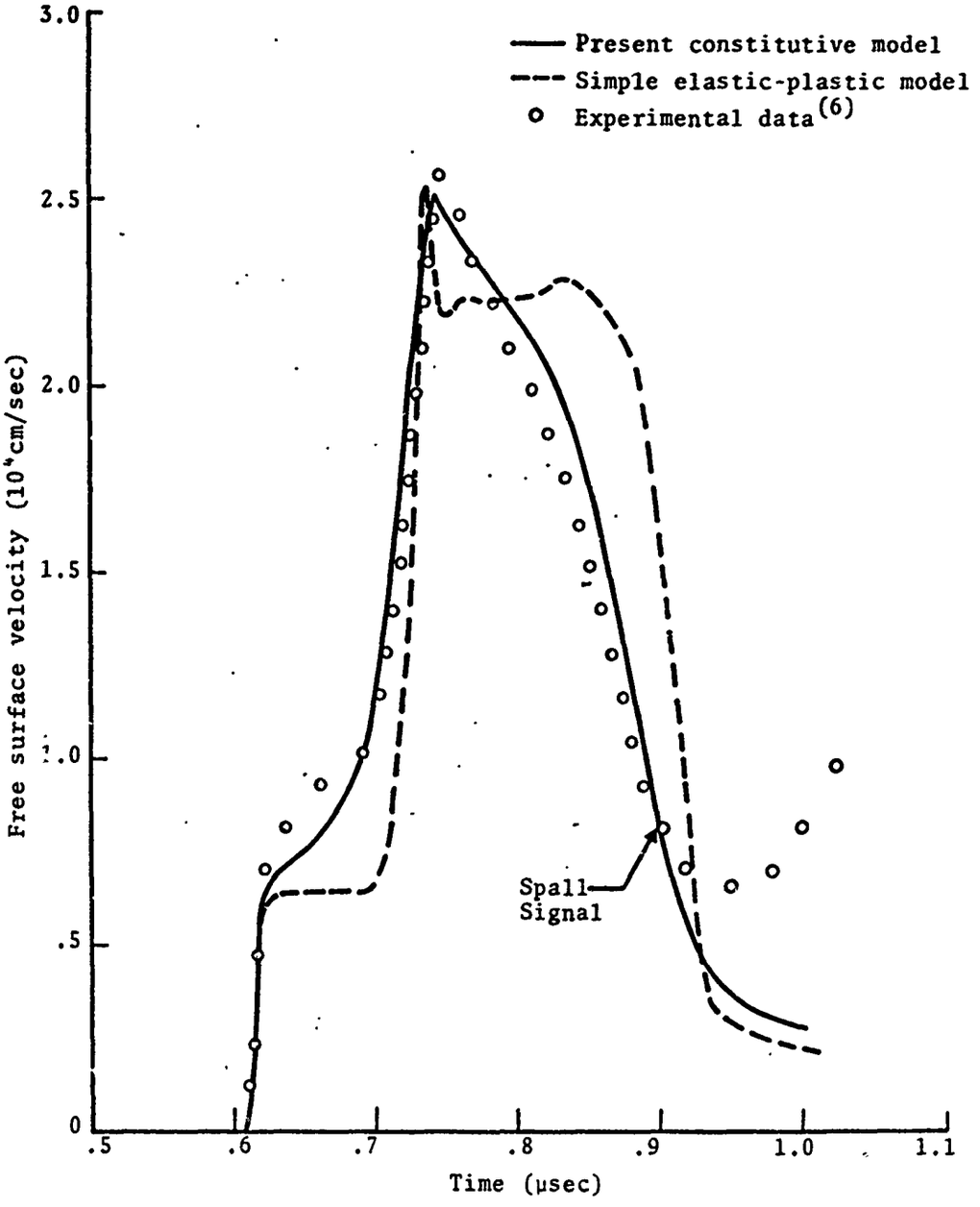

Figure 15. Comparison of computed and observed free surface velocity history for shot 111.

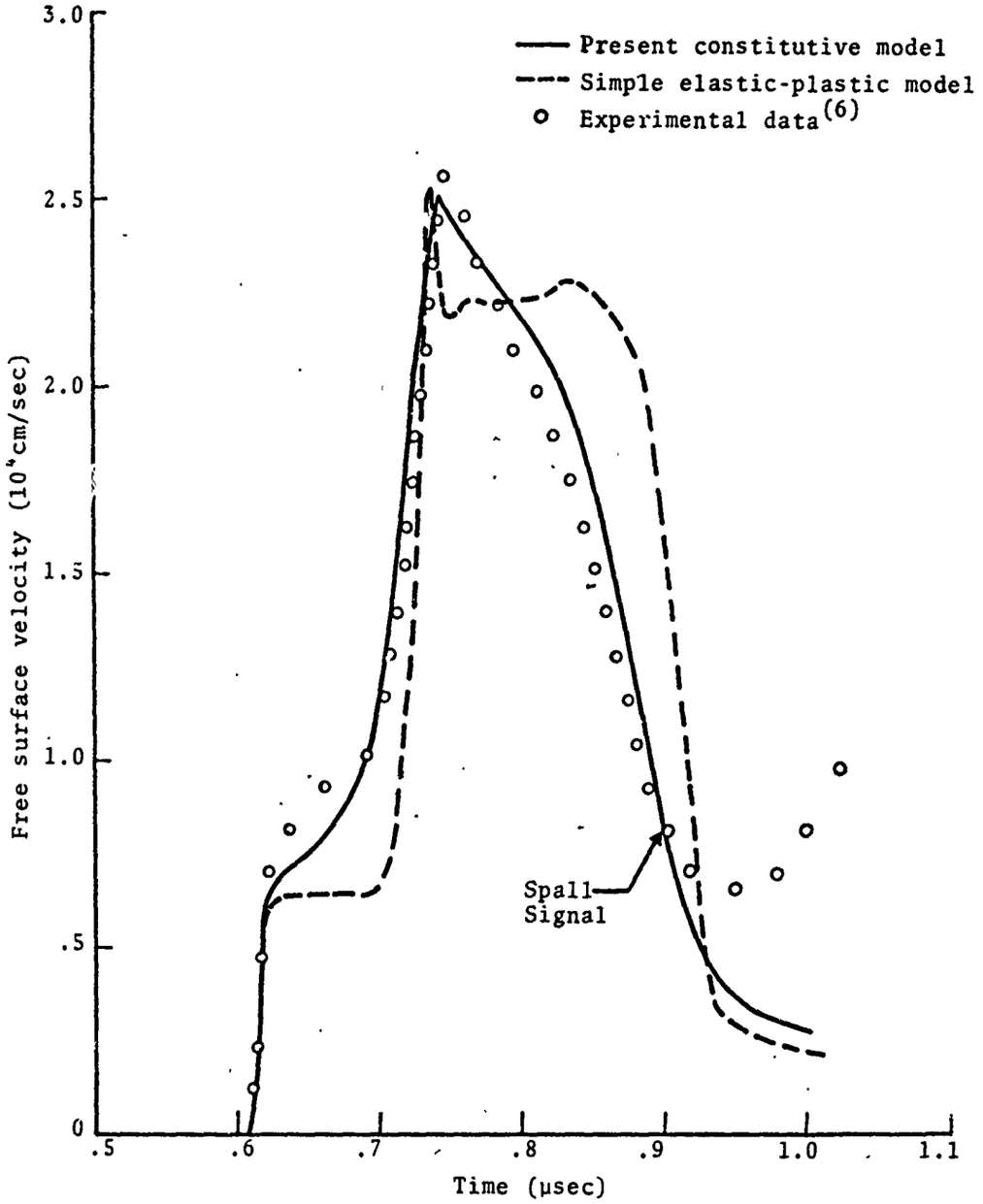

Figure 15. Comparison of computed and observed free surface velocity history for shot 111.

discrepancy between the results for the two models is in the shapes of the release waves, and this is most pronounced in shot 112. It appears that the approximate agreement between the computed peak free surface velocity for both models is fortuitous to some extent, inasmuch as the significant differences in the shapes of the release wave profiles for these models would undoubtedly lead to differences in peak stress for further attenuation.

C. High Pressure, Thin Pulse Attenuation

As a final proof-test of the constitutive model developed herein, the attenuation of a high pressure (102 kbar) thin stress pulse was calculated numerically and the results were compared with experimental data obtained by Isbell, et al. for shots 73, 74, and 79 reported in Ref. 6. In these experiments very thin 6061-T6 aluminum flyer plates backed by plexiglass were impacted at nearly identical velocities on 6061-T6 aluminum targets, of different thickness, backed by fused quartz. A summary of the important features of these shots is given in the following table:

Table IV

Summary of Shots 73, 74, and 79

Shot No.	Flyer Thickness* (mm)	Target Thickness* (mm)	Impact Velocity (mm/μsec)	Peak Stress (kbar)
73	0.269	2.520	1.242	103
74	0.252	5.067	1.238	102
79	0.252	1.029	1.235	102

*Thickness of the 6061-T6 aluminum portion only.

Numerical studies were carried out for the above shots using the present constitutive model for 6061-T6 aluminum and constitutive models for plexiglass and fused quartz given, respectively, in Refs. 63 and 62. The results of these numer-

ical studies together with the corresponding experimental data from Ref. 6 are shown in Fig. 17. Here, the calculated and observed particle-velocity history at the aluminum-fused quartz interface is depicted for the three target thicknesses studied. As an inspection of this figure will reveal, the agreement between the calculated and observed attenuation is excellent, as well as the agreement between the qualitative features of the wave profiles. The residual interface velocity of about 0.350 mm/μsec, which persists after the passage of the release portion of the stress pulse, is due primarily to the plexiglass backing on the flyer plate. It therefore appears that the present constitutive model can be used to accurately predict the attenuation of thin stress pulses in 6061-T6 aluminum for initial impact stresses of 100 kbar or less. No attempt to check on the ability of the present model to predict attenuation for initial stresses in excess of 100 kbar has been made in the present study.

In the next section we shall investigate the effect that the differences in dynamic response between the present model and the simple elastic-plastic model have on the calculation of incipient spallation thresholds in 6061-T6 aluminum.

D. Differences in the Evaluation of Spall Criteria Resulting from the Use of the Present Constitutive Model and the Simple Elastic-Plastic Model

The numerical studies of spallation in metals which have been reported in the past have been based, to the authors' knowledge, solely on the use of a simple elastic-plastic constitutive model. Because of this, questions inevitably arise regarding the extent to which the evaluation of particular spall criteria would be influenced by the use of a more realistic material model. In the case of most metals, there is reason to believe that the analysis of spall data for problems involving thin attenuated stress pulses would be the most sensitive to the constitutive description.

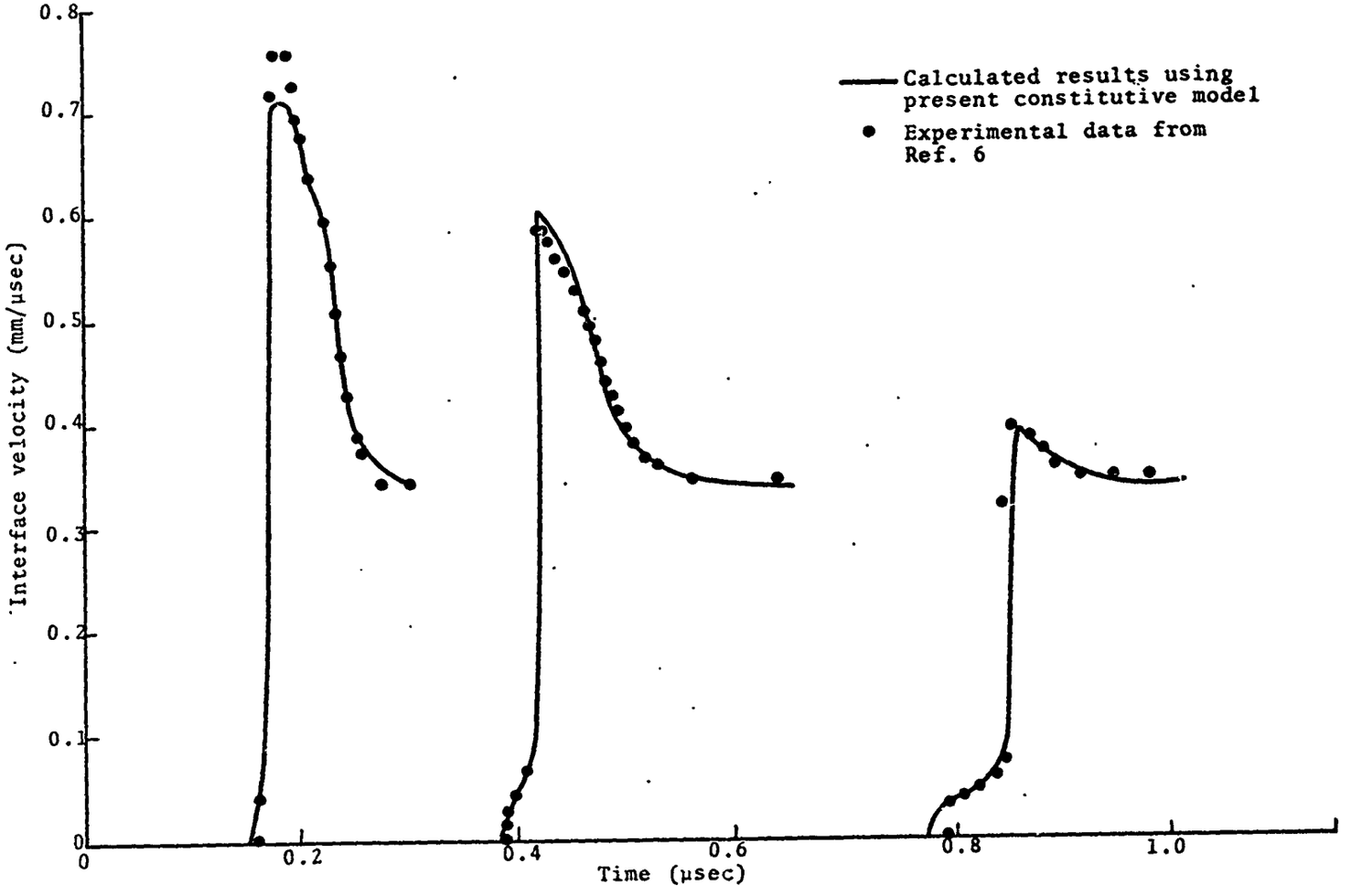

Figure 17. Thin stress pulse attenuation in 6061-T6 aluminum (initial impact stress of 102 kbar)

In an attempt to shed some light on this question, numerical studies were performed on two impact problems involving attenuated waves which resulted in incipient material damage to the target.* The details of these problems are described below in Table V.

Table V

Summary of Incipient Spall Problems

Problem No.	Thickness (cm)	Thickness (cm)	Velocity (mm/μsec)	Experimental Investigator
1	0.046	0.402	0.345	GM[6]
2	0.013	0.328	1.120	ETI[65]

With the exception of problem 2, where a Mylar flyer plate was used, the flyer plate and target material was 6061-T6 aluminum. The constitutive equation used in the numerical study for Mylar was taken from Ref. 63.

Using both the present constitutive model and the simple elastic-plastic model, two spall criteria were examined in the numerical studies. Attenuation was directed specifically to the cumulative damage criterion and the tensile strain criterion, since both of these have received attention recently in connection with 6061-T6 aluminum.[66-68]

1. The Cumulative Damage Criterion

The cumulative damage criterion, originally suggested by Tuler and Butcher[66] for use in conjunction with uniaxial strain configurations, is based on the consideration of a function F, defined at a point as

$$F(\sigma_1, t) = \int_0^{\Delta t} [\sigma_1 - (\sigma_1)_0]^{\lambda} dt, \quad \text{for } \sigma_1 \geq (\sigma_1)_0 \qquad (5.2)$$

*The results reported in this section represent only one aspect of the investigation of spall in metals carried out by S^3 under the PREDIX program; for additional results, see Ref.64.

Here, σ_1 denotes the tensile stress component in the direction of the only nonvanishing component of strain;* $(\sigma_1)_0$ is a (constant) tensile stress, below which fracture is not expected to occur on the time scales considered here; λ is a coefficient, and Δt represents the width of the tensile pulse at the stress level $\sigma_1 - (\sigma_1)_0$. The cumulative damage criterion states that spall will take place in the material at the point(s) where the function F equals or exceeds a critical value K. For incipient spall, the maximum value of the function F equals K.

An effort to correlate the currently available incipient spall data for 6061-T6 aluminum by the cumulative damage criterion has recently been reported by Fisher.[68] In this study it was found that the following values for the coefficients in the cumulative damage criterion

$$\begin{aligned} (\sigma_1)_0 &= 4.25 \text{ kbar} \\ \lambda &= 4.3 \\ K &= 2\text{-}3\times10^3 (\text{kbar})^{\lambda} \mu\text{sec} \end{aligned} \qquad (5.3)$$

provide the best correlation of the experimental spall data for 6061-T6 aluminum at room temperature. It should be noted that except for $(\sigma_1)_0$, the above values for the coefficients differ from those originally suggested in Ref. 66; however, much more experimental spall data for 6061-T6 aluminum was available at the time the above values of coefficients were determined than when Tuler and Butcher did their original analysis. In the work reported here, the coefficients were assigned the values listed above in Eq. (5.3).

A summary of the numerical results obtained in this study is given below in Table VI. Here, the computed values of (1) the peak tensile stress, $(\sigma_1)_{max}$, (2) the pulse width, Δt, at the stress level $\sigma_1 = (\sigma_1)_0$, (3) the maximum value of the function F, and (4) the distance x_s, between the front surface of the target and the predicted spall location are given for both material models.

*Following the sign convention adopted throughout Ref. 66, tensile stresses are taken as positive in this section.

Table VI

Summary of Results for Cumulative Damage Criterion

Problem No.	Peak Stress $(\sigma_1)_{max}$ (kbar)		Pulse Width Δt (μsec)		$F_{max} \times 10^{-3}$ (kbar$^{\lambda}$μsec)		Spall Location, x_s (cm)	
	PM*	SEPM**	PM	SEPM	PM	SEPM	PM	SEPM
1	15.4	15.4	0.221	0.199	2.72	2.74	0.329	0.343
2	16.1	19.9	0.132	0.124	1.65	4.73	0.280	0.295

*Present Model

**Simple Elastic-Plastic Model

The computed tensile stress histories at the predicted spall locations in problems 1 and 2 are shown in Figs.18 and 19. Here, the results for both the present constitutive model and the simple elastic-plastic model are depicted. A dashed line at the stress level σ = 4.25 kbar has been included on each of these figures to indicate the point at which the pulse widths given in Table V were determined.

An inspection of Table VI and Figs. 18 and 19 shows that the discrepancy between the calculated results for the two constitutive models is much greater in problem 2 than in problem 1. In problem 1, the results for each constitutive model are in reasonably good agreement with one another. As reference to Table VI will confirm, the calculated values of the peak tensile stress and the maximum of the function F are almost the same. Differences arise between the computed pulse widths and spall locations, but these are small, being on the order of 10%. It must therefore be concluded that at least for problem 1, the differences in the tensile stress histories evident in Fig. do not have a significant effect on the evaluation of the cumulative damage criterion.

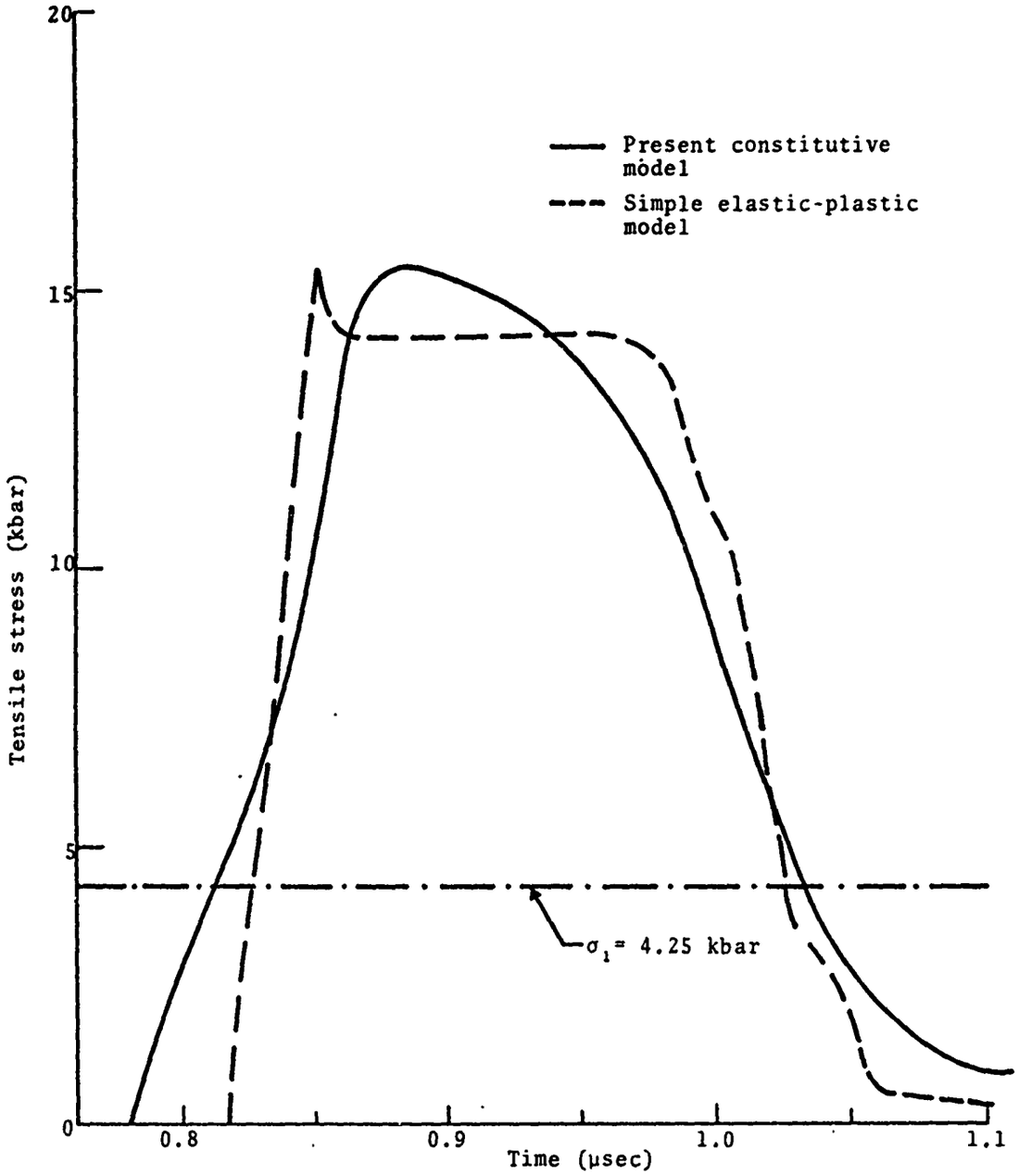

Figure 18. Comparison of tensile stress histories at predicted spall locations for problem 1.

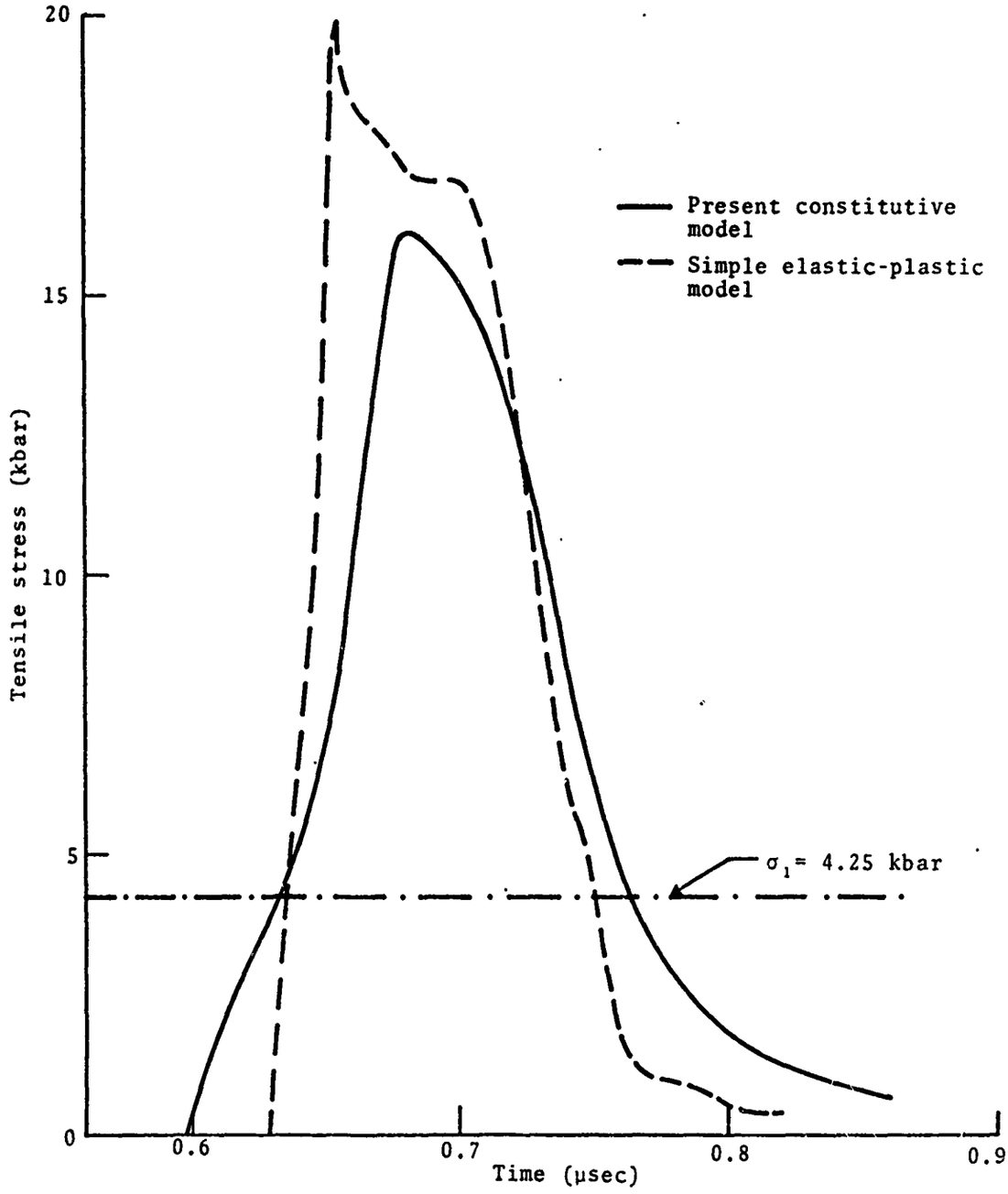

Figure 19. Comparison of tensile stress histories at predicted spall locations for problem 2.

In problem 2, the situation is considerably different. Significant differences which have bearing on the cumulative damage criterion arise in this problem. Of the two problems studied, problem 2 involves much greater stress attenuation and has the narrower tensile pulse width. The calculated peak tensile stresses in this problem differ by almost 24%, and the computed values of F_{max}, which depend strongly on the peak tensile stress, differ by nearly a factor of three. On the other hand, there is reasonable agreement between the computed pulse widths and spall locations.

The extent to which the use of the present constitutive model in the numerical studies modifies results obtained from the use of the simple elastic-plastic model is illustrated in Fig. 20. Here, the results obtained in the present study for problems 1 and 2 are shown together with previously reported spall results[6] for 6061-T6 aluminum.[68] Ideally, the points shown in Fig. 20 would fall on a horizontal line $F_{max} = K$ if the cumulative damage criterion correlated the data. Some of the observed scatter can, however, be attributed to the uncertainties involved in experimentally determining the incipient spall thresholds.

It should be emphasized that, with the exception of problems 1 and 2, the results shown in Fig.20 pertain entirely to experiments wherein the initial stress waves are unattenuated. Several of the unattenuated wave problems were reexamined using the present constitutive model and from this, very little change occurred in the results for these problems from that shown in the figure.

From this limited study, it appears that even in a material such as 6061-T6 aluminum which exhibits relatively small strain hardening and strain rate effects, significant differences can arise in the evaluation of the cumulative damage criterion, particularly in problems involving attenuated stress waves and thin stress pulses.

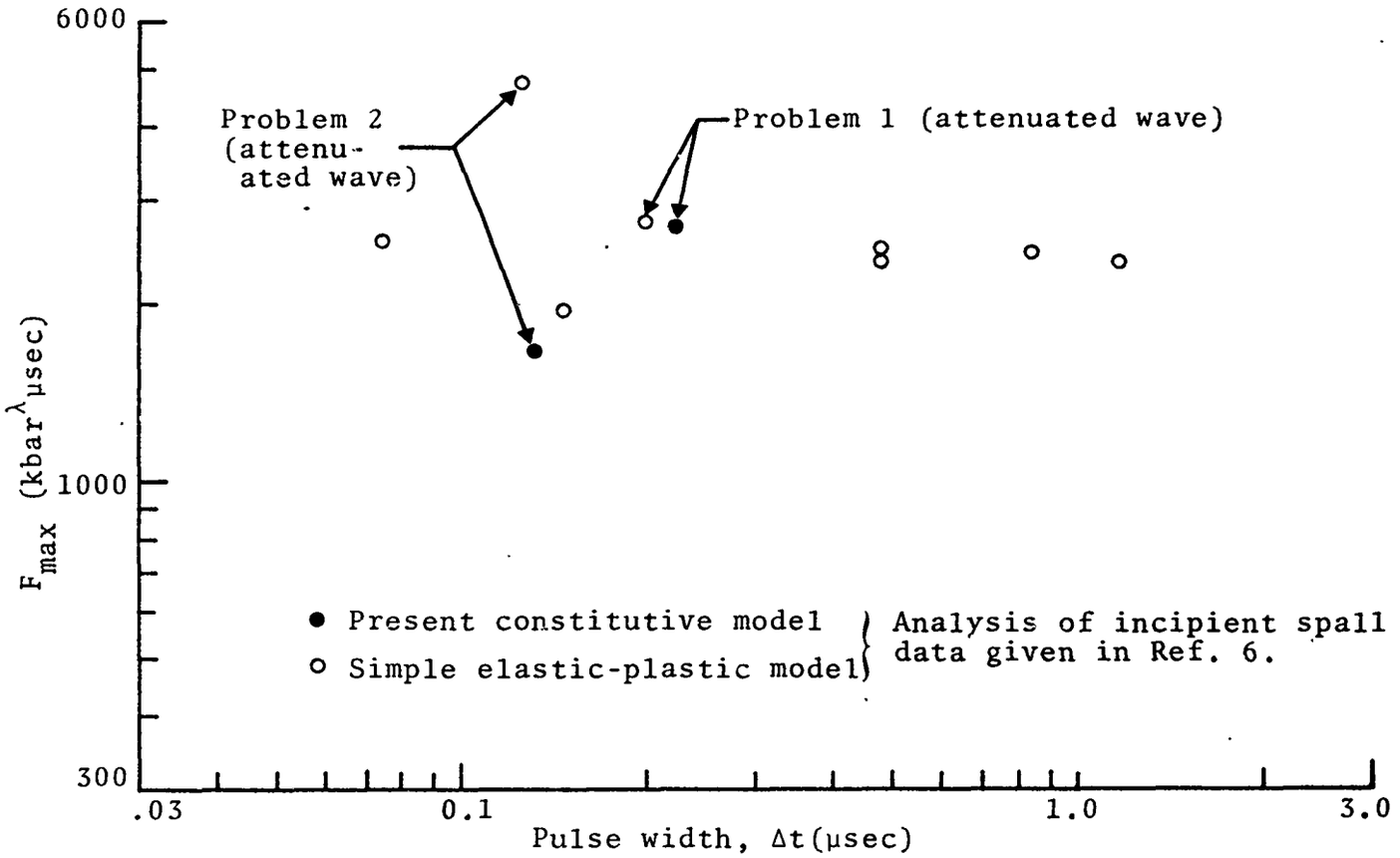

Figure 20. The effect of the constitutive description on the evaluation of the cumulative damage criterion for 6061-T6 aluminum.

2. The Tensile Strain Criterion

A spall criterion based on tensile strain has recently been proposed and applied to several metals by Tuler.[67] In this criterion, incipient spall is predicted at the positions(s) in the material where the tensile strain, ε_T, has its maximum absolute value, provided the following equation is satisfied:

$$(|\varepsilon_T|_{max})^{\lambda_1} \Delta t = K_1 \tag{5.4}$$

Here, $|\varepsilon_T|_{max}$ denotes the maximum of the absolute value of ε_T, Δt is the width of the tensile strain pulse, and λ_1, K_1 are coefficients.

To determine the sensitivity of this criterion to differences in the constitutive model for 6061-T6 aluminum, problems 1 and 2 were reexamined numerically, using both the present constitutive model and the simple elastic-plastic model. The important results of this study are summarized below in Table VII and depicted in Figs. 21-23.

Table VII

Summary of Results for Tensile Strain Criterion

Problem No.	$\|\varepsilon_T\|_{max}$		Pulse Width, Δt (μsec)		Spall Location, x_s (cm)	
	PM*	SEPM**	PM	SEPM	PM	SEPM
1	.0174	.0183	0.221	0.199	0.329	0.343
2	.0179	.0250	0.132	0.124	0.280	0.295

*Present Model

**Simple Elastic-Plastic Model

Due to the tailing off of the tensile strain beyond its peak value, the meaning of the term "pulse width" is somewhat

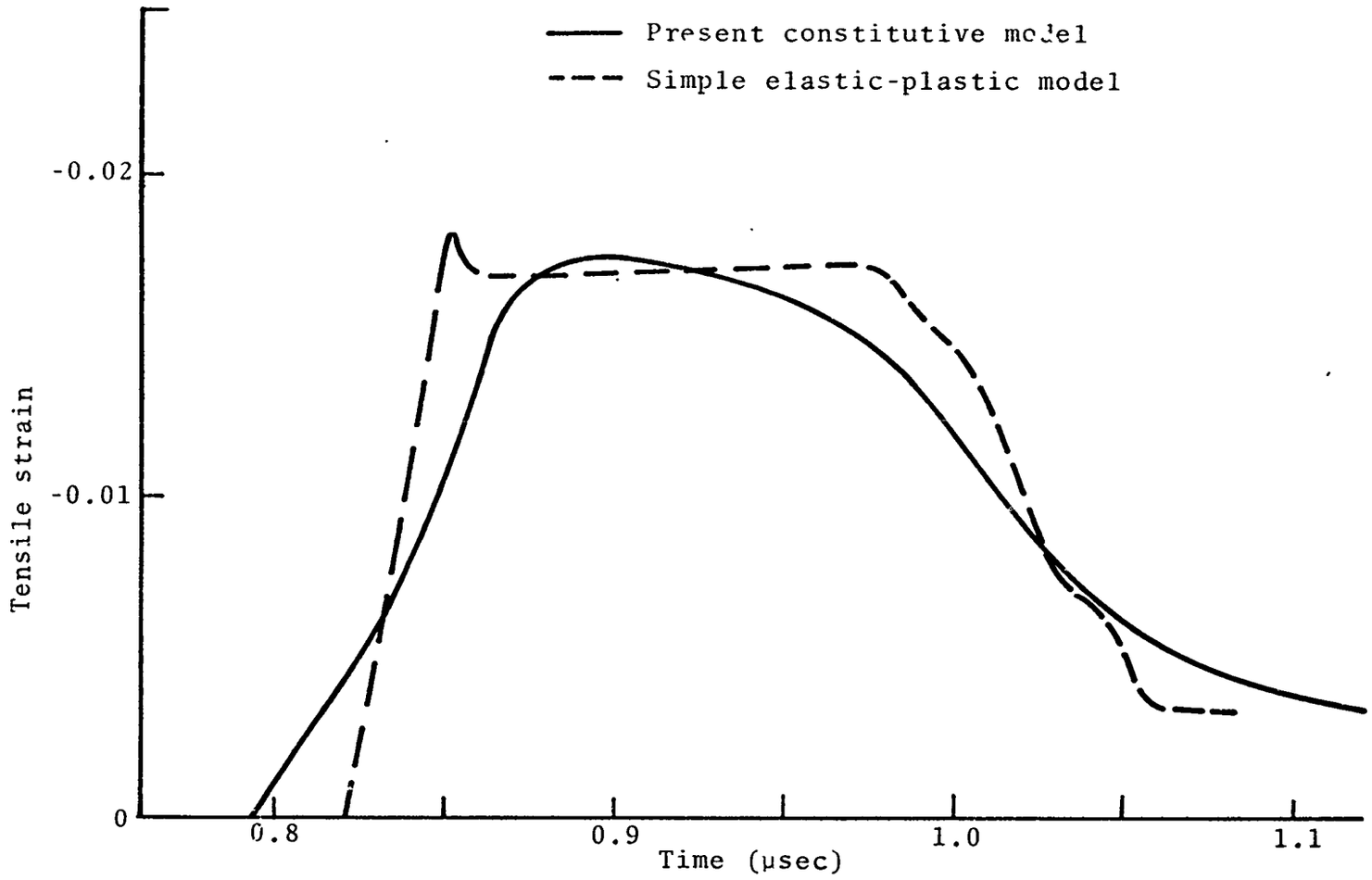

Figure 21. Comparison of tensile strain histories at predicted spall locations for problem 1.

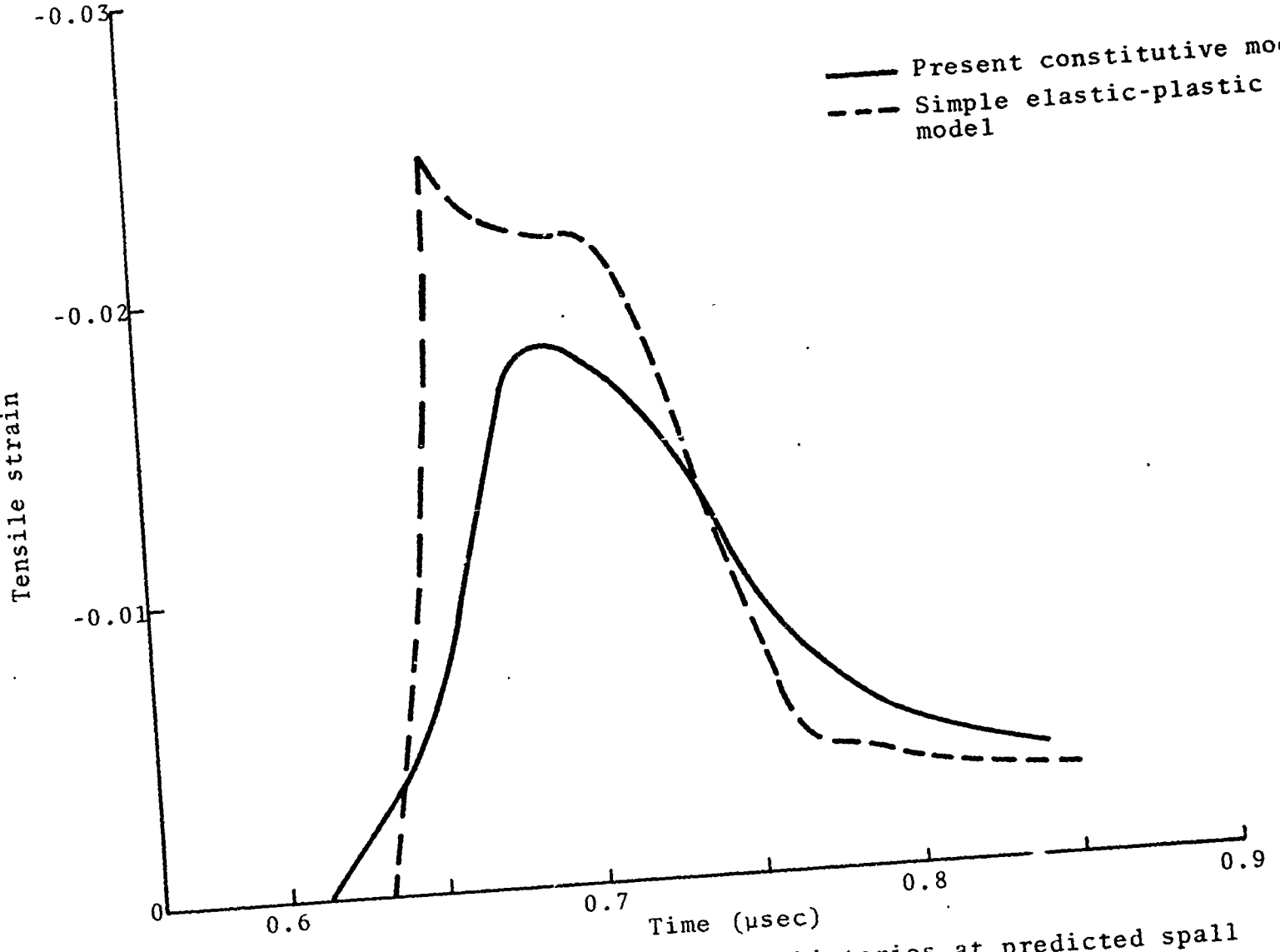

Figure 22. Comparison of tensile strain histories at predicted spall locations for problem 2.

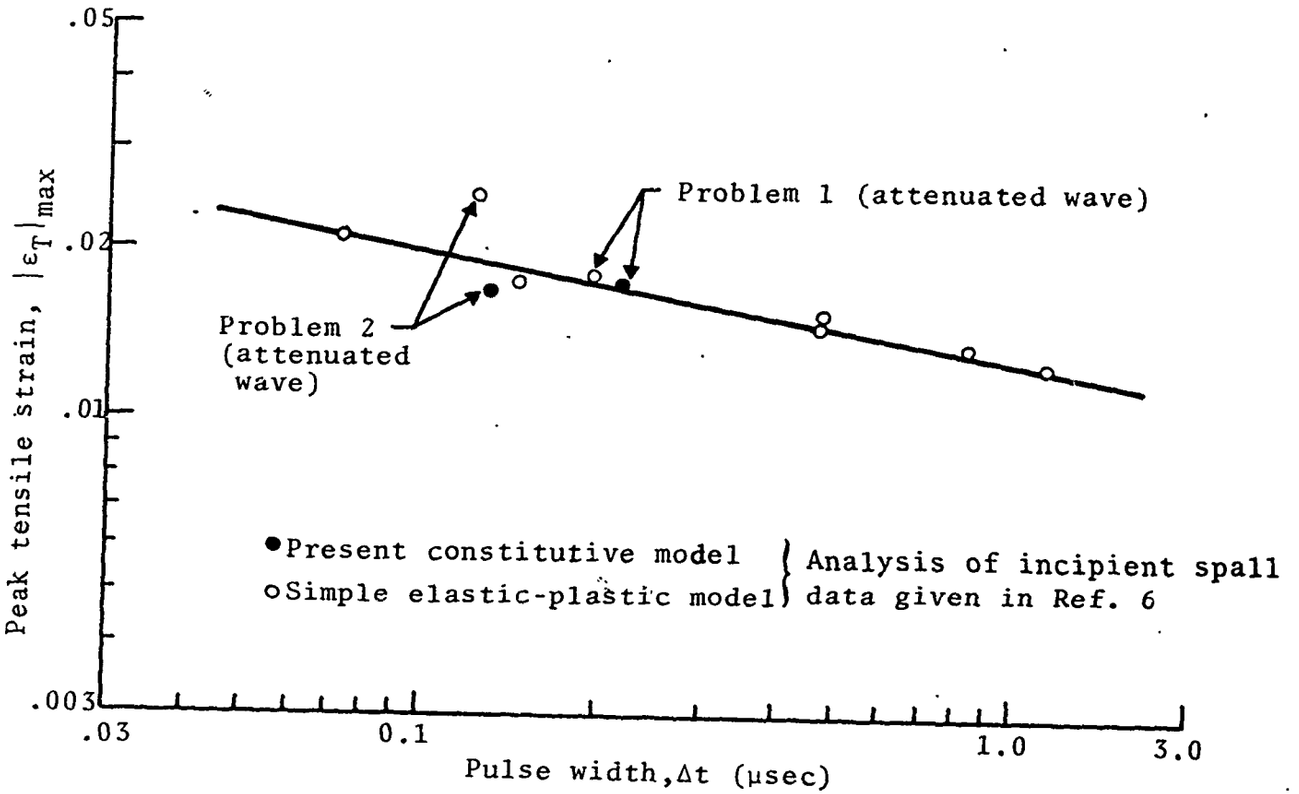

Figure 23. The effect of the constitutive description on the evaluation of the tensile strain criterion for 6061-T6 aluminum.

obscure, as reference to Figs. 21 and 22 will reveal. Because of this, we have used the width of the corresponding tensile stress pulse to correlate the spall results, and it is this pulse width which is listed in Table VII. In addition, the spall location, x_s, listed in Table VII represents the distance from the front surface of the target to the point in the target where the greatest tensile strain occurred.

The influence which the different material models have on the evaluation of the tensile strain criterion is illustrated in Fig. 23 where results previously reported in Ref. 67 are depicted together with the present results for problems 1 and 2. From this figure it is clear that the greatest discrepancy between the results for the two models occurs, as before, in problem 2, where the calculated peak tensile strains differ by almost 40%.

3. Closure

While there is at the present time no generally accepted criterion for spallation in metals, two criteria have been considered here which have received recent attention in connection with 6061-T6 aluminum, namely, the cumulative damage and tensile strain criteria. Numerical studies were carried out for several problems in which incipient material damage was observed to determine the sensitivity of the two spall criteria to differences in the constitutive model. For this purpose the present constitutive model, which accounts for strain hardening, strain rate, and a Bauschinger effect, and the simple elastic-plastic model, which neglects the above effects, were used in the numerical studies.

Compared with other metals, such as α-titanium, beryllium, and tantalum, 6061-T6 aluminum exhibits relatively small strain hardening and strain rate effects. Nevertheless, the present results indicate that the inclusion of strain hardening, strain

rate, and a Bauschinger effect in the constitutive model can have a significant effect on the evaluation of spall criteria for such a material, especially in problems involving attenuated waves and thin stress pulses.

VI. CONCLUSION

The present work was initiated with the goal of developing a constitutive model for use in computer codes which will provide a more realistic description of the dynamic response of metals than the simple elastic-plastic model. Throughout this study, the emphasis has been placed on high strain rate phenomena which accompany plastic wave propagation. Very little, however, is presently known about the micromechanical mechanisms that govern plastic flow at high strain rates. Present day experimental techniques for mapping the stress-strain-strain rate relationship for metals, e.g., the split Hopkinson bar, are generally limited to strain rates not exceeding 10^3 sec^{-1}. Because of this, there is no direct experimental data available in the range of strain rates of importance in plastic wave propagation, namely, 10^3-10^7 sec^{-1}. Thus it becomes necessary to resort to the use of indirect experimental data, such as elastic precursor decay and steady wave profiles, in order to gain some insight into the high strain rate plastic response of these materials.

An attempt has been made in the present work to utilize, whenever possible, current knowledge of dislocation theory in the formulation of the constitutive model. It is not the intent, however, to imply that the present model has physical significance at the microstructural level; as noted above, the micromechanical mechanisms that govern the mobility and multiplication of dislocations at high strain rates are not well understood at the present time. In most instances, only simple models of the mechanisms can be constructed and, even to accomplish this, considerable speculation is required. In other instances, where dislocation theory cannot provide guidance in defining and characterizing a particular plastic flow mechanism, a phenomenological approach has been followed.

On the basis of this philosophy, a constitutive model of metals has been developed which exhibits the following general features of plastic flow:

- strain hardening
- thermal activation
- a Bauschinger effect
- viscous drag
- dislocation multiplication and annihilation
- a limiting dislocation velocity (relativistic effect)

A numerical scheme for incorporating the constitutive model into one-dimensional finite-difference codes has been developed and implemented in the RIP code. A complete documentation of this scheme has been given in Ref. 69.

A procedure for evaluating the coefficients in the constitutive model for a given material has been described and specifically illustrated for 6061-T6 aluminum at room temperature. In this case, the types of experimental data required to evaluate the coefficients in the model were:

- quasi-static stress-strain curves and elastic moduli
- precursor decay curves
- plastic loading wave profiles
- plastic release wave profiles

When the effect of thermal activation on the high strain rate response cannot be disregarded, as was possible in the case of 6061-T6 aluminum studied here, additional experimental data are required before the thermal component of the strain rate dependent portion of the shear stress can be isolated from the viscous drag component. This can be accomplished, however,

in a rather straightforward manner with a uniaxial stress machine through tests involving both strain rate changes at constant temperature and temperature changes at constant strain rate (see Ref. 70).

Although 6061-T6 aluminum does not exhibit large strain hardening and strain rate effects at room temperature compared with most metals of current interest in reentry vehicle design, the evaluation of spall criteria for this material was found to be sensitive to the inclusion of strain rate, strain hardening, and a Bauschinger effect in the constitutive description; this was particularly true in problems involving very thin attenuated stress pulses, which are the type expected to arise in a material suddenly exposed to nuclear radiation. There is reason to believe that spall criteria which depend on either the stress gradient, stress rate, or strain rate may be influenced even more strongly by the constitutive description than the two criteria examined here. Therefore, in materials which exhibit greater strain hardening and strain rate effects than 6061-T6 aluminum, the simple elastic-plastic model may be unreliable for use in spall studies; when this is the case, a more realistic constitutive model will be required before meaningful analysis of spall results can be made.

As noted in the beginning, the effects of temperature changes and heating rate on the constitutive relation have not been considered in the present study. The sudden exposure of a metal component to radiation, however, can produce increases in the temperature of the component large enough to affect its dynamic response. It is well-known that metals show increased strain rate sensitivity as the temperature is raised. Because of this, the discrepancy between actual material behavior and that predicted with the simple elastic-plastic model can be expected to become increasingly greater as the temperature increases. At elevated temperatures, the need for a more realistic constitutive model becomes even more important.

REFERENCES

1. Herrmann, W., "Non-linear Stress Waves in Metals," ASME Symposium on Wave Propagation in Solids, Los Angeles, Nov. 1969.

2. Jones, O.E., F.W. Neilson, and W.B. Benedick, "Dynamic Yield Behavior of Explosively Loaded Metals Determined by a Quartz Transducer Technique," J. Appl. Phys. 33, 1962, p.3224.

3. Taylor, J.W., and M.H. Rice, "Elastic-Plastic Properties of Iron," J. Appl. Phys. 34, 1963, p.364.

4. Barker, L.M., B.M. Butcher, and C.H. Karnes, "Yield-Point Phenomenon in Impact-Loaded 1060 Aluminum," J. Appl. Phys. 37, 1966, p.1989.

5. Karnes, C.H., Symposium on the Mechanical Behavior of Materials under Dynamic Loads, San Antonio, Texas, 1967.

6. Isbell, W.M., D.R. Christman, S.G. Babcock, T.E. Michaels, and S.J. Green, "Measurements of Dynamic Properties of Materials: Results for Metals," Materials and Structures Laboratory, General Motors Technical Center, 1970.

7. Barker, L.M., C.D. Lundergan, and W. Herrmann, "Dynamic Response of Aluminum," J. Appl. Phys. 35, 1964, p.1203.

8. Hartman, W.F., "Determination of Unloading Behavior of Uniaxially Strained 6061-T6 Aluminum from Residual Strain Measurements," J. Appl. Phys. 35, 1964, p.2090.

9. Erkman, J.O., and A.B. Christensen, "Attenuation of Shock Waves in Aluminum," J. Appl. Phys. 38, 1967, p.5395.

10. Curran, D.R., "Nonhydrodynamic Attenuation of Shock Waves in Aluminum," J. Appl. Phys. 34, 1963, p.2677.

11. Barker, L.M., "Fine Structure of Compression and Release Wave Shapes in Aluminum Measured by the Velocity Interferometer Technique," Proc. Sym. on Behavior of Dense Media Under High Dynamic Pressure, Paris, Sept. 1967.

12. Herrmann, W., R.J. Lawrence, and D.S. Mason, "Effect of Strain Hardening and Strain Rate in Elastic-Plastic Wave Propagation," presented at Nuclear Survivability Working Group on Propulsion and Ordnance Systems, Kirtland AFB, New Mexico, December 1969.

13. Dorn, J.E., J. Mitchell, and F. Hauser, "Dislocation Dynamics," Experimental Mechanics, November 1965, p.1.

14. Taylor, J.W., "Dislocation Dynamics and Dynamic Yielding," J. Appl. Phys. 36, 1965, p. 3146.

15. Gilman, J.J., "Progress in the Microdynamical Theory of Plasticity," Proc. Fifth U.S. National Congredd Applied Mechanics, 1966.

16. Wilkins, M.L., "Le Calcul de la Resistance Dynamique d'un Materiau," IUTAM Symp. High Dynamic Pressure, Paris, 1967.

17. Johnson, J.N., and L.M. Barker, "Dislocation Dynamics and Steady Plastic Wave Profiles in 6061-T6 Aluminum," J. Appl. Phys. 40, 1969, p.4321.

18. Jones, A.H., C.J. Maiden, and W.M. Isbell, "The Effect of High-Pressure Shock Waves on Metals: Mechanical and Metallurgical Behavior," Mechanical Behavior of Materials Under Pressure, H.L1.E. Pugh, Ed., Elsevier Publishing Co. (in press).

19. Nolder, R.L., and G. Thomas, "The Substructure of Plastically Deformed Nickel," Acta Met. 12, 1964, p.227.

20. Tegart, W.J.M., Elements of Mechanical Metallurgy, Macmillan Co., New York, 1966.

21. Johari, O., and G. Thomas, "Substructure of Explosively Loaded Cu and Cu-Al Alloys," Acta Met. 12, 1964, p.1153.

22. Kaybyshev, O.A., "Dislocation Structure of Copper after High-Velocity Deformation," Fiz. Met. Metalloved 23, 1967, p.505.

23. Gilman, J.J., "Dislocation Dynamics and the Response of Materials to Impact," Appl. Mechs. Rev. 21, 1968, p.767.

24. Klassen-Neklyudova, M.V., Mechanical Twinning of Crystals, Consultants Bureau, Inc., New York, 1964.

25. Deformation Twinning, Gordon and Breach Co., New York, 1964.

26. Johnson, J.N., "Constitutive Relation for Rate-Dependent Plastic Flow in Polycrystalline Metals," J. Appl. Phys. 40, 1969, p.2287.

27. Argon, A.S., "Dislocation Dynamics," Mat. Sci. and Engrg. 3, 1968/1969, p.24.

28. Gilman, J.J., "Dynamical Dislocation Theory of Crystal Plasticity. II. Easy Glide and Strain Hardening," J. Appl. Phys. 36, 1965, p.3380.

29. Akulov, N.S., "On Dislocation Kinetics," Acta Met. 12, 1964, p.1195.

30. Seeger, A., Dislocations and Mechanical Properties of Crystals, John Wiley, New York, 1957.

31. Conrad, H., "Thermally Activated Deformation of Metals," J. Metals, 1964, p.582.

32. Kumar, A., F.E. Hauser, and J.E. Dorn, "Viscous Drag on Dislocations in Aluminum at High Strain Rates," Acta Met. 16, 1968, p.1189.

33. Wiedersich, H., "Hardening Mechanisms and the Theory of Deformation," J. Metals, 1964, p.425.

34. Conrad, H., "The Cryogenic Properties of Metals," in High Strength Materials, John Wiley, New York, 1964.

35. Gilbert, A., B.A. Wilcox, and G.T. Hahn, "The Effect of Strain Rate on Dislocation Multiplication in Polycrystalline Molybdenum," Phil. Mag. 12, 1965, p.649.

36. Kressel, H., and N. Brown, "Lattice Defects in Shock-Deformed and Cold-Worked Nickel," J. Appl. Phys. 38, 1967, p.1618.

37. Conrad, H., and H. Wiedersich, "Activation Energy for Deformation of Metals at Low Temperatures," Acta Met. 8, 1960, p.128.

38. Dorn, J.E., "Low-Temperature Dislocation Mechanisms," in Dislocation Dynamics, McGraw-Hill, New York, 1968.

39. Ferguson, W.G., "Dislocation Damping in Aluminum at High Strain Rates," J. Appl. Phys. 38, 1967, p.1863.

40. Dharan, C.K. Hari, "The Dynamic Behavior of Aluminum at High Strain Rates," (Doctoral Dissertation, Univ. of Calif. Berkeley), published as UCRL Report 18549, 1968.

41. Frank, F.C., Proc. Phys. Soc. (London), A62, 1969, p.131.

42. Eshelby, J.D., Proc. Phys. Soc. (London), A62, 1949, p.307.

43. Weertman, J., "High Velocity Dislocations" in Response of Metals to High Velocity Deformation, Interscience, 1961.

44. Gillis, P.P., J.J. Gilman, and J.W. Taylor, "Stress Dependences of Dislocation Velocities," Phil. Mag. 1969, p.187.

45. Lindholm, U.S., "Some Experiments in Dynamic Plasticity Under Combined Stress," Symp. Mech. Behavior of Matls. Under Dynamic Loads, San Antonio, September 1967.

46. Nevill, G.E., and C.D. Myers, "Strain Rate Effects During Reverse Loading," J. Mechs. and Phys. of Solids 16, 1968, p.187.

47. Mott, N.F., "The Behavior of Metals Under Reversed Stresses," in Dislocations and Mechanical Properties of Crystals, John Wiley and Co., New York, 1957.

48. Milligan, R.V., and W.H. Koo, "The Bauschinger Effect in Copper and Copper-Zinc Alloys," Watervliet Arsenal, Report WVT-7022, May 1970.

49. Duwez, P., "On the Plasticity of Crystals," Phys. Rev. 47, 1935, p.494.

50. Mróz, Z., "On the Description of Anisotropic Work Hardening," J. Mechs. Phys. Solids 15, 1967, p.163.

51. Como, M., and S. D'Agostini, "Strain Hardening Plasticity with a Bauschinger Effect," Meccanica 4, 1969, p.146.

52. Lubliner, J., "A Generalized Theory of Strain-Rate Dependent Plastic Wave Propagation in Bars," J. Mechs. Phys. Solids 12, 1964, p.59.

53. Holt, D.L., S.G. Babcock, S.J. Green, and C.J. Maiden, "The Strain Rate Dependence of the Flow Stress in Some Aluminum Alloys," Trans. of the ASM 60, June 1967.

54. Fowles, G.R., "Shock Wave Compression of Hardened and Annealed 2024 Aluminum," J. Appl. Phys. 32, 1961, p.1475.

55. Maiden, C.J., and S.J. Green, "Compressive Strain-Rate Tests on Six Selected Materials at Strain Rates from 10^{-3} to $10^{4}sec^{-1}$, J. Appl. Mechs. 1966.

56. Duvall, G.E., "Propagation of Plane Shock Waves in a Stress-Relaxing Medium," in Stress Waves in Anelastic Solids, Springer-Verlag, New York, 1964.

57. Ahrens, T.J., and G.E. Duvall, "Stress Relaxation Behind Elastic Shock Waves in Rocks," J. Geo. Res. 71, 1966, p.4349.

58. Johnson, J.N., and W. Band, "Investigation of Precursor Decay in Iron by the Artificial Viscosity Method," J. Appl. Phys. 38, 1967, p.1578.

59. Herrmann, W., D.L. Hicks, and E.G. Young, "Attenuation of Elastic-Plastic Stress Waves," paper presented at the 17th Sagamore Conference on Shock Waves and Mechanical Properties of Solids, Raquette Lake, New York, September 1970.

60. Band, W., "Studies in the Theory of Shock Propagation in Solids," J. Geophys. Res. 65, 1960, p.695.

61. Band, W., and G.E. Duvall, "Physical Nature of Shock Propagation," Am. J. Phys. 29, 1961, p.780.

62. Barker, L.M., and R.E. Hollenbach, "Shock Wave Studies of PMMA, Fused Silica, and Sapphire," report SC-DC-70-4655, Sandia Laboratories, Albuquerque, 1970.

63. Kohn, B.J., "Compilation of Hugoniot Equations of State," Air Force Weapons Laboratory,report AFWL-TR-69-38, 1970.

64. Kruger, R.A., R.H. Fisher, H.E. Read, and J.R. Triplett, "A Theoretical Investigation of the Dynamic Response of Metals," Systems, Science and Software,report No. 3SR-308, December 1970.

65. Keller, D.V., and F.R. Tuler, "PREDIX Metals Report," Effects Technology, Inc., report CR-70-06, 1970.

66. Tuler, F.R., and B. Butcher, "A Criterion for the Time Dependence of Dynamic Fracture," Int. J. Frac. Mechs. 4, 1968, p.431.

67. Tuler, F.R., "Tensile Strain as a Criterion for Spallation in Metals," paper presented at 17th Sagamore Conference on Shock Waves and Mechanical Properties of Solids, Raquette Lake, N.Y., September 1970.

68. Fisher, R.H., R.A. Kruger, and H.E. Read, "Summary of S^3 Presentation," Minutes of the Sixth PREDIX Meeting, Effects Technology, Inc., report ETI-CR-69-11, November 1969.

69. Fisher, R.H., R.A. Cecil, and G.A. Lane, "RIP, A One-Dimensional Material Response Code," Systems, Science and Software (in preparation).

70. Conrad, H., "Thermally Activated Deformation of α-Titanium Below 0.5 T_m," Canadian J. of Phys. 45, 1967, p.581.

APPENDIX

AN ALTERNATIVE BAUSCHINGER MODEL

An alternative approach for treating the rate-independent shear stress component, τ_μ, during reversed straining of metals which exhibit a Bauschinger effect is presented in this appendix. The approach described here is motivated largely by ideas presented initially by Duwez[49] and later by Mróz[50]; it differs from the approach discussed earlier in the text in that (1) it is based on concepts of pure kinematic hardening and (2) it completely prescribes the reverse-loading path directly from the initial loading path. In other words, when the dependence of τ_μ on ε_p for initial plastic loading has been determined, the reverse loading path is set; no additional parameters are required to specify the reverse loading path for this model. Models similar to this have been applied by Duwez[49] and Herrmann, et al.[12] to describe reverse loading behavior in copper and aluminum, respectively.

To further amplify the preceding ideas, let us turn to Fig. 24, where the dependence of τ_μ on ε_p for the alternative Bauschinger model is depicted. We shall describe the deformation process and the model as one traverses the path a-b-c-d-e shown in this figure. Between points 0 and a, elastic loading takes place with a corresponding increase in the magnitude of τ_μ from zero to τ_0, the initial yield shear stress. Plastic loading occurs between a and b, where the increase in τ_μ due to strain hardening is given by some expression of the form

$$\tau_\mu = f(\varepsilon_p) \qquad (A.1)$$

where the function f is taken in the present work to have the form

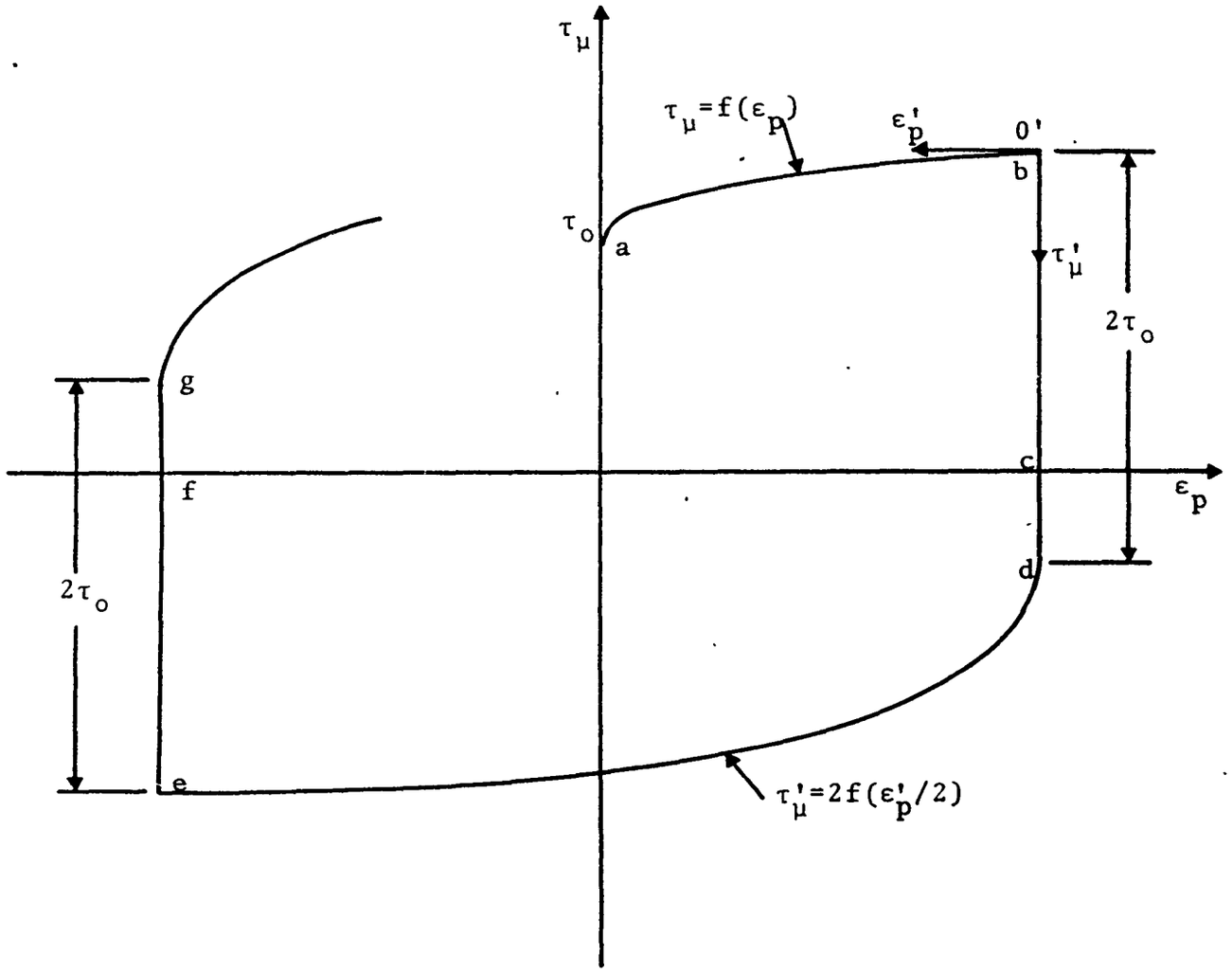

Figure 24. Dependence of τ_μ on ε_p for the alternative Bauschinger model.

$$f = \tau_0 \sqrt{1 + a(\varepsilon_p)^m} \ , \qquad (A.2)$$

in accordance with Eq. (3.18). At point b, elastic unloading begins and the stress τ_μ decreases elastically to zero with no change in the plastic strain. Reverse loading of τ_μ occurs elastically between c and d and, at point d, reverse plastic flow is initiated. Following Duwez and Mroz, the shear stress at which reverse plastic flow first occurs in this model (point d) is determined by subtracting the quantity $2\tau_0$ from the value of τ_μ reached at the end of the initial loading process. Let us note parenthetically that this feature of the model is acceptable from the thermodynamical standpoint only so long as the reverse yield point (point d) falls in the region $\tau_\mu \leq 0$; if the drop of $2\tau_0$ from point b should place point d in the region $\tau_\mu > 0$, the subsequent unloading process would lead to negative plastic work and, therefore, prove to be unacceptable thermodynamically. Consequently, the use of this model appears to be restricted to the range of initial plastic deformations for which point d falls within the region $\tau_\mu \leq 0$. Returning now to Fig. 24, τ_μ follows a strain hardening path between d and e during reverse loading which is described by the expression

$$\tau'_\mu = 2f(\varepsilon'_p/2) \qquad (A.3)$$

where the primes refer to the coordinate system centered at point b (as shown), and f denotes the function used to prescribe the initial loading path, which was given earlier in Eq. (A.2). Because this model is based on pure kinematic hardening, the path e-f-g-b is similar to the path b-c-d-e and the hysteresis loop will be closed, as shown.

A comparison of the reverse loading paths determined from this model with the corresponding experimental paths for several values of plastic prestrain is shown in Fig. 25 for 6061-T6 aluminum. The experimental curves are the same as those which

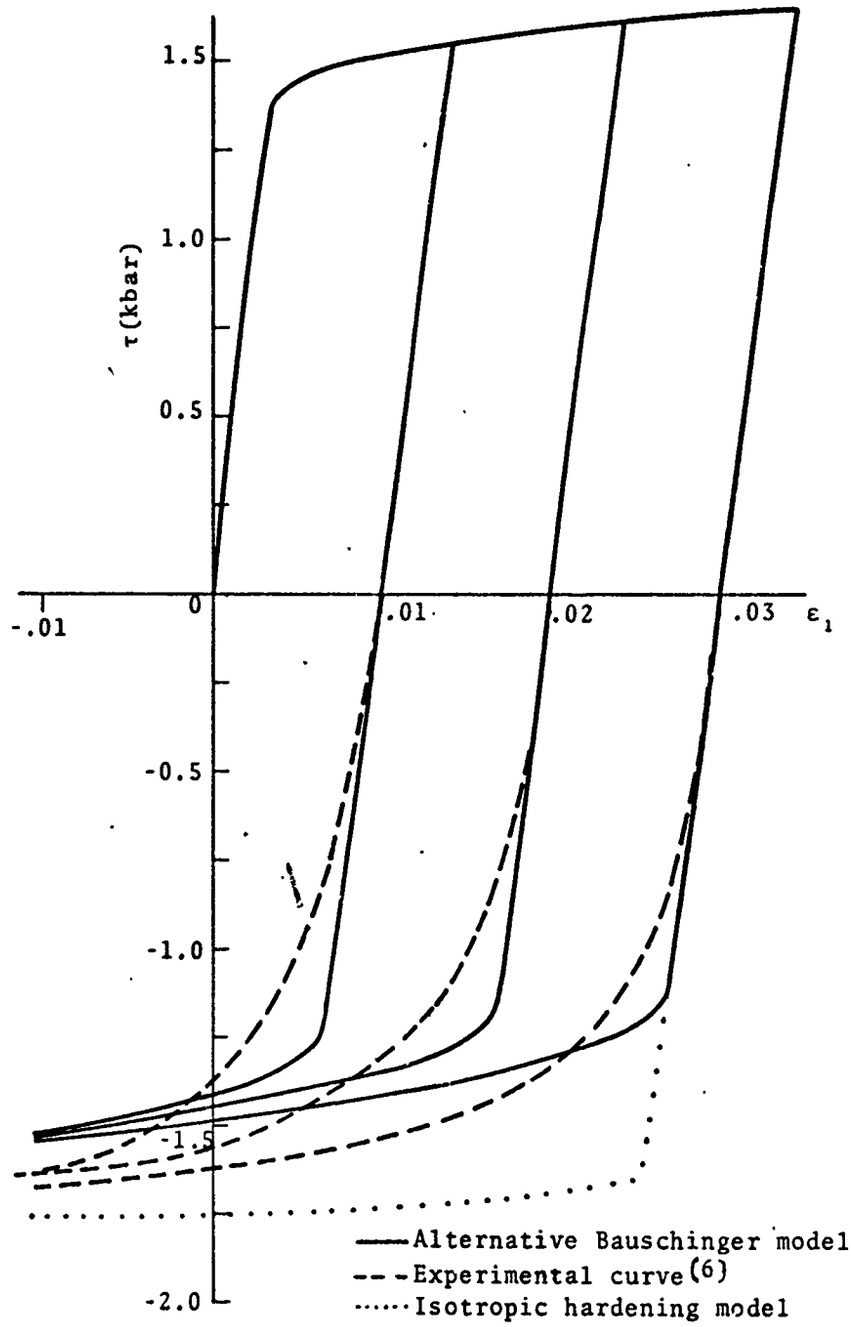

Figure 25. Comparison between the reverse loading paths determined by the alternative Bauschinger model and those determined experimentally for several values of plastic prestrain in 6061-T6 aluminum.

were given earlier in Fig. 7 and they were determined by Isbell, et al.[6] from uniaxial stress tests carried out under quasi-static conditions. For purposes of comparison, the reverse loading path predicted by an isotropic hardening model for a plastic prestrain of 0.03 is also shown on this figure. As a comparison of Figs. 7 and 25 will reveal, the Bauschinger model described in the main text shows better agreement with the experimental curves than the alternative Bauschinger model described here; this is not too surprising, however, inasmuch as the Bauschinger model described in the text has two adjustable coefficients and can be refined more to agree with experimental data than the alternative Bauschinger model, which has no adjustable coefficients.

DOCUMENT CONTROL DATA - R & D

(Security classification of title, body of abstract and indexing annotation must be entered when the overall report is classified)

1 ORIGINATING ACTIVITY (Corporate author)	2a. REPORT SECURITY CLASSIFICATION
Systems, Science and Software P.O. Box 1620 La Jolla, California 92037	UNCLASSIFIED 2b. GROUP

3 REPORT TITLE

Dislocation Dynamics and the Formulation of Constitutive Equations for Rate-Dependent Plastic Flow in Metals

4 DESCRIPTIVE NOTES *(Type of report and inclusive dates)*

Final Report

5. AUTHOR(S) *(First name, middle initial, last name)*

Harold E. Read, John R. Triplett, and Robert A. Cecil

6. REPORT DATE	7a. TOTAL NO. OF PAGES	7b. NO. OF REFS
December 1970	115	70

8a CONTRACT OR GRANT NO.	9a. ORIGINATOR'S REPORT NUMBER(S)
DASA 01-70-C-0055 b. PROJECT NO. NWER XAXA c. Task and Subtask AA106 d.	3SR-502 9b. OTHER REPORT NO(S) *(Any other numbers that may be assigned this report)* DASA 2638

10 DISTRIBUTION STATEMENT

Approved for public release; distribution unlimited.

11 SUPPLEMENTARY NOTES	12. SPONSORING MILITARY ACTIVITY
n/a	Director Defense Atomic Support Agency Washington, D.C. 20305

13 ABSTRACT

A rate-dependent constitutive model is developed which describes a broad spectrum of elastic-plastic response in isotropic metals, ranging from quasi-static behavior through the thermally activated intermediate strain rate regime, up to the high strain rate region where phonon viscosity and relativistic effects appear to control the flow process. Upon reverse straining from a plastically pre-strained state, the constitutive model exhibits a rate-dependent Bauschinger effect.

An attempt has been made to utilize, wherever possible, current knowledge in the theory of dislocation dynamics in formulating the constitutive model. In most cases, only simple models of governing deformation mechanisms can be constructed and, even to accomplish this, considerable speculation is required. Where dislocation theory is unable to provide guidance in defining and characterizing a particular mechanism, a phenomenological approach has been followed.

The advanced constitutive model developed here has been incorporated into the one-dimensional, finite-difference RIP code. The application of this model to 6061-T6 aluminum is described.

DD FORM 1 NOV 65 1473

14. KEY WORDS	LINK A		LINK B		LINK C	
	ROLE	WT	ROLE	WT	ROLE	WT
Shock Waves						
Dislocation Dynamics						
Constitutive Equations						
Spallation						
Aluminum						